ICARUS 85, 394–443 (1990)

Tidal Evolution of the Uranian Satellites

III. Evolution through the Miranda–Umbriel 3:1, Miranda–Ariel 5:3, and Ariel–Umbriel 2:1 Mean-Motion Commensurabilities[1]

WILLIAM C. TITTEMORE

Department of Planetary Sciences, Lunar and Planetary Laboratory, University of Arizona, Tucson, Arizona 85721

AND

JACK WISDOM

Department of Earth, Atmospheric, and Planetary Sciences, Massachusetts Institute of Technology, Cambridge, Massachusetts 02139

Received January 27, 1989; revised November 20, 1989

Tidal evolution has significantly affected the history of the Uranian satellite system. The presence of large chaotic zones at past mean-motion commensurabilities among the Uranian satellites has resulted in significant changes in the orbital elements of some of the satellites, while allowing them to escape from the commensurabilities and evolve to their present nonresonant configuration. Miranda and Umbriel have probably passed through the 3:1 commensurability, resulting in Miranda's current anomalously high inclination, and constraining the Q of Uranus to be less than 39,000 (W. C. Tittemore and J. Wisdom 1989, *Icarus* 78, 63–89). The orbits of both satellites become chaotic during evolution through the eccentricity resonances associated with the 3:1 commensurability. During this phase of evolution, the orbital eccentricity of Miranda can be driven up to a value of about 0.05. Miranda can then escape from the 3:1 commensurability with a relatively large orbital eccentricity, which can damp to the current value in the time since resonance passage. Tidal friction may have heated the interior of Miranda to a temperature near the eutectic melting point of $NH_3 \cdot H_2O$, but most likely did not result in the melting of significant quantities of water ice. Miranda and Ariel passed through the 5:3 mean-motion commensurability if the Q of Uranus is less than about 12,000. During evolution through this commensurability, the semimajor axis ratio (a_M/a_A) decreased. As the orbits enter a large chaotic zone associated with this commensurability, both the eccentricity and inclination of Miranda's orbit jump to values up to six times higher than the values approaching the resonance. Upon escaping from the resonance, the orbit of Miranda may have retained moderately high eccentricity and inclination, or e_M and i_M may have decreased back to values comparable to those approaching the resonance. If the Q of Uranus is smaller than about 11,000, Ariel and Umbriel would have encountered the 2:1 mean-motion commensurability. However, capture into this resonance is very likely if the eccentricities of the orbits approaching the resonance were comparable to the current values: the probability of escape would not have been significant unless the initial eccentricities were of order 0.03 or larger. It is therefore unlikely that these satellites encountered this resonance, constraining the Q of Uranus to be greater than 11,000. The specific dissipation function of Uranus is therefore well constrained: $11{,}000 < Q < 39{,}000$.

[1] Contribution 89-07 of the University of Arizona Theoretical Astrophysics Program.

0019-1035/90 $3.00

1. INTRODUCTION

The Uranian satellite system contains a rich variety of features of interest to planetary scientists. Voyager 2 revealed that the satellites Miranda, Ariel, and Titania have had spectacular geological histories (Smith *et al.* 1986), despite their small sizes and low current temperatures. Sources of internal heat for these satellites must have been present at some point in time to account for the exotic features observed on their surfaces. In addition, there are some interesting anomalies in the orbits of the Uranian satellites. For one, the satellites are not currently involved in any low-order mean-motion resonances, in contrast to the satellite systems of Jupiter and Saturn. Also, the orbital eccentricities of the inner large satellites are anomalously large when the time scale of damping due to satellite tides is taken into consideration (Squyres *et al.* 1985). Finally, the orbital inclination of Miranda is more than an order of magnitude larger than those of the other satellites (Whitaker and Greenberg 1973, Veillet 1983).

Tidal evolution is an important process in planetary satellite systems. Most of the commensurabilities in the Jovian and Saturnian systems are probably the result of tidal evolution of the orbits (Goldreich 1965). Tidal heating of Io in the Laplace resonance explains the geological activity on this satellite (Peale *et al.* 1979). Tides raised on Uranus by its major satellites tend to increase in the orbital semimajor axes, as energy is dissipated in the planetary interior. Because the major satellites move in eccentric orbits, the tidal distortion of the satellites caused by the planet varies periodically. Internal friction dissipates energy in the satellites, tending to decrease the orbital semimajor axes and eccentricities, and heating the satellite interiors.

Two features of the Uranian system distinguish it from the Saturnian and Jovian systems: the oblateness of the planet is relatively small, and the satellite-to-planet mass ratios are relatively large. The importance of the small oblateness of Uranus was pointed out by Dermott (1984), who suggested that since resonances at mean-motion commensurabilities among the Uranian satellites are not well separated, there might be chaotic behavior. He speculated that chaotic behavior at past orbital commensurabilities might explain some of the currently observed dynamical features. Significant secular interactions between the satellites (Greenberg 1975, Dermott and Nicholson 1986, Laskar 1986) resulting from the relatively large satellite masses may also contribute to chaotic behavior. Since there are large increases of eccentricity and inclination at the asteroidal resonances (Wisdom 1982, 1983, 1987b), it is natural to speculate that similar chaotic behavior among the Uranian satellites might lead to significant changes in the orbits and tidally heat the satellites.

To address this problem in a rigorous manner, we have been carrying out a systematic study of mean-motion resonances which may have been encountered by the Uranian satellites as the orbits evolved due to tidal friction. We have found significant chaotic zones at low-order mean-motion commensurabilities between the Uranian satellites (Tittemore and Wisdom 1987, 1988a,b, 1989, Tittemore 1988). The presence of these chaotic zones significantly affects the mechanisms and outcomes of resonance passage. Satellites may spend a considerable period of time evolving within a commensurability, during which orbital eccentricities and/or inclinations may vary significantly, and then escape from the resonant interaction, allowing the satellites to evolve to their present nonresonant configuration. The standard integrable theory of evolution through resonances (Goldreich and Peale 1966, Counselman and Shapiro 1970, Yoder 1979a, Henrard 1982, Henrard and Lemaitre 1983, Borderies and Goldreich 1984, Lemaitre 1984) has limited applicability to the Uranian satellite system.

Our approach has been to model the most important interactions involving the orbital

TABLE I

URANIAN SATELLITES

Satellite	R^a (km)	$m/M_U{}^a$	$a/R_U{}^a$	T^a (days)	e^b	i^c (radians)
Miranda	242 ± 5	$8.63 \pm 2.6 \times 10^{-7}$	4.96	1.41	0.0014 ± 0.0002	0.0737 ± 0.0028
Ariel	580 ± 5	$1.55 \pm .28 \times 10^{-5}$	7.29	2.52	0.0017 ± 0.0002	0.0054 ± 0.0019
Umbriel	595 ± 10	$1.47 \pm .28 \times 10^{-5}$	10.15	4.15	0.0043 ± 0.0002	0.0063 ± 0.0014
Titania	805 ± 5	$4.00 \pm .21 \times 10^{-5}$	16.65	8.70	0.0025 ± 0.0001	0.0025 ± 0.0005
Oberon	775 ± 10	$3.37 \pm .19 \times 10^{-5}$	22.27	13.46	0.0003 ± 0.0001	0.0018 ± 0.0004

[a] Stone and Miner (1986). $M_U = 8.69 \times 10^{25}$ kg, and $R_U = 26{,}200$ km (French *et al.* 1985).
[b] Peale (1988).
[c] Veillet (1983).

eccentricities or inclinations of satellites near a resonance by a Hamiltonian system with a parameter that evolves due to tidal friction. The parameter changes at a rate determined primarily by the tidal specific dissipation function (Q) of the planet. Tidal dissipation in the satellites may also affect the rate at which the model parameter changes, and affects the orbital eccentricities through direct tidal damping, which introduces frictional terms into the equations of motion. The time scale over which tidal effects become important is in general much longer than the dynamical time scale of the resonant interaction, and therefore tidal effects act as slow changes in the Hamiltonian. As a first approximation, we have only modeled the effects of planetary tides on the resonant interactions. This has allowed us to explore the dynamical environment of the most important resonances among the Uranian satellites, and to determine constraints on the extent to which the satellite system has tidally evolved. We have used nominal orbital and physical properties of the satellites in our models (see Tables I and II), to represent as closely as possible the evolution of the physical system.

In some cases, a two-degree-of-freedom Hamiltonian model is appropriate, allowing detailed study of the dynamics using surfaces of section. We have developed algebraic mappings from these models (see, e.g., Tittemore and Wisdom 1988a), similar to those developed by Wisdom (1982, 1983) to study resonant asteroidal motion, which reduce the amount of computer time needed to carry out the numerical simulations. We have integrated many trajectories through the commensurabilities using the mappings, to determine probabilities of various outcomes, and have tested the effects of various perturbations on our models.

During our program of study of the Uranian satellite system, we have found that a large chaotic zone exists at the Ariel-Umbriel 5 : 3 commensurability (Tittemore and Wisdom 1988a, henceforth referred to as TW-I). During evolution through this commensurability, the orbital eccentricities of Ariel and Umbriel may have increased moderately within the chaotic zone, before the satellites escaped from the resonance. However, the increases in the orbital eccentricity

TABLE II

TIDAL PARAMETERS

Satellite	ρ^a (g/cm^3)	μ^b (dyn/cm^2)	$k_2{}^c$	Q
Miranda	1.26 ± 0.39	4×10^{10}	1.4×10^{-3}	100
Ariel	1.65 ± 0.30	10^{11}	4.3×10^{-3}	100
Umbriel	1.44 ± 0.28	10^{11}	3.3×10^{-3}	100

[a] Stone and Miner (1986).
[b] Shear modulus, $\approx 4 \times 10^{10}$ dyn/cm^2 (water ice), $\approx 6.5 \times 10^{11}$ dyn/cm^2 (rock).
[c] $k_{2i} = \dfrac{\frac{3}{2}}{1 + 19\mu_i/2\rho_i g_i R_i} \approx \dfrac{3\rho_i g_i R_i}{19\mu_i}$,
$k_2 = 0.104$ (Gavrilov and Zharkov 1977).

of Ariel at this resonance do not appear to be sufficient to significantly affect its thermal evolution. We have also found that the current anomalously high orbital inclination of Miranda can be accounted for by passage through the 3 : 1 commensurability with Umbriel (Tittemore and Wisdom 1987, Tittemore and Wisdom 1989, henceforth referred to as TW-II). The satellites are temporarily captured into one of the inclination resonances, until a *secondary resonance*, or commensurability between the resonant libration frequency and the frequency difference between neighboring resonant arguments, drags the satellites into a large chaotic zone at large i_M, whereupon the satellites can escape from the inclination resonance region. The requirement that the satellites have passed through this commensurability constrains the Q of Uranus to be less than 39,000 [using $k_2 = 0.104$ (Gavrilov and Zharkov 1977)]. We also found that the orbital eccentricity of Miranda increases dramatically during evolution through this commensurability (Tittemore and Wisdom 1987, TW-II), possibly providing a significant internal heat source. This phase of lution is further discussed in Section 2.1.

We have also carried out a careful evaluation of the effect of the simulated rate of tidal evolution on the dynamical outcome. In the integrable single-resonance theory, the dynamics of resonance passage are independent of rate if a particular "adiabatic criterion" is satisfied, that is, the action of a trajectory (area in phase space) is approximately invariant except at the point of transition across the separatrix. This occurs when the fractional change in the libration frequency in one libration period due to tidal evolution is small (see Sections 2.1.1 and 2.2.1 and TW-II). In cases where the evolution is dominated by quasiperiodic behavior (TW-II), the single-resonance adiabatic criterion may be used to determine the simulated rate of tidal evolution at which the dynamics become independent of rate. However, in cases where the evolution is dominated by chaotic behavior (TW-I, see also below), the dynamics of resonance passage may be extremely sensitive to the simulated rate of tidal evolution, even if the simulated rate is orders of magnitude slower than the rate predicted by the single-resonance adiabatic criterion. In such cases, the relevant criterion is based on a "chaotic" adiabatic invariant (e.g., Brown *et al.* 1987). In the case of chaotic Hamiltonian systems with two degrees of freedom, the adiabatic invariant is the phase space volume enclosed by the energy surface containing the chaotic zone. This is a natural generalization of the concept of adiabatic invariants in integrable systems (e.g., Lenard 1959, Kruskal 1962, Arnold 1963). Approximate conservation of the chaotic adiabatic invariant requires that the chaotic zone be well explored by the trajectory on time scales much shorter than the time scale of resonance passage. We are continuing to examine the applicability of chaotic adiabatic invariants to orbital resonances. In some cases, however, we have found that adiabatic invariants do not exist even at tidal evolution rates that are within our constraints on the physical rate, for example, in the Miranda–Umbriel 3 : 1 commensurability during evolution through the eccentricity resonances when the inclination of Miranda is high (see Section 2.1). In this case, high-dimensional chaos is important, and the dynamics are not well approximated by a two-degree-of-freedom model.

Dermott *et al.* (1988) have also found chaotic variations at the Miranda–Umbriel 3 : 1 commensurability, by integrating the full gravitational equations of motion at the resonance for a relatively short time with the orbital eccentricity and inclination of Miranda artifically enhanced. Although the integration of the full gravitational equations of motion includes all of the higher-order resonant dynamical effects, this approach requires significantly longer computational times: direct numerical integrations require about three orders of magnitude more computer time than the algebraic mapping methods we have employed (Wisdom 1982). Therefore, using direct numerical integra-

tions, it is not yet feasible to simulate tidal evolution of trajectories fully through a commensurability at rates within our constraints on the physical rate. However, as we show (see Section 2.1), at the 3 : 1 Miranda–Umbriel commensurability, it is necessary to use simulated tidal evolution rates within our constraints on the physical rate, or there will be rate-induced artifacts in the dynamics. Even the short numerical integrations carried out by Dermott *et al.* use too high a simulated tidal evolution rate (see Section 2.1), and therefore the dynamics are significantly affected by rate-induced artifacts. A number of techniques used by those authors to reduce the computing time for numerical integrations that evolve all the way through the commensurability also introduce artifacts into the dynamics. First, the authors use the single-resonance adiabatic criterion to judge whether the simulated rate of tidal evolution is slow enough. As we have shown in TW-I and TW-II and here in Section 2.1, this is not a sufficient criterion. The authors also artificially increase the mass of Umbriel, simultaneously increasing the J_2 of Uranus. The justification given for this is to increase the single-resonance adiabatic rate and, thereby, further reduce the computing time. However, changing the masses and J_2 significantly changes the dynamical characteristics of the problem. Finally, the authors cause trajectories to ultimately escape from the resonance by increasing the simulated rate of tidal evolution by a factor of 20 in the middle of the integration, which also significantly alters the dynamics and probably artificially drags the trajectory out of the chaotic zone. Therefore, although the large increases in eccentricity and inclination and eventual disruption of the resonance found by the authors are interesting, they do not represent the dynamics of the actual Miranda–Umbriel system. The results of their numerical integrations of Miranda through a series of first-order resonances with Ariel are also affected by similar problems. However, those resonances were probably never encountered, because if they had been, Ariel and Umbriel must have passed through the 2 : 1 commensurability, which we have shown to be highly unlikely (see Section 2.3).

Marcialis and Greenberg (1988) have proposed an alternate model for the tidal heating of Miranda, in which the damping of the orbital eccentricity during a phase of chaotic rotation at some point in its early history provides the energy source. However, a number of key assumptions made by the authors are not well justified: (a) The authors have not determined the size of the chaotic zone for parameters appropriate to Miranda. Their assertion that a large chaotic zone exists is dependent upon Miranda having a large orbital eccentricity of order 0.1, which cannot be primordial, since the orbital eccentricity damping time scale of Miranda is only of order 10^8 years (see Section 2.1). (b) The authors do not demonstrate a mechanism for transferring Miranda from the synchronous rotation state to the chaotic zone. The resonance overlap criterion (see Wisdom *et al.* 1984) cannot by itself be used to determine whether a satellite is attitude unstable. For example, Phobos and several other small, irregularly shaped satellites satisfy the resonance overlap criterion for the synchronous and 3/2 rotation states, and have large chaotic zones in the spin–orbit phase space (Wisdom 1987a), but are not currently in a chaotic rotation state. (c) For a body in a chaotic tumbling state, tidal evolution of the spin and orbit is determined by the damping of the "rotational Jacobi integral" due to tidal dissipation, not just the damping of the orbital eccentricity (see Wisdom 1987a). These problems must be addressed before this mechanism can be considered viable.

We present here the results of our continuing studies of the Uranian satellite system. Section 2 explores the evolution of Miranda and Umbriel through the 3 : 1 mean-motion commensurability. Tittemore and Wisdom (1987, see also TW-II) found that during evolution through this commensurability,

the orbital eccentricity of Miranda may also have increased dramatically. We more fully explore this phase of the evolution here. Following an initial phase of temporary capture into one or more of the second-order eccentricity resonances associated with this commensurability, the satellites enter a large chaotic zone. In the planar-eccentric approximation, the maximum and minimum eccentricities in the chaotic zone increase in a very regular manner, indicating the existence of a chaotic adiabatic invariant. However, because of the high inclination of Miranda's orbit that develops during the prior passage through the inclination resonances, there is a strong coupling between the eccentricity and inclination resonances, and the actual variations of eccentricity are much more irregular than the planar approximation, although the maximum values of eccentricity are similar in both models. During evolution through the large chaotic zone, the orbital eccentricity of Miranda varies chaotically from zero to about 0.05. Chaotic variations occur over time scales comparable to the resonance passage time scale even for simulated tidal evolution rates within our constraints for the physical rate of evolution, due to significant high-dimensional chaotic wandering. This indicates that a chaotic adiabatic invariant does not exist in the three-dimensional case at physical rates of tidal evolution. Miranda may have retained a relatively large value of eccentricity after the satellites escaped from the resonant interaction. In the time since the satellites encountered this commensurability, the inclination of Miranda's orbit would have remained high, explaining the current anomalously high value, while the orbital eccentricity would have damped to the current value. Tidal heating of Miranda may have raised its internal temperature to a value near the eutectic melting point of ammonia hydrate, but most likely did not result in the melting of large quantities of water ice.

The 5 : 3 mean-motion commensurability involving Miranda and Ariel, which would have been encountered if Q is less than 12,000 [using $k_2 = 0.104$ (Gavrilov and Zharkov 1977)], is discussed in Section 2.1. This commensurability is similar to the 3 : 1 Miranda–Umbriel commensurability in that the mass of Ariel is much greater than that of Miranda, so the orbital elements of Miranda are more strongly affected by the resonance passage than are those of Ariel. It is similar to the 5 : 3 Ariel–Umbriel commensurability (TW-I) in that they involve the same combinations of resonance angles for the two satellites, and because the orbits are relatively close together, there is a relatively strong secular interaction between the satellites which significantly affects the orbit of Miranda. However, passage through this resonance differs from the previously considered ones in a significant way: for the nominal masses of Miranda and Ariel (see Table I), the semimajor axis ratio (a_M/a_A) *decreases* due to tidal dissipation in the planet. Upon encountering this resonance, the orbital eccentricity and inclination of Miranda suddenly increase by about a factor of 6 as the satellites evolve through a large chaotic zone. The changes in the orbit of Ariel are relatively insignificant. Miranda may leave this resonance with an orbital eccentricity and inclination comparable to or somewhat larger than the current values. The maximum rate of tidal heating of Miranda at this resonance was about one-third the maximum rate at the 3 : 1 commensurability with Umbriel. Both the structure of the phase space and the numerical experiments indicate that there is no mechanism of capture into this resonance, a conclusion also reached by Peale (1988) using arguments based on the available energy.

Finally, the Ariel–Umbriel 2 : 1 mean-motion commensurability is discussed in Section 2.3. The probability of capture was very high if the satellites approached this resonance with orbital eccentricities comparable to the current values. For such small initial eccentricities, the evolution is dominated by quasiperiodic behavior: although secondary resonances among fundamental

frequencies affect the amplitude of libration in the resonance, the chaotic zones associated with the secondary resonances are small. Once captured into the resonance, the satellites would have evolved to the equilibrium eccentricity of Ariel without the resonance becoming unstable. For much larger initial eccentricities, significant chaotic zones are present at this resonance; however, eccentricities of order 0.03 would have been required for the probability of escape to be significant. Therefore, it is unlikely that the satellites ever encountered this commensurability. The 2 : 1 commensurability is probably a dynamical "barrier" to the tidal evolution of the satellite system. Therefore, the specific dissipation function (Q) of Uranus is constrained to be greater than 11,000 [using $k_2 = 0.104$ (Gavrilov and Zharkov 1977)].

There are significant chaotic zones associated with all of the resonances considered in this investigation. The dynamics are exciting. The mechanisms of resonance passage are significantly different than in the integrable theories of resonance passage. There are some similarities between different resonances, but each has unique properties, resulting in a rich variety of dynamical behavior in the Uranian satellite system. The dynamics of the individual resonances may be used to constrain the evolution of the system as a whole. Since passage through the 3 : 1 resonance with Umbriel can explain the current inclination of Miranda's orbit, it is likely that the satellites have tidally evolved at least enough to encounter this commensurability. This sets an upper limit of 39,000 on the specific dissipation function (Q) of Uranus. Requiring that Ariel and Umbriel did not encounter the 2 : 1 commensurability constrains Q to be greater than 11,000. This rather narrow range may be useful in modeling the interior of Uranus.

2. RESONANCE DYNAMICS

In this section, we describe in detail the dynamics of the Miranda–Umbriel 3 : 1, Miranda–Ariel 5 : 3, and Ariel–Umbriel 2–1 mean-motion commensurabilities. We have considered three models for each commensurability. First, we consider the planar-eccentric approximation, in which the resonant motion can be described by a two-degree-of-freedom Hamiltonian, and the dynamics can be studied in detail using surfaces of section. We have carried out a systematic survey of each commensurability, determining capture probabilities, studying the effects of the rate of tidal evolution on the dynamics, and determining the structure of the phase space at different points in the evolution. This has allowed us to gain a detailed understanding of the dynamical mechanisms affecting the evolution of the orbital eccentricities at these resonances. For the planar-eccentric models, numerical calculations have been carried out using the algebraic mappings. The development of the planar-eccentric Hamiltonian models is given in Appendix I, and the development of tidal parameters is given in Appendix II. In calculating the numerical values of the Hamiltonian coefficients and other quantities, the adopted unit of time is one year, of mass is the mass of Uranus, and of length is the radius of Uranus (see Appendix I), unless otherwise specified.

We also consider the effects of perturbations on the planar-eccentric dynamical models. There are important resonant terms involving the inclinations at each commensurability. The inclinations are coupled to the eccentricities through nonlinear terms. We have developed Hamiltonian models for the study of the three-dimensional resonant behavior (Appendix I) and algebraic mappings to carry out the numerical integrations.

In addition, for each commensurability we determine the effects of perturbations due to other satellites on the resonant behavior. The secular interactions between the major Uranian satellites result in significant variations of the eccentricities and inclinations (Dermott and Nicholson 1986, Laskar 1986), and the frequencies are comparable to the important frequencies at reso-

nances. We have developed Hamiltonian models for the motion at a mean-motion commensurability perturbed by the secular interactions of the two resonant satellites with a third (see Appendix I). At the Miranda–Umbriel 3 : 1 commensurability, we consider the perturbations due to Ariel; at the Miranda–Ariel 5 : 3 commensurability, those due to Umbriel; and at the Ariel–Umbriel 2 : 1 resonance, those due to Titania. Numerical integrations of the averaged equations of motion were carried out using the Bulirsch–Stoer (1966a,b) algorithm.

2.1. The Miranda–Umbriel 3 : 1 Commensurability

2.1.1. The Planar-Eccentric Model

We consider first the interaction between Miranda and Umbriel in the planar-eccentric approximation, initially ignoring the fact that it is likely that the orbital inclination of Miranda was comparable to its current value at the time of encountering the eccentricity resonances. Although in fact the large orbital inclination of Miranda significantly affects the evolution through the eccentricity resonances (see Section 2.1.2), consideration of the planar model enables us to understand many qualitative features of the evolution through the eccentricity resonances.

The tidal parameter is defined to be $\delta = 3n_U - n_M - \dot{\tilde{\omega}}_M - \dot{\tilde{\omega}}_U$ (see Appendix I). At this commensurability, the orbital semimajor axis of Miranda increases much more rapidly than that of Umbriel. The time rate of change of δ is approximated by (see Appendix II)

$$\dot{\delta} \approx -\dot{n}_M \approx \frac{3}{2} n_M \frac{\dot{a}_M}{a_M}. \tag{1}$$

The equilibrium eccentricity at this resonance is $e_M = 0.026$, if $Q = 11{,}000$ for Uranus and $Q = 100$ for Miranda (see Appendix II). However, as we will show, the interaction between the satellites at such eccentricities is chaotic, and an equilibrium configuration may not be achieved.

The dynamical properties of the 3 : 1 commensurability were determined by integrating sets of trajectories through the resonance. The initial coordinates for each trajectory in a set were determined from the physical parameters $a_M = 4.8630$, $a_U = 10.1179$, $e_M = 0.005$, and $e_U = 0.005$, together with the initial angles $\sigma_M = \pi/2$, and $\sigma_U = 3\pi/2$, from which the coordinates $x_M = 0.0$, $y_M = 0.0009213$, $x_U = 0.0$, and $y_U = -0.004574$, and the parameter $\delta = -0.6153$ were computed for an initial trajectory. These eccentricities are comparable to the current eccentricities of the Uranian satellites. From this initial point, the coordinates of 199 additional points, spaced in time by 100 mapping periods ($T = 2\pi/40$ years) were computed using the mapping without tidal dissipation. These points formed the initial coordinates of the trajectories, each starting with the same energy, δ, and action (area enclosed by a trajectory in phase space), but with different phases. These trajectories were then tidally evolved through the resonance using the mapping.

As in TW-I and TW-II, we have carried out a study to determine the influence of the simulated rate of tidal evolution on the dynamics of the 3 : 1 resonance, by integrating sets of trajectories through the resonance at different dissipation rates. The simulated rate of tidal evolution is parameterized by the effective specific dissipation function of Uranus, as usual designated by $\mathfrak{Q}$, which is distinguished from the physical specific dissipation function Q for Uranus, which is presumably fixed and unknown. We wish to determine a simulated rate of tidal evolution sufficiently slow that the dynamics of resonance passage are not affected by rate-induced artifacts.

Plotted in Fig. 1 are the mean escape orbital eccentricities of Miranda and Umbriel for each set of trajectories as a function of dissipation rate. The mean escape orbital eccentricity of Miranda is quite high, of order 0.02, for $\mathfrak{Q} > 1$. For $\mathfrak{Q} < 0.1$, the escape orbital eccentricities of Miranda and Umbriel are the same as the initial values:

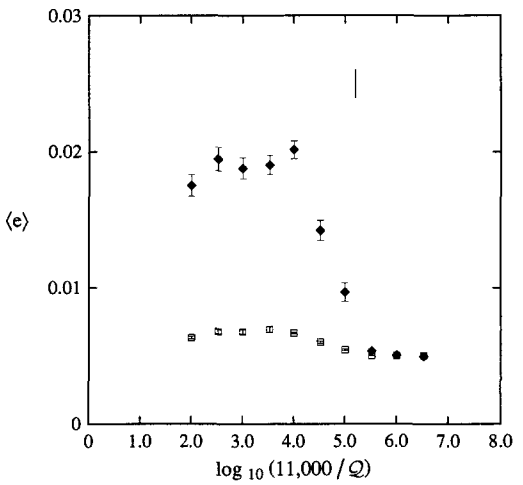

FIG. 1. Mean escape orbital eccentricities of Miranda (◆) and Umbriel (□) for ensembles of 200 trajectories as a function of tidal dissipation rate, expressed in terms of the effective specific dissipation function of Uranus $\mathcal{Q}$. The single-resonance adiabatic rate for the e_U^2 resonance is denoted by the vertical bar ($\mathcal{Q} = 0.07$, $\dot{a}_M/a_M = 9.4 \times 10^{-9}$ per orbit period). For simulated tidal evolution rates larger than this the trajectories are dragged through the resonance without displaying any interesting behavior. However, the dynamics are sensitive to the rate even for rates an order of magnitude slower than this.

they have been dragged through the resonance without displaying any interesting behavior. Between these values of $\mathcal{Q}$, the average escape eccentricity varies significantly.

As we have done for the circular-inclined problem (TW-II), we can compare the simulated tidal evolution rate at which dynamical artifacts appear to the adiabatic rate based on the single-resonance model. The first eccentricity resonance to be encountered is the e_U^2 resonance. We express the simulated rate of tidal evolution as the change of libration frequency of the e_U^2 resonance considered independently in one libration period divided by the libration frequency: $(\Delta\omega_L/\omega_L)$. In the single-resonance model, the action (area enclosed by a trajectory in the phase space) is approximately conserved if this nondimensional quantity is less than about unity, since the dynamical time scale is then much shorter than the tidal time scale.

The libration frequency of the e_U^2 resonance considered independently is given by (see TW-II for details of analogous calculations in the circular-inclined approximation)

$$\omega_L^2 = -4H(\delta - \delta_0) \qquad (2)$$

where $\delta_0 = 2(C - D) - 16B\Sigma_M$ is the value at which libration zones first appear in the phase space of this resonance. The change in the libration frequency of the e_U^2 resonance in one period is $\Delta\omega_L \simeq -4\pi H\dot{\delta}/\omega_L^2$, where $\dot{\delta} \approx 4.1 \times 10^{-4}/\mathcal{Q}$. For $e_M = e_U = 0.005$ well before the resonance is encountered, $\delta_0 = -0.29$, and the trajectory encounters the resonance at $\delta = 0.5$. Therefore, the single-resonance theory predicts that for the e_U^2 resonance with $e_M = e_U = 0.005$, $\Delta\omega_L/\omega_L \approx 0.07/\mathcal{Q}$. In the single-resonance approximation, then, the results of numerical simulations should be independent of the simulated tidal evolution rate if $\mathcal{Q} > 0.07$. We have denoted the single-resonance adiabatic rate in Fig. 1 by the vertical bar in the upper right of the figure. The results shown in Fig. 1 indicate that for simulated tidal evolution rates higher than this value, not much of dynamical interest happens. However, the dynamical outcome appears to be sensitive to the simulated rate of tidal evolution for rates about an order of magnitude slower than the rate predicted by the single-resonance adiabatic criterion. Therefore, the single-resonance approximation is not sufficient to determine the adiabatic rate in the planar-eccentric model. A large chaotic zone dominates the evolution through the eccentricity resonances, and the relevant adiabatic criterion for the planar-eccentric model is based on a chaotic adiabatic invariant.

The slowest rate used to integrate many trajectories, $\mathcal{Q} = 110$ ($\dot{a}_M/a_M \approx 6 \times 10^{-12}$ per orbit period), appears to be slow enough to represent the dynamics of passage through this commensurability well in the planar-eccentric approximation. Numerical

simulations of resonance passage at this rate show that the chaotic zone is well explored on time scales much shorter than the tidal evolution time scale (e.g., Fig. 3, see below), indicating that a chaotic adiabatic invariant is approximately conserved.

In Fig. 2, the distributions of time-averaged escape eccentricities for Miranda and Umbriel for $\mathfrak{Q} = 110$ are shown. As in the circular-inclined problem (see TW-II), the orbit of Umbriel is also significantly affected by the resonant interaction, although the changes in eccentricity are small compared to those of Miranda. It is quite possible for the orbit of Miranda to attain orbital eccentricities much larger than the single-resonance equilibrium value of about 0.026 during passage through this resonance, even in the planar approximation. The high orbital eccentricity of Miranda remaining after escape from the resonance can damp to the current value in the time since resonance passage.

Again, for this problem we can "freeze" the energy and δ of a trajectory at any point in the evolution and study the structure of the phase space by computing surfaces of section, to understand the qualitative behavior of the trajectory. The surfaces of section chosen plot y_M versus x_M when $x_U = 0$, which we designate section I, and σ_U versus Σ_U when $x_M = 0$ ($\sigma_M = \pi/2$), which we designate section II. Initial conditions on the surface of section are determined by solving a quartic equation (see TW-I). As with the circular-inclined model (TW-II), the phase space is simple enough that we need only study one quartic root family for each surface of section: the second largest root for section I and the largest root for section II. On section I, e_M is the radial distance from the origin, while the resonant argument σ_M is measured counterclockwise from the positive abcissa. On section II, e_U is plotted along the right ordinate axis for scale.

Figure 3 shows the variations of the orbital eccentricities of Miranda and Umbriel for one of the trajectories evolved through the 3:1 commensurability in the planar-eccentric approximation. The maximum and minimum orbital eccentricities are plotted in a small interval of δ ($\Delta\delta \approx 0.0035$). Well before the resonance is encountered, the motion is regular. Both orbital eccentricities are nearly constant: the mutual secular

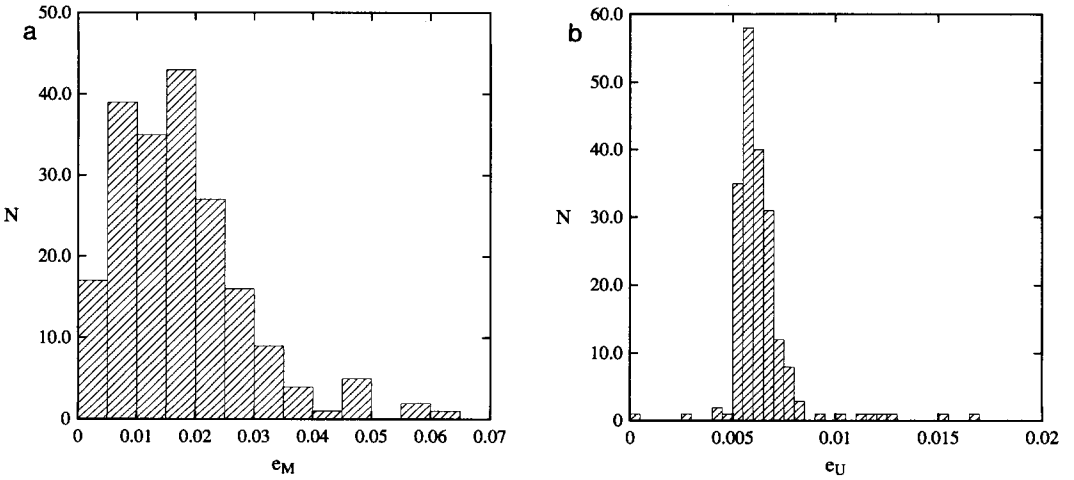

FIG. 2. Distributions of escape orbital eccentricities of Miranda (a) and Umbriel (b) for an ensemble of 200 trajectories evolved through the resonance with $\mathfrak{Q} = 110$, or $\dot{a}_M/a_M = 6 \times 10^{-12}$ per orbit period. Both orbits are affected by the resonant interaction. The high orbital eccentricity of Miranda retained after escape from the resonance can damp to the current value in the time since resonance passage.

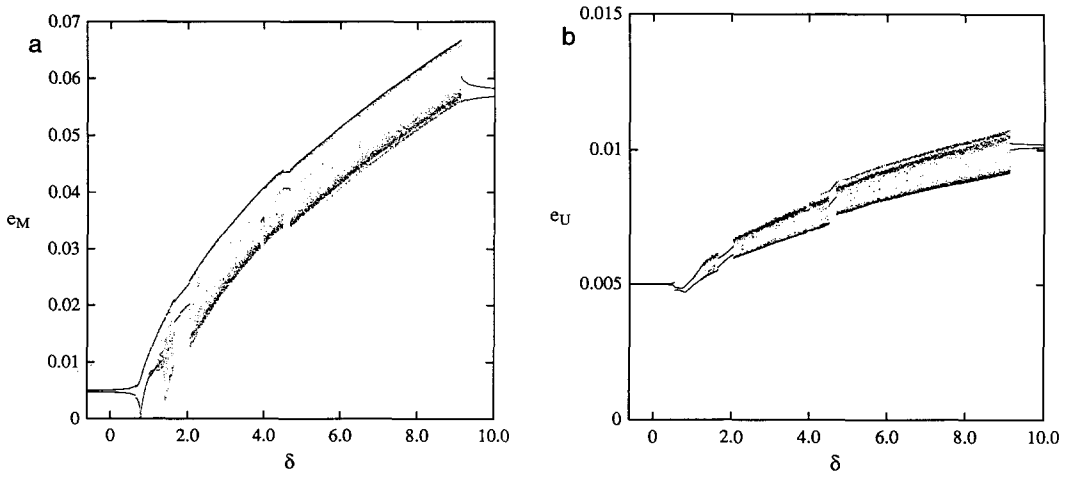

FIG. 3. Evolution of the orbital eccentricities of Miranda (a) and Umbriel (b) during passage through the 3 : 1 commensurability in the planar-eccentric approximation, with $\dot{a}_M/a_M = 6 \times 10^{-12}$ per orbit period ($\mathcal{Q} = 110$). The maximum and minimum eccentricities are plotted in intervals $\Delta\delta = 0.0035$. After initially being captured into the mixed ($e_M e_U$) resonance, the trajectory enters a large chaotic zone and the orbital eccentricity of Miranda evolves to a large value before the trajectory escapes from the resonance.

interactions are quite weak. As the resonance is approached, the amplitude of eccentricity variation increases slightly. At $\delta \approx 0.5$, the trajectory encounters the e_U^2 resonance, which it is not captured into, resulting in the slight decrease of average e_U visible in Fig. 3b. Shortly thereafter, the trajectory encounters the mixed ($e_M e_U$) resonance, at $\delta \approx 0.8$. Figure 4a displays the phase space (section II) through which the trajectory has evolved at this point in its evolution. The two large islands and narrow chaotic zone visible in the center of the figure are associated with the e_U^2 resonance. At the bottom left of the figure is the libration region associated with the $e_M e_U$ resonance, surrounded by a chaotic zone. Between the two primary resonant libration regions are smaller chains of islands and narrow chaotic zones, associated with low-order commensurabilities between the circulation frequencies of the e_U^2 and $e_M e_U$ resonant arguments. Near the $e_M e_U$ resonance, the spacing between these secondary resonant zones is smaller than the widths of the islands, and gives a complicated appearance to the chaotic zone at the bottom of the figure. The trajectory displayed in Fig. 3 has just been captured into the $e_M e_U$ resonance, and is in the libration region in the lower left of the figure.

As this trajectory evolves within the $e_M e_U$ resonance, the orbital eccentricities of both satellites increase. Shortly after being captured, though, the trajectory encounters a chain of four islands associated with a secondary resonance between the libration frequency of the $e_M e_U$ resonance and the frequency of circulation of the e_U^2 resonant argument. Figure 4b shows the phase space inhabited by the trajectory displayed in Fig. 3 just after capture into this secondary resonance. The trajectory from Fig. 3 generates two loops in the chain of four islands within the zone of libration of the $e_M e_U$ resonance in the bottom left of the figure. The chaotic zone surrounding the libration region has grown, having "swallowed" more neighboring secondary resonant island chains that were separate in Fig. 4a.

The trajectory is "dragged" out of the $e_M e_U$ libration zone by the secondary reso-

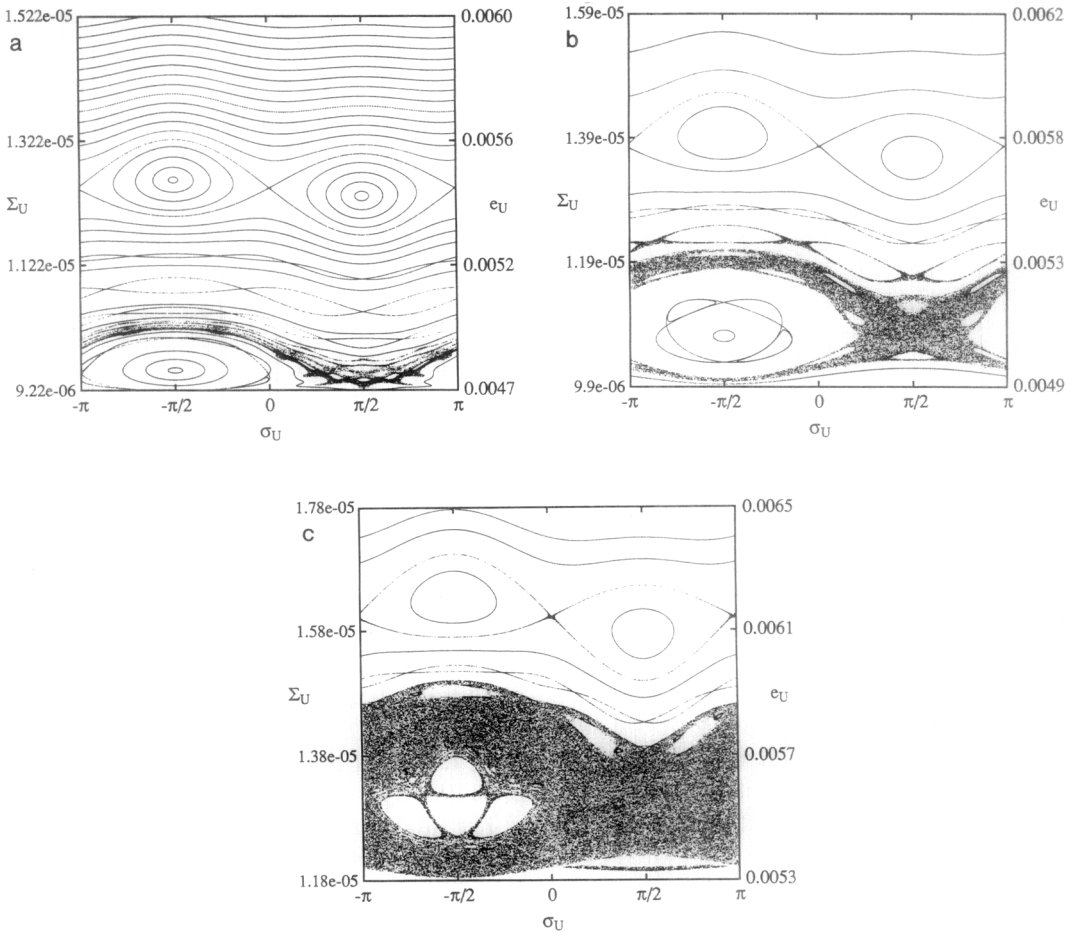

FIG. 4. Surfaces of section II showing the phase space available to the trajectory displayed in Fig. 3. (a) $\delta = 0.804$. The trajectory has escaped from the e_U^2 resonance (center), and has just been captured into the $e_M e_U$ libration zone at lower left. A large chaotic zone is forming at the $e_M e_U$ resonance. (b) $\delta = 1.01$. The trajectory has been captured in a secondary resonance in the $e_M e_U$ libration zone, and generates the two loops in the chain of four islands. The chaotic zone has increased in extent. (c) $\delta = 1.385$. The trajectory has been dragged into the large chaotic zone. The $e_M e_U$ resonance has become unstable.

nance, and enters the chaotic region. This mechanism of escape from resonance through secondary resonance capture was first identified in our study of the Miranda–Umbriel 3 : 1 inclination resonances (TW-II). However, in contrast to the inclination resonances, the trajectory spends a considerable period of time in the chaotic zone before escaping from the eccentricity resonances. Both eccentricities continue to increase, and as they do, the extent of the chaotic region in phase space increases. Figure 4c shows section II after the system has entered the chaotic zone. The $e_m e_U$ libration zone has become unstable due to a period 3 secondary resonance. The period 3 secondary resonance visible in Figs. 4a and b between the primary libration zones has been absorbed into the large chaotic zone. Eventually, the chaotic separatrix associated with the e_U^2 resonance also merges with the large chaotic zone. Figure 5 shows section I at the same point in the evolution as Fig. 4b. The heavy solid curve

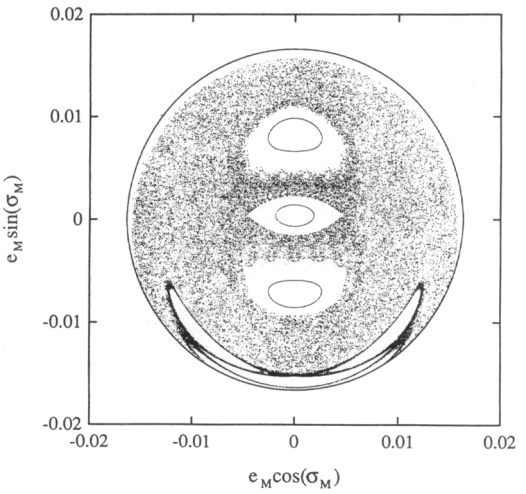

FIG. 5. Surface of section I showing the phase space available to the trajectory displayed in Fig. 3 at $\delta = 1.385$ (see also Fig. 4c). The $e_M e_U$ resonance zone is at the bottom of the figure. The e_M^2 resonance zone has appeared at the center of the figure.

is the energy surface boundary of the surface of section, within which trajectories are constrained. The large chaotic zone fills much of the displayed region of the phase space, but remnants of the individual second-order eccentricity resonances are still visible at this point in the evolution. The unstable libration region of the $e_M e_U$ resonance is visible at the bottom of the figure. The quasiperiodic zone in the center of the figure is the region into which trajectories eventually escape from the eccentricity resonances. The two quasiperiodic zones above and below center are libration regions associated with the e_M^2 resonance. The chaotic zone becomes much more uniform in structure as the system continues to evolve.

As the trajectory evolves within the large chaotic zone, the eccentricities vary between well-defined maximum and minimum values, forming a smooth "envelope" of eccentricities visible in Fig. 3. At a particular value of δ, these "envelopes" correspond to the boundaries of the chaotic zones on the surfaces of section of the frozen Hamiltonian. This indicates that the chaotic zone is being well explored on a time scale much shorter than the time scale over which δ evolves significantly due to tides. This in turn indicates that while the trajectory is in the chaotic zone, a chaotic adiabatic invariant is being approximately conserved. Note also that at values of δ of approximately 2 and 4.5, the trajectory is temporarily recaptured into a quasiperiodic resonant region.

For small initial eccentricities, the locations of secondary resonances are well predicted by the analytical techniques we employed in our study of the inclination problem (see TW-II), allowing us to analytically determine the point of transition from quasiperiodic to chaotic behavior.

2.1.2. The Eccentric-Inclined Model

In TW-II, we introduced the eccentric-inclined Miranda–Umbriel 3 : 1 resonance model, and showed that the inclination of Miranda's orbit remains high during chaotic evolution through the eccentricity resonances at the 3 : 1 commensurability. (See Note at end of Appendix I.) We further explore the dynamics of this resonance here.

The tidal evolution parameter δ is defined to be the nonresonant contributions to $3n_U - n_M - \frac{1}{2}(\dot{\bar{\omega}}_M + \dot{\bar{\omega}}_U + \dot{\Omega}_M + \dot{\Omega}_U)$ (see Appendix I). Initial conditions for trajectories to be numerically evolved through the resonance were generated as follows. From an initial set of coordinates, calculated from the orbital elements $a_M = 4.86345$, $a_U = 10.1179$, $e_M = e_M = 0.005$, $i_M = i_U = 0.005$ radian, $\sigma_M = \sigma_U = 0$, $\psi_M = \psi_U = 0$, points were computed without tidal dissipation, spaced in time by 100 mapping iterations, or 15.7 years ($\Omega = 40$).

This model comprises three eccentricity resonances, three inclination resonances, and secular interactions. The eccentricities are coupled to the inclinations through nonlinear terms; this model has four degrees of freedom. For chaotic systems with two degrees of freedom, such as the planar-eccentric case described above, chaotic zones are isolated from each other in phase space by quasiperiodic zones, and thus the variations possible within a chaotic zone are

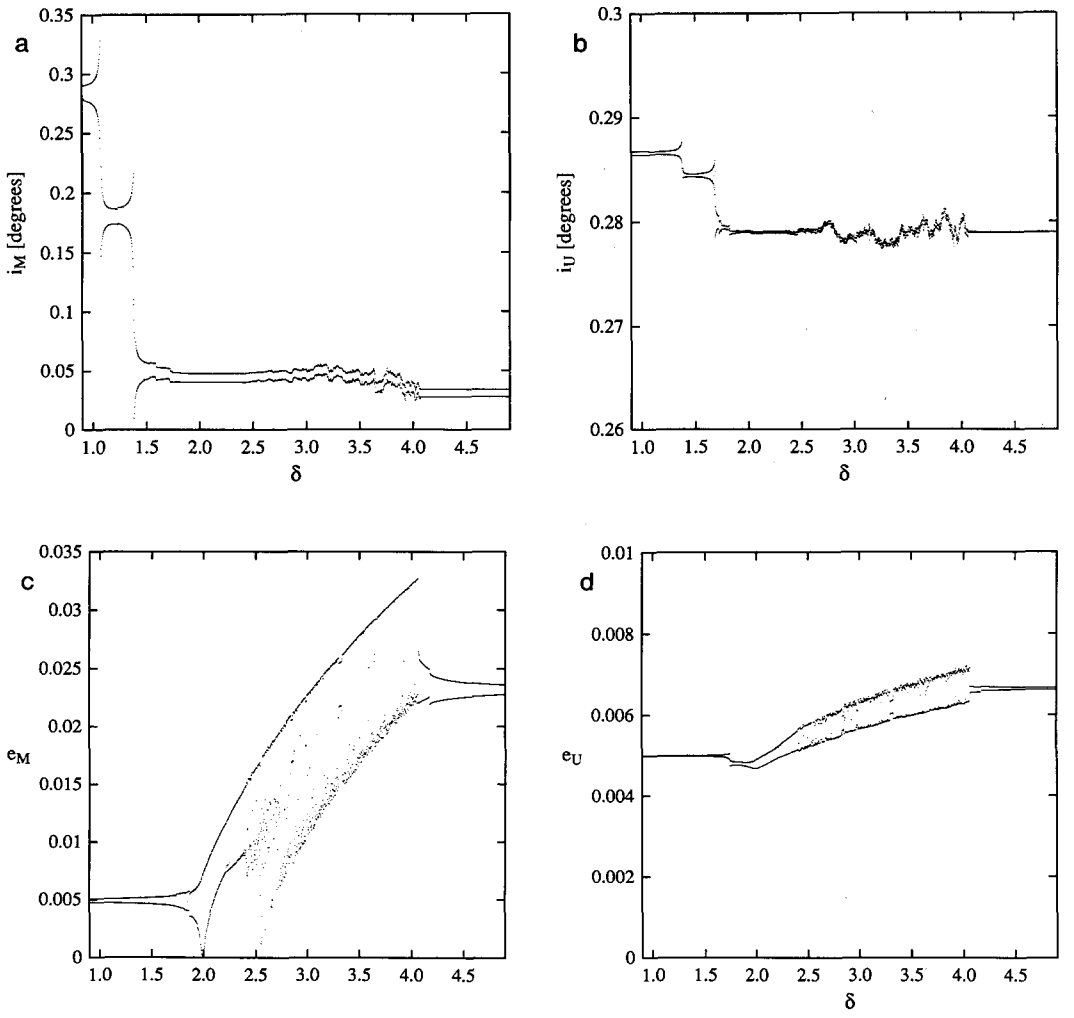

FIG. 6. Eccentricity and inclination variations of a trajectory evolved through the 3 : 1 Miranda–Umbriel mean-motion commensurability ($\dot{a}_M/a_M = 6 \times 10^{-12}$ per orbit period). (a) Orbital inclination of Miranda. (b) Orbital inclination of Umbriel. (c) Orbital eccentricity of Miranda. (d) Orbital eccentricity of Umbriel. The inclination resonances are encountered first, and the satellites escape from them, leaving both satellites with low inclinations. Evolution through the large chaotic zone associated with the eccentricity resonances is qualitatively similar to that in the planar-eccentric approximation (compare with Fig. 3).

restricted. In systems with more than two degrees of freedom, though, chaotic zones are not isolated. (see, e.g., Chirikov 1979, Hénon 1983). Therefore, where this higher-dimensional chaos is important, the trajectory may wander far from its initial state, over a long enough time scale, exploring a much larger volume of phase space than the two-degree-of-freedom system. The extent of these chaotic wanderings will depend on the diffusion time scale compared to the tidal evolution time scale. Since this higher-dimensional diffusion occurs generally over a much longer time scale than the fundamental dynamical periods in the problem (Chirikov 1979), a chaotic adiabatic criterion which is based on the trajectory exploring all of the chaotic zone before significant tidal

evolution takes place may not exist for higher-dimensional systems. Therefore, where this higher-dimensional chaos is significant, the dynamical outcome may be sensitive to the simulated tidal evolution rate, even for rates implied by our constraints on the physical Q of Uranus.

In the planar-eccentric two-degree-of-freedom model, the conservation of a chaotic adiabatic invariant is indicated by the smooth "envelope" of maximum and minimum eccentricities in the chaotic zone, which show that the chaotic zone is well explored by the trajectory on a time scale much shorter than the tidal evolution time scale. Figure 6 shows the inclination and eccentricity variations of Miranda and Umbriel for a trajectory that escapes from all the inclination resonances, thus encountering the eccentricity resonances with both inclinations small. In each plot, the maximum and minimum eccentricity or inclination is plotted in intervals of $\Delta\delta = 0.0033$. For this trajectory, the nonlinear coupling between inclination and eccentricity resonances is weak, because both orbital inclinations are small. All of the elements vary chaotically during evolution through the eccentricity resonances, but we still see a smooth "envelope" of the maximum and minimum eccentricities in the chaotic zone (Figs. 6c and d), as we did in the planar approximation (Fig. 3). This indicates that an adiabatic invariant is being nearly conserved.

The rate of tidal evolution used for the trajectory in Fig. 6 was $\dot{a}_M/a_M = 6 \times 10^{-12}$ per orbit period ($\mathcal{Q} = 110$), the same rate used for the trajectory displayed in Fig. 3 in the planar approximation. To test whether the behavior is similar at physical rates, we have taken the state variables of the trajectory shown in Fig. 6 in the chaotic zone ($\delta = 2.649$), and continued the integration with $\mathcal{Q} = 11{,}000$. The orbital eccentricity variations of Miranda for this experiment are shown in Fig. 7. The maximum and minimum boundaries of the chaotic zone are still well defined, confirming the near conservation of a chaotic adiabatic invariant at physical rates. The planar-eccentric model is therefore a good approximation if the orbital inclinations are small.

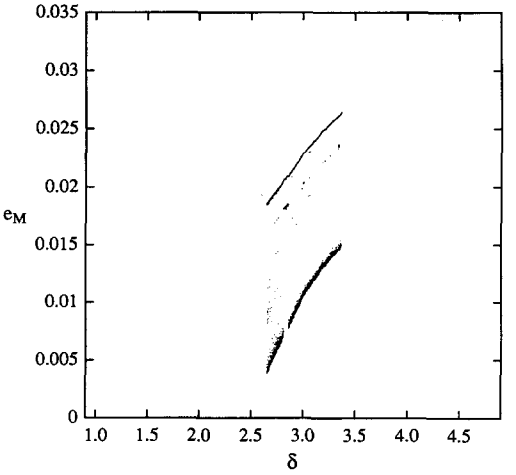

FIG. 7. Eccentricity variations of Miranda in the chaotic zone of the 3 : 1 commensurability with Umbriel, at a simulated rate of tidal evolution of $\dot{a}_M/a_M = 6 \times 10^{-14}$ per orbit period ($Q = 11{,}000$) within our constraints on the physical Q of Uranus. With both inclinations small, the boundaries of the chaotic zone vary smoothly.

However, with a high inclination of Miranda's orbit resulting from temporary capture into the inclination resonances, we see markedly different behavior. Figure 8 shows the inclination and eccentricity variations of Miranda and Umbriel evolved through the 3 : 1 commensurability with the three-dimensional mapping with $\mathcal{Q} = 11{,}000$. The maximum and minimum eccentricities and inclinations are plotted in intervals of $\Delta\delta = 0.0037$, and the region between the maximum and minimum envelopes has been shaded, to better show how the elements vary. We have not artifically enhanced the simulated rate of tidal evolution in this calculation; $\mathcal{Q}$ is within our constraints on the physical Q of Uranus set by the dynamics. In this example, the trajectory is captured into the i_M^2 resonance. The evolution through the inclination resonances is not significantly affected by the

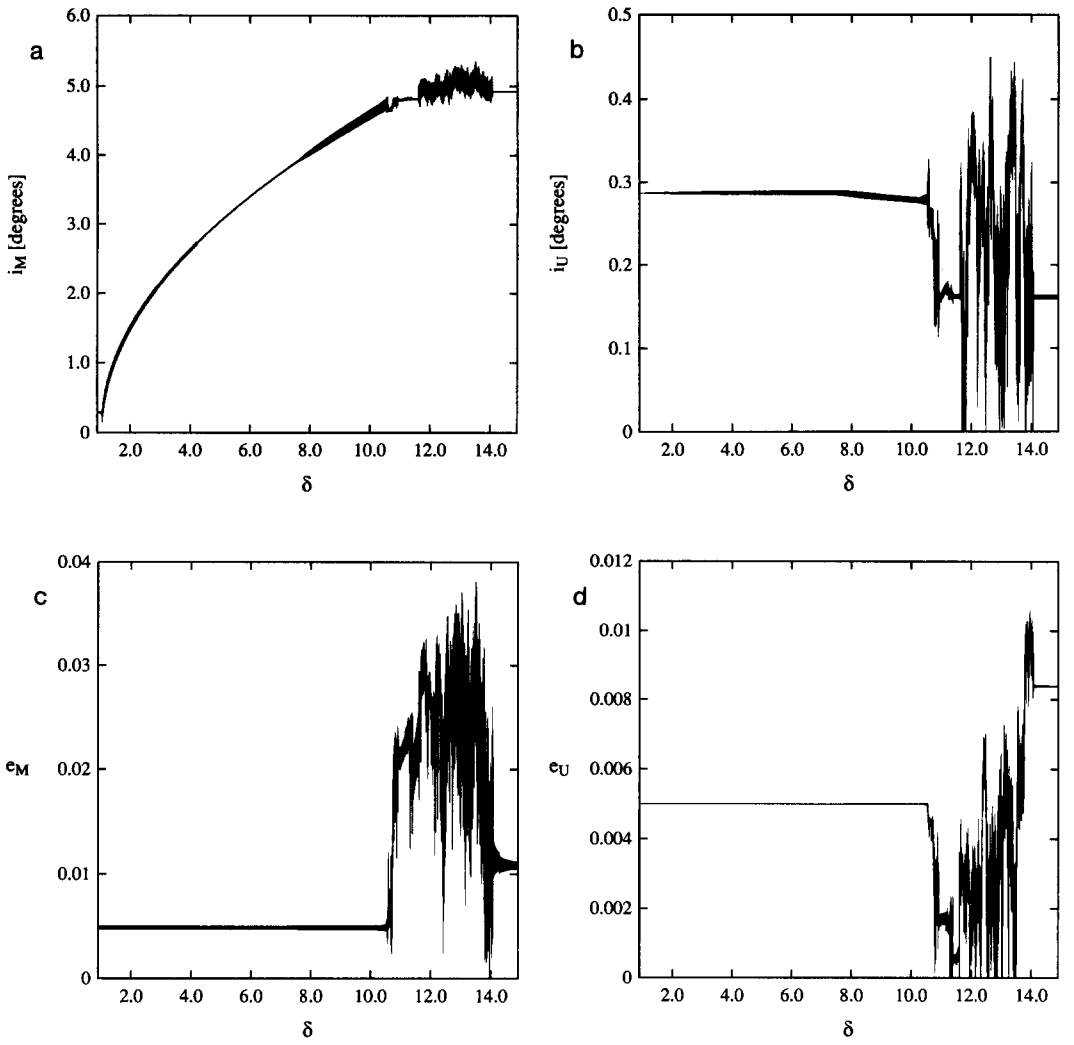

FIG. 8. Eccentricity and inclination variations of a trajectory evolved through the 3 : 1 Miranda-Umbriel mean-motion commensurability with $\mathcal{Q} = 11{,}000$ ($\dot{a}_M/a_M = 6 \times 10^{-14}$ per orbit period), within our constraints on the physical Q of Uranus. (a) Orbital inclination of Miranda. (b) Orbital inclination of Umbriel. (c) Orbital eccentricity of Miranda. (d) Orbital eccentricity of Umbriel. The maximum and minimum values are plotted in intervals of $\Delta\delta = 0.0066$. This figure represents about 10^{11} orbit periods of Miranda. In this case, the trajectory is captured into the i_M^2 resonance, and i_M evolves to a high value. With the orbital inclination of Miranda high at the point of encounter of the eccentricity resonances, the orbital eccentricity of Miranda varies extremely irregularly within this chaotic zone, even on timescales comparable to the resonance passage timescale. The orbital inclination of Miranda remains high.

nonresonant variations in eccentricity, as we previously showed in TW-II. At $\delta \approx 8.0$, the trajectory in Fig. 8 is captured into the 2 : 1 secondary commensurability between the libration frequency of the i_M^2 resonant argument and the circulation frequency of the i_U^2 resonant argument (see TW-II).

This 2 : 1 secondary resonance eventually drags the trajectory displayed in Fig. 8 into the chaotic zone associated with the inclina-

tion resonances. During evolution through this chaotic zone, both the inclinations and the eccentricities vary chaotically. With a high orbital inclination of Miranda, the nonlinear coupling between the eccentricity and inclination resonances is strong and causes significant variations in the orbital eccentricity of Miranda. The trajectory escapes from the inclination resonances, becomes briefly quasiperiodic, and then enters the large chaotic zone associated with the eccentricity resonances, which dominates the rest of the evolution through the commensurability. The variations of the eccentricities and inclinations of both satellites are very irregular in this chaotic zone. Note, however, that the variations in orbital inclination of Miranda are relatively small: it maintains a large average value. As the trajectory evolves further in the chaotic zone, the maximum eccentricity of Miranda's orbit becomes larger, reaching a maximum value of about 0.04 before the trajectory escapes from the commensurability. After escape, the orbital eccentricity of Miranda is about 0.011. The chaotic variations in the orbital eccentricity and inclination of Umbriel are not large compared to those of Miranda.

Even though this trajectory was computed with a simulated tidal evolution rate within the physical bonds, the orbital elements vary extremely irregularly on time scales comparable to the resonance passage time scale: there is not a smooth "envelope" to the chaotic eccentricity variations as seen in the previous example.There is no evidence for an adiabatic invariant when both the orbital inclination and eccentricity of Miranda are large, even at this very slow simulated tidal evolution rate. The dynamics are sensitive to the simulated rate, even if the Q of Uranus is within our constraints. *Therefore, to avoid dynamical artifacts, simulated tidal evolution rates must be within the physical constraints.* The resonant mapping methods first developed by Wisdom (1982, 1983) have made this computationally feasible.

Although the eccentric-inclined model has too many degrees of freedom to study using surfaces of section, we can verify the presence of the secondary resonances. In Fig. 9a, the i_U^2 resonant argument, $\psi_U = \frac{1}{2}(3\lambda_U - \lambda_M - 2\Omega_U)$, is plotted against the i_M^2 resonant argument, $\psi_M = \frac{1}{2}(3\lambda_U - \lambda_M - 2\Omega_M)$ for the trajectory shown in Fig. 8 at

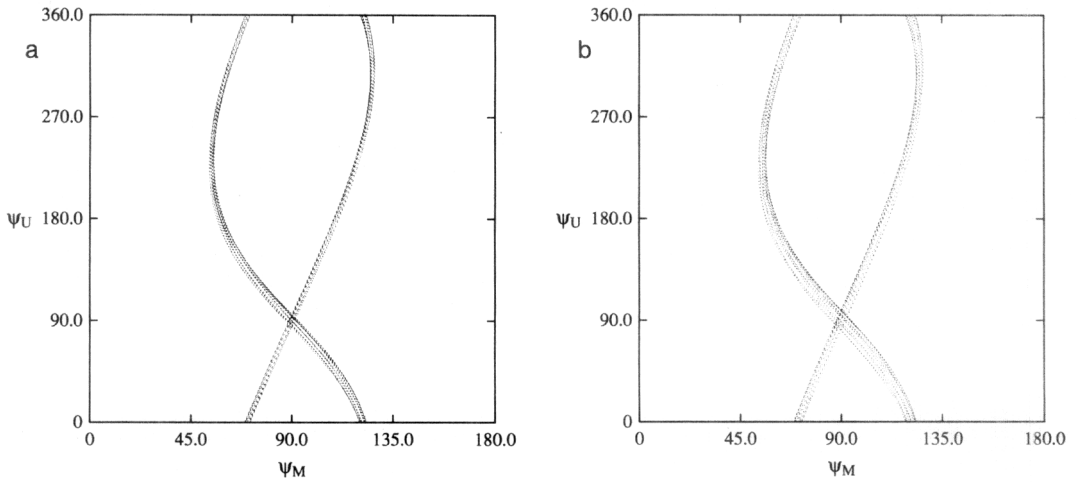

FIG. 9. Variation of the resonant arguments $\psi_M = \frac{1}{2}(3\lambda_U - \lambda_M - 2\Omega_M)$ and $\psi_U = \frac{1}{2}(3\lambda_U - \lambda_M - 2\Omega_U)$ for the trajectory displayed in Fig. 8 at $\delta = 9.147$. (a) Computed using the mapping. (b) Computed using unaveraged differential equations.

$\delta = 9.147$. Points were computed using the mapping with an iterative time step of 57.37 days. ψ_M is librating in this figure as ψ_U circulates. In addition, the trajectory is nearly periodic: it is librating in the 2 : 1 secondary resonance region (see Fig. 12 of TW-II for a surface of section of this region of phase space in the circular-inclined model).

As a further check of the secondary resonance mechanism for escape from this resonance, we have explored the same region of phase space using direct unaveraged numerical integrations. Our Hamiltonian models utilize Jacobi coordinates (see Appendix I). We have taken the Jacobi coordinates of the trajectory shown in Fig. 9a, and converted them to the following Uranus-centered orbital elements: $a_M = 4.863473$, $a_U = 10.117934$, $e_M = 0.00497385$, $e_U = 0.00500281$, $i_M = 4.416421$ degree, $i_U = 0.279794$ degree, $\lambda_M = \lambda_U = 0$, $\tilde{\omega}_M = 45.013320$ degree, $\tilde{\omega}_U = 21.380209$ degrees, $\Omega_M = 271.650075$ degrees, and $\Omega_U = 282.078623$ degrees. We carried out a direct unaveraged numerical integration of the gravitational equations of motion for the resonant system, in Uranus-centered coordinate, including planetary oblateness terms of order J_2. The integration was carried out using the Bulirsch–Stoer integrator, with a relative precision of 10^{-9} per step size of approximately 0.069 day (about 1/20th of an orbital period of Miranda), and points were plotted in intervals of approximately 57.37 days. Figure 9b shows the variations of ψ_M and ψ_U for Miranda and Umbriel using unaveraged differential equations. The variations of the resonant arguments on this plot are virtually identical to those in Fig. 9a, indicating that the eccentric-inclined Hamiltonian model and mapping represent the actual dynamics of the 3 : 1 Miranda–Umbriel resonance well.

We have further explored the evolution of Miranda through the 3 : 1 mean-motion commensurability. We have generated starting conditions for trajectories with large i_M, using the state variables of the trajectory displayed in Fig. 8 at $\delta = 10.397$, just before it enters the chaotic zone associated with the inclination resonances. From these coordinates, we have generated three new sets of coordinates, by integrating the mapping forward in time, without tidal dissipation, spaced in time by 100 mapping iterations (15.7 years). This provides a set of initial conditions with identical values of δ and the Hamiltonian, but with different angular phases. These different initial conditions have each been integrated forward in time through the eccentricity resonances using the mapping, with $\mathfrak{Q} = 11{,}000$, to provide some idea of the possible range of behavior of trajectories at this resonance. Figure 10 shows the orbital eccentricity variations of Miranda for the three trajectories, displayed in the same format as Fig. 8c. For each case, the variations of eccentricity are extremely irregular, with the trajectory in Fig. 10a reaching a maximum value of about 0.05. Upon escape from the resonance, Miranda may have a relatively large orbital eccentricity (Fig. 10b), or a value comparable to the value before the resonance was encountered (Fig. 10a). The mechanism by which trajectories enter the large chaotic zone appears to depend on the behavior during passage through the chaotic zone associated with the inclination resonances. For example, in Fig. 10a, the eccentricity varies chaotically between $10.5 < \delta < 11.4$, but leaves the chaotic zone with a relatively low value. It then becomes temporarily trapped in the $e_M e_U$ resonance between $11.5 < \delta < 12.3$, exhibiting behavior similar to what is seen in the planar-eccentric model. The trajectory displayed in Fig. 10b shows a similar temporary capture phase. However, the trajectories displayed in Figs. 10c and 8c do not show the temporary capture phase. There appear to be other mechanisms for entering the chaotic zones in these cases. For each of the trajectories displayed in Fig. 10, the orbital inclination of Miranda remains large during evolution through the chaotic zones, and the variations in the orbital elements of Umbriel are relatively small.

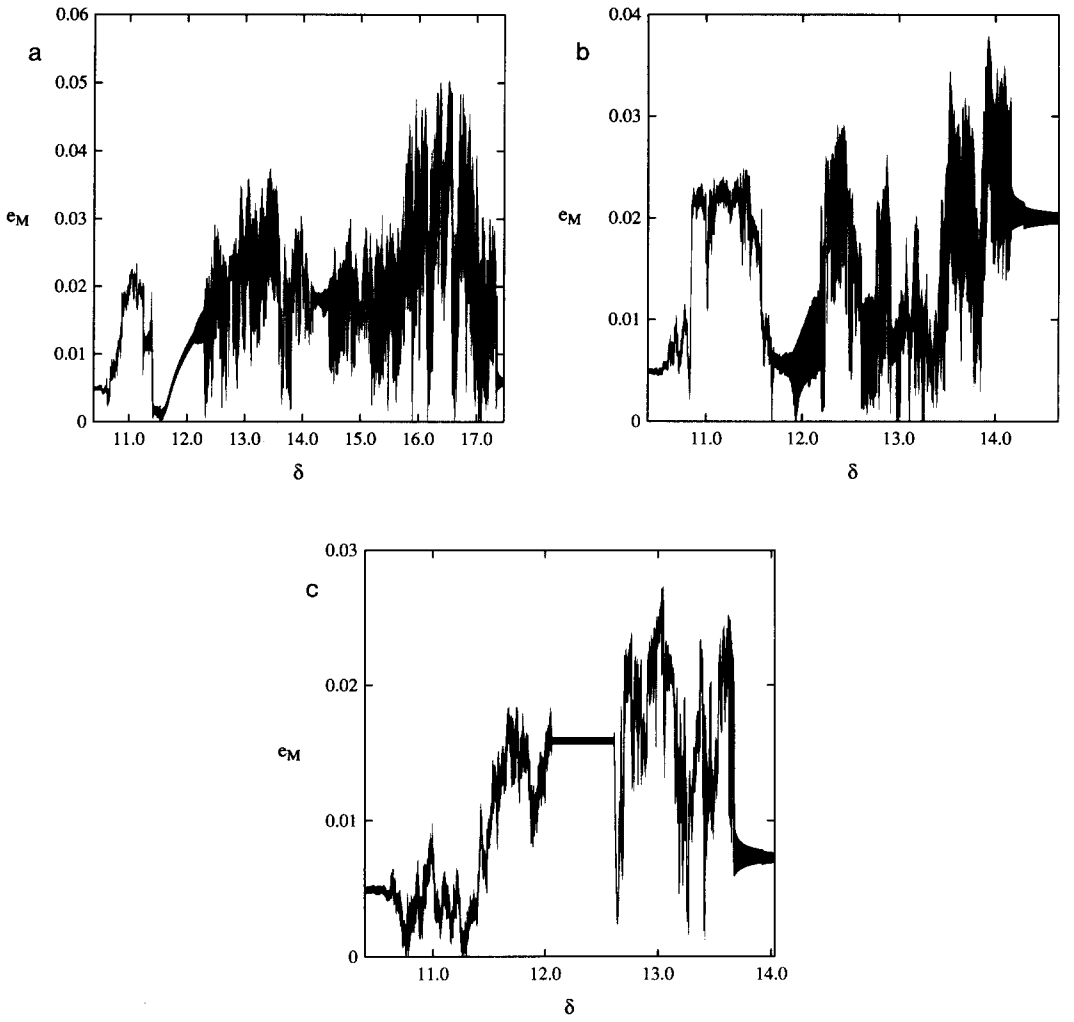

FIG. 10. Eccentricity variations of Miranda for three trajectories evolved through the 3 : 1 Miranda–Umbriel eccentricity resonances with i_M having a high initial value ($\mathcal{Q}$ = 11,000). The maximum and minimum values are plotted in intervals of $\Delta\delta$ = 0.0033. As in Fig. 8, the orbital eccentricity of Miranda varies extremely irregularly within the chaotic zone.

2.1.3. *Secular Perturbations*

Figure 11 shows an example of the evolution of the orbital eccentricity of Miranda during evolution through the 3 : 1 mean-motion commensurability with Umbriel, including secular perturbations due to Ariel, with $\dot{a}_M/a_M = 6 \times 10^{-13}$ per orbit period. The initial orbital parameters for this trajectory were $a_M = 4.8631$, $a_A = 7.0846$, $a_U = 10.1179$, $e_M = e_A = e_U = 0.005$, $\phi = 0$, $\tilde{\omega}_M = 0$, $\tilde{\omega}_A = -\pi/2$, and $\tilde{\omega}_U = \pi/2$. In Fig. 11, the maximum and minimum eccentricities are plotted in the intervals of $\Delta\delta$ = 0.0033, with the resulting envelope shaded to better display the variations. The behavior of e_M is qualitatively similar to that in the planar-eccentric case, with the average value increasing during evolution through the chaotic zone. The orbital eccentricities of both other satellites vary chaotically, but these variations are relatively small. However, as

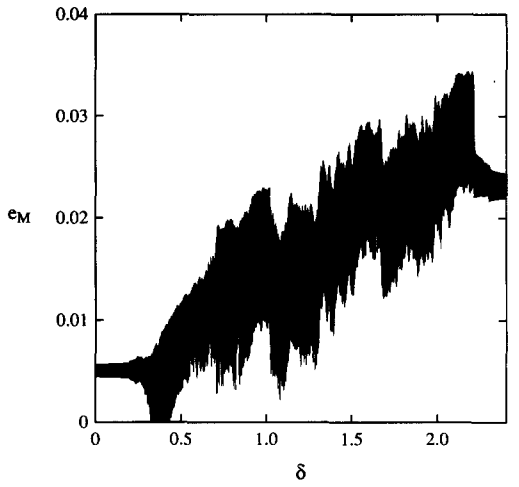

FIG. 11. Eccentricity variations of Miranda for a trajectory evolved through the 3:1 Miranda–Umbriel eccentricity resonances, perturbed by the secular variations of Ariel. The maximum and minimum eccentricities are plotted in intervals of $\Delta\delta = 0.0033$. The eccentricity variations are more irregular than in the unperturbed case.

in the eccentric-inclined model, the maximum and minimum boundaries of the chaotic zone are not well defined, indicating that there is no chaotic adiabatic invariant. This has been verified by integrating a trajectory through the chaotic zone with $\dot{a}_M/a_M = 6 \times 10^{-14}$ per orbit period ($\mathcal{Q} = 11{,}000$). The initial coordinates were those of the trajectory displayed in Fig. 11 at $\delta = 1.374$. For this trajectory, the maximum and minimum eccentricity envelopes were very irregular.

2.2. The Miranda–Ariel 5:3 Commensurability

2.2.1. The Planar-Eccentric Model

At this resonance, the mean motion of Ariel decreases more rapidly than that of Miranda. The time rate of change of $\delta = 5n_A - 3n_M - \dot{\tilde{\omega}}_M - \dot{\tilde{\omega}}_A$ (see Appendix I) is approximated by

$$\dot{\delta} \approx -0.492(5\dot{n}_A) \approx -0.492\frac{15}{2}n_A\frac{\dot{a}_A}{a_A}. \quad (3)$$

Because a_M/a_A is decreasing, there is not an equilibrium eccentricity configuration for this resonance in the single-resonance approximation (see also Peale 1988).

The initial coordinates of the trajectories to be numerically evolved through the commensurability were determined from an initial state with the following orbital parameters: $a_M = 4.6361$, $a_A = 6.5110$, $e_M = 0.005$, $e_A = 0.005$, $\sigma_M = 90°$, and $\sigma_A = 90°$. From this initial state, the 19 other states in the ensemble were determined by integrating the equations of motion forward in time with the mapping without tidal dissipation, spacing successive states 66 mapping iterations ($\Omega = 40.0$ year^{-1}, $\Delta t = 66 \times 2\pi/\Omega = 10.4$ years). Each of these initial states was then integrated forward in time with tidal dissipation included.

Ensembles of 20 trajectories were evolved through the resonance at different simulated rates of tidal evolution, to determine the effect of the simulated rate of tidal evolution on the dynamics. Figure 12 shows the results of this study of the effect of the rate of tidal evolution on the dynamics. Plotted are the averages of the maximum orbital eccentricities in the chaotic zone as a function of the rate expressed in terms of $\mathcal{Q}$. There is a dependence of the maximum eccentricity of Miranda on $\mathcal{Q}$ for $\mathcal{Q} < 11$ ($\dot{a}_A/a_A \approx 2.4 \times 10^{-10}$ per orbit period); for slower dissipation rates (larger $\mathcal{Q}$), the dynamics in the chaotic zone appear to become independent of the rate of evolution. Therefore, the trajectory explores the chaotic region well on time scales much shorter than the evolution time scale, and there appears to be a chaotic adiabatic invariant for $\mathcal{Q} > 11$.

At this resonance, the single-resonance adiabatic criterion is insufficient to determine where the dynamics become independent of the simulated rate of tidal evolution. Because the orbit of Ariel is evolving outward more rapidly than that of Miranda, the first eccentricity resonance to be encountered is the e_M^2 resonance. We compute $(\Delta\omega_L/\omega_L)$ for this resonance. The libration

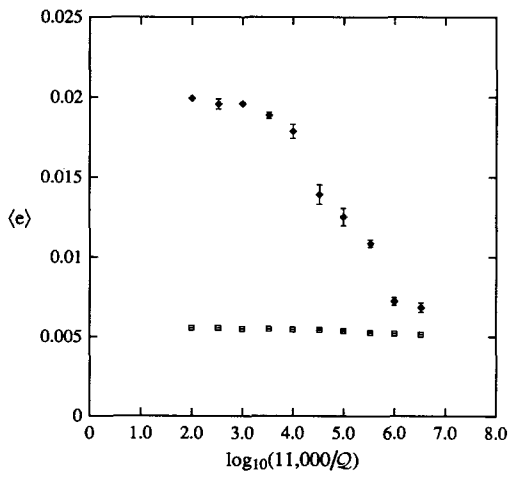

FIG. 12. Maximum eccentricities of Miranda (◆) and Ariel (□) in the chaotic zone of the 5 : 3 commensurability, related to the rate of tidal evolution expressed in terms of the effective specific dissipation function of Uranus $\mathcal{Q}$. For $\mathcal{Q} > 10$, trajectories explore the full extent of the chaotic region before escaping from the resonance; for higher rates, the dynamics are not well represented. The single-resonance adiabatic rate for the e_M^2 resonance is denoted by the vertical bar ($\mathcal{Q} = 0.0063$, $\dot{a}_A/a_A \approx 4 \times 10^{-7}$ per orbit period). For simulated tidal evolution rates larger than this, the trajectories are dragged through the resonance without displaying any interesting behavior. Note that the dynamics are sensitive to the rate for rates more than three orders of magnitude slower than this. Clearly, the single-resonance adiabatic criterion is not sufficient for the planar-eccentric case.

frequency of this resonance is given by

$$\omega_L^2 = -4F(\delta - \delta_0) \qquad (4)$$

where $\delta_0 = 2(C - D) - 16B\Sigma_U$. The change in the libration frequency of the (e_M^2) resonance in one libration period due to tidal evolution of the orbits is $\Delta\omega_L \simeq -4\pi F\dot{\delta}/\omega_L^2$, where $\dot{\delta} \approx -1.8 \times 10^{-3}/\mathcal{Q}$ in our units, at low eccentrities. For $e_M = e_U = 0.005$ well before the resonance is encountered, $\delta_0 = 7.03$. When the resonance is encountered at $\delta = 8.46$, $\Delta\omega_L/\omega_L \approx -0.0063/\mathcal{Q}$. In the single-resonance approximation, dynamical artifacts should appear if $\mathcal{Q} < 0.0063$, or $\dot{a}_A/a_A \approx 4 \times 10^{-7}$ per orbit period. The single-resonance adiabatic rate is denoted by the vertical bar in the upper right of Fig. 12. However, Fig. 12 reveals that the chaotic zone is not fully explored in the tidal evolution time scale until the simulated rate of evolution is approximately *three orders of magnitude* slower than the criterion based on the single-resonance approximation.

Figure 13 shows the evolution of this same ensemble of trajectories in δ, ΔE parameter space at a simulated tidal evolution rate of $\dot{a}_A/a_A = 2.4 \times 10^{-11}$ per orbit period ($\mathcal{Q} = 110$). ΔE is defined as

$$\Delta E = \varepsilon - E_2 \qquad (5)$$

where ε is the energy of the Hamiltonian, and

$$E_2 = \begin{cases} 0, & \delta < -2(C - D) + 4F \\ -(\delta + 2(C - D) - 4F)^2/64B, & \\ & \delta \geq -2(C - D) + 4F \end{cases} \qquad (6)$$

(see TW-I). If the Hamiltonian is equal to $E_2(\Delta E = 0)$, the quartic equation that deter-

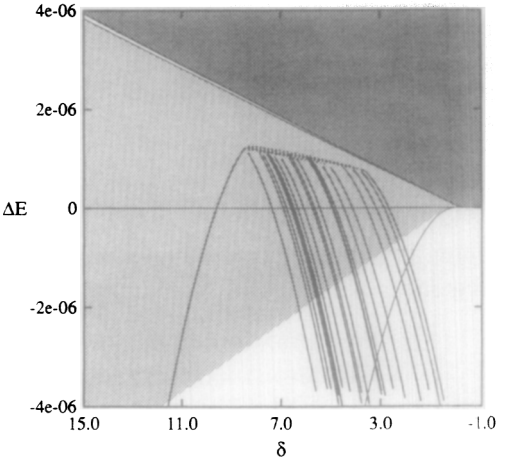

FIG. 13. Twenty trajectories in δ, ΔE space with $\mathcal{Q} = 110$. The mean initial eccentricities of the orbits are $e_M = 0.0045$ and $e_A = 0.0050$. Solid lines indicate quasiperiodic behavior; dashed lines indicate chaotic behavior. Evolution of the energy during the chaotic phase of evolution is quite regular, indicating the existence of a chaotic adiabatic invariant. Trajectories escape from the resonance via the chaotic zone at irregular intervals, evolving to large negative ΔE.

mines initial conditions on the surface of section has no solutions at zero eccentricity on the section. If the Hamiltonian is greater than $E_2(\Delta E > 0)$, there is a finite area on the surface of section near the origin in which the quartic equation has no solutions. Within this area, points cannot be generated on the surface of section.

In Fig. 13, δ decreases with time, and trajectories evolve toward the right. Trajectories are excluded from the heavily shaded region in the upper right of the figure. The lightly shaded region represents the range of values of Hamiltonian and the parameter δ where large-scale chaos is present in the phase space. The extent of this region was numerically determined using surfaces of section. The surfaces of section used for this purpose plot x_M versus y_M when $x_A = 0$. For different values of ΔE and δ, the initial conditions of 20 trajectories were determined, with initial coordinates equally spaced on the ordinate axis of the surface of section. For each trajectory, the rate of growth of distance between nearby trajectories (Lyapunov exponent) was evaluated. Where one or more trajectories indicate a positive Lyapunov exponent, large-scale chaotic behavior is present.

In the small unshaded region near the boundary of the excluded zone, the resonant arguments $\sigma_M = \frac{1}{2}(5\lambda_A - 3\lambda_M - 2\tilde{\omega}_M)$ and $\sigma_A = \frac{1}{2}(5\lambda_A - 3\lambda_M - 2\tilde{\omega}_A)$ must librate about $\pm\pi/2$, because of the shape of the energy surface boundary. This region disappears as δ decreases, indicating that permanent capture into quasiperiodic libration does not occur during passage through this commensurability via the capture mechanism described in TW-I. Tidal evolution drives trajectories into the unshaded region of parameter space in the lower right of this figure, where there is no known mechanism of capture into resonance. [Peale (1988) also concludes that capture into this resonance cannot occur, using arguments based on the available energy.]

The trajectories shown in Fig. 13 initially evolve to positive ΔE in a regular fashion, then enter a large chaotic zone. Solid lines indicate quasiperiodic behavior, and dashed lines indicate chaotic behavior in this figure. The evolution of the energies is also very regular during the chaotic phase, until the trajectory escapes to a quasiperiodic region of phase space and evolves to large negative ΔE. The regularity of the evolution of ΔE while the trajectories are chaotic is further evidence for the approximate conservation of a chaotic adiabatic invariant. There is not an obvious pattern to the escape process: trajectories "drop out" of the chaotic zone in a seemingly random manner.

Figure 14 shows the distribution of average orbital eccentricities of Miranda after escape from the resonance. For reference, the time-averaged initial value of about 0.0045 is shown by the vertical bar in the upper part of the figure. For most trajectories, the average orbital eccentricity of Miranda is higher than the value approaching the resonance, which is qualitatively in agreement with the predictions of the single-resonance theory. However, a few trajecto-

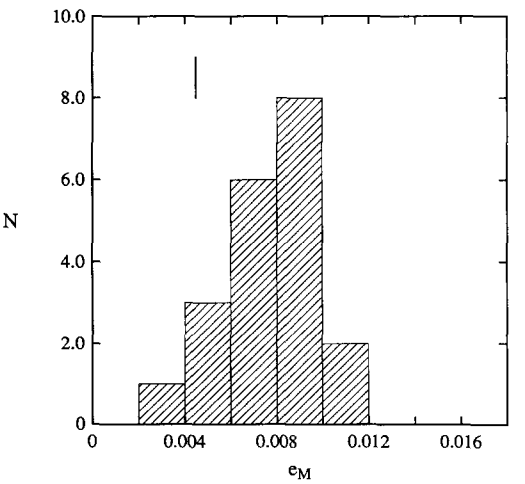

FIG. 14. Distribution of time-averaged orbital eccentricities of Miranda for the trajectories displayed in Fig. 13. The vertical bar at the top of the figure indicates the average eccentricity prior to resonance encounter. Most trajectories escape from the resonance with an average eccentricity larger than the initial value, but in a few cases the average eccentricity decreases during resonance passage.

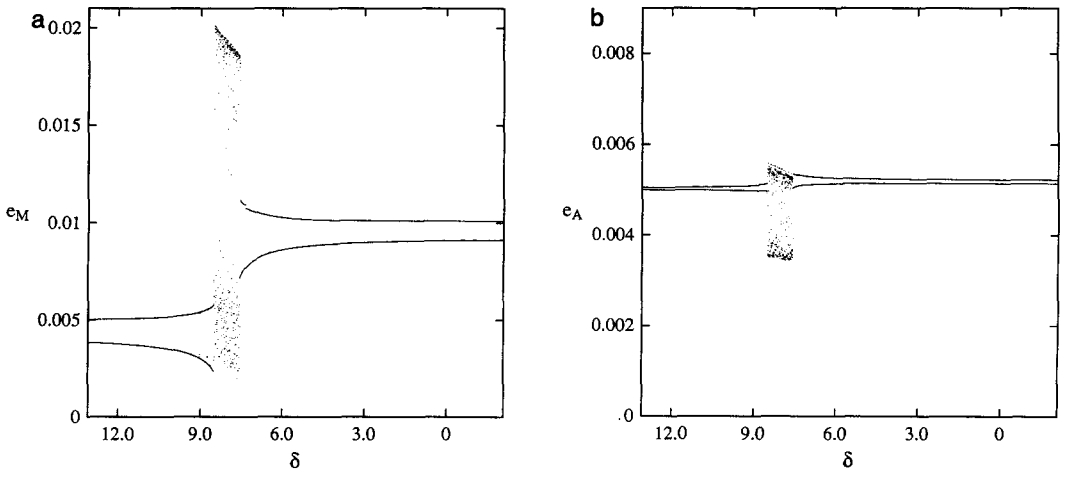

FIG. 15. Variations of the orbital eccentricities of Miranda (a) and Ariel (b) during evolution through the 5 : 3 mean-motion commensurability. $\dot{a}_A/a_A = 2.4 \times 10^{-11}$ per orbit period ($\mathfrak{Q} = 110$). The maximum and minimum values are plotted in intervals of $\Delta\delta = 0.005$. Upon entering the chaotic zone, the maximum orbital eccentricity of Miranda suddenly jumps to relatively high values. The final eccentricities of both orbits are larger than the initial values.

ries evolve to lower eccentricity, which cannot happen in the single-resonance theory. Also, the mean value of the time-averaged orbital eccentricities of Ariel decreases from about 0.005 prior to resonance encountered to about 0.0048 after escape, with a scatter of about 10% about this value.

There is a correlation between the orbital eccentricities upon escape from the resonance and the length of time spent in the chaotic zone. Figures 15 and 16 show the evolution of the orbital eccentricities of two different trajectories in this ensemble. In these figures, the maximum and minimum

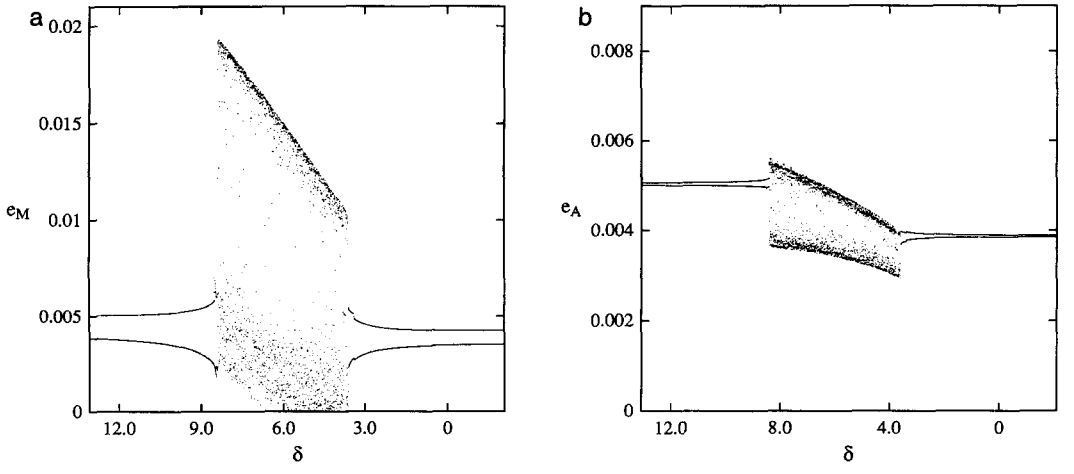

FIG. 16. Variations of the orbital eccentricities of Miranda (a) and Ariel (b) during evolution through the 5 : 3 mean-motion commensurability. $\dot{a}_A/a_A = 2.4 \times 10^{-11}$ per orbit period ($\mathfrak{Q} = 110$). The maximum and minimum values are plotted in intervals of $\Delta\delta = 0.005$. The final eccentricities are smaller than the initial values.

eccentricities in a small interval of δ ($\Delta\delta \approx 0.005$) are plotted versus δ. In each case, the eccentricity "envelopes" are smooth and well defined well before the resonance is encountered. The orbital eccentricities initially oscillate with amplitudes determined by the strength of the secular coupling. As the trajectories approach the resonance, the amplitude of oscillation increases. There may be a sudden small change in the oscillation amplitude, just before the large chaotic zone is entered, when the trajectory crosses a secondary commensurability (see below). When the trajectory enters the chaotic zone, the maximum orbital eccentricity of Miranda suddenly jumps to a value approximately four times the maximum prior to resonance encounter. The orbital eccentricity of Miranda varies irregularly between about 0.002 and 0.02. Meanwhile, the orbital eccentricity of Ariel also varies chaotically, but through a much smaller range. As the trajectories tidally evolve through the chaotic zone, the eccentricities continue to vary in an irregular manner, but within well-defined limits which both decrease as δ decreases. The presence of these well-defined "envelopes" further indicates that the trajectory fully explores the chaotic zone on time scales much shorter than the time scale of tidal evolution, and that therefore a chaotic adiabatic invariant is conserved.

Eventually, the trajectories escape from the resonance. The trajectory shown in Fig. 15, after only a short time in the chaotic zone, escapes with an average orbital eccentricity of Miranda approximately twice the value prior to resonance encounter. The orbital eccentricity of Ariel also increases a tiny amount. For a trajectory that spends a long time in the chaotic zone, such as the one shown in Fig. 16, the average eccentricities of both orbits are lower after escape from the resonance than before the resonance was encountered. In both cases, escape from the chaotic zone is accompanied by slight sudden changes in the oscillation amplitude of the eccentricities associated with passage through secondary resonances.

To better understand the qualitative features of the dynamics of resonance passage, we have studied the evolution of the trajectory shown in Fig. 16 using surfaces of section. The surfaces of section chosen for study plot y_M versus x_M when $x_A = 0$ (defined as section I) and y_A versus x_A when $x_M = 0$ (defined to be section II). The section condition $x_i = 0$ corresponds to 2 or 4 values of the conjugate y_i, due to the quartic nature of the Hamiltonian. These values of y_i are obtained numerically by solving a quartic equation, and are designated a–d in descending numerical order (see TW-I). For section I, there are two high-eccentricity quartic root "families" and two low-eccentricity root families. Unfortunately, to display all of the features of the phase space, it is necessary to plot surfaces of section corresponding to at least two of these root families, as was the case in the Ariel–Umbriel 5:3 resonance problem (TW-I). For section II, the phase space is even more complicated due to the appearance of an excluded region near the origin for $\Delta E > 0$. We have chosen here to display sections Ia and Ib. On these plots, e_M is the radial distance from the origin.

Figure 17 shows sections I just after the trajectory in Fig. 16 has entered the chaotic zone, at $\delta = 8.337$. The heavy solid curve enclosing each plot is the energy surface boundary, which constrains where points can be generated on the section. On both sections Ia and Ib there is a quasiperiodic zone near the origin and a large chaotic zone which extends to the energy surface boundary. The trajectory has entered the chaotic zone from the quasiperiodic zone on section Ib (Fig. 17b), and will eventually escape from the resonance into the quasiperiodic zone on section Ia (Fig. 17a). The chaotic zone acts as a bridge between these two regions. By studying this figure, it is possible to understand the origin of the sudden large jump in orbital eccentricity experienced by Miranda as it enters the chaotic zone. Prior

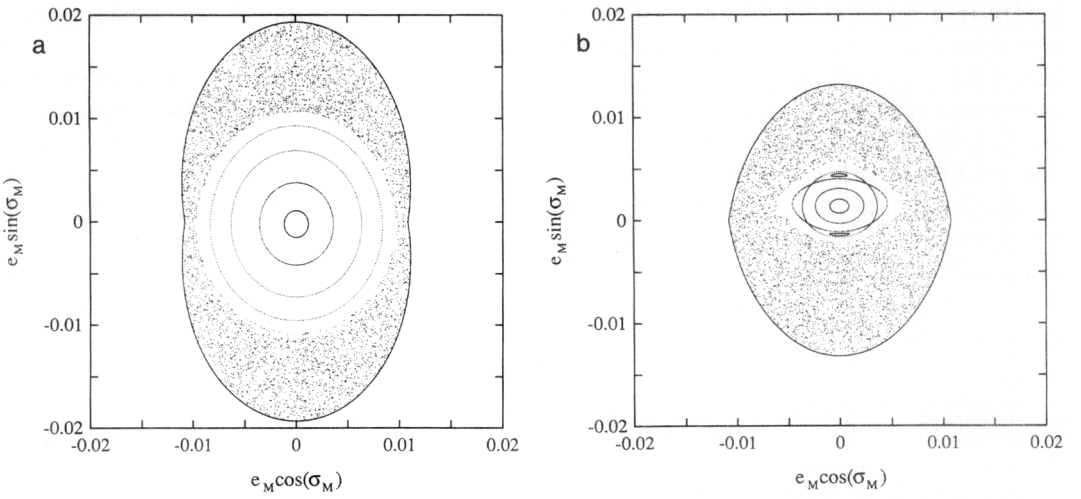

FIG. 17. Sections I showing the phase space available to the trajectory in Fig. 15 just after entering the chaotic zone, at $\delta = 8.337$. The chaotic zone extends from the edge of the quasiperiodic region on section I*b* (b) to the energy surface boundary on section I*a* (a), explaining the sudden jump in e_M when the chaotic zone is entered.

to resonance encounter, the trajectory is confined to the quasiperiodic region in Fig. 17b. The evolution in this region involves the secular interaction between the satellites, and the orbital eccentricity of Miranda never gets above about 0.005. When the trajectory enters the large chaotic zone, a much more extensive region of phase space is available to the trajectory, including the chaotic zone in Fig. 17a. The chaotic zone extends all the way out to the energy surface boundary, which constrains the extent of motion. On section Ia, the energy surface boundary extends to an orbital eccentricity of Miranda of about 0.02, about four times the maximum in the quasiperiodic zone before resonance encounter. In the chaotic zone, the orbital eccentricity varies irregularly between a value corresponding to the maximum extent of the energy surface boundary on Fig. 17a and a minimum value corresponding to the outer edge of the quasiperiodic region on Fig. 17b. Because the time scale of evolution within the chaotic zone is much shorter than the tidal evolution time scale, we see the sudden jump in the maximum orbital eccentricity of Miranda in Figs. 15 and 16. Clearly, to fully explore the chaotic zone, a tidally evolving trajectory must reach the maximum eccentricity in the chaotic zone as defined by the energy surface boundary of the surface of section. This explains the fact that the mean maximum eccentricity reached by trajectories levels off for slow simulated tidal evolution rates at a value corresponding to the maximum distance of the energy surface boundary from the origin on the phase plane (see Fig. 12).

Note that there is a chain of four islands associated with a secondary resonance visible in the quasiperiodic region in Fig. 17b. The appearance of this and other secondary resonances at the edge of the chaotic zone may result in the transfer of trajectories into the chaotic zone.

As a trajectory evolves through the commensurability, surfaces of section generated for the "frozen" Hamiltonian at successive points in the evolution qualitatively resemble Fig. 17, but occupy a smaller region of the phase plane, and the maximum extent of the chaotic zone decreases.

We have also studied the evolution of tra-

jectories with higher initial eccentricities ($e_M = e_A \approx 0.01$), and similar relative increases in the orbital eccentricity of Miranda have been found.

2.2.2. *The Eccentric-Inclined Model*

The tidal evolution parameter δ is defined to be the nonresonant contributions to $5n_A - 3n_M - \frac{1}{2}(\dot{\tilde{\omega}}_M + \dot{\tilde{\omega}}_A + \dot{\Omega}_M + \dot{\Omega}_A)$ (see Appendix I). Because both the orbital eccentricity and the inclination of Miranda are significantly affected by this resonance, it is expected, based on the results of Section 2, that higher-dimensional chaos may be important, and therefore the dynamical outcome is sensitive to the simulated rate of evolution. Therefore, we have used a simulated rate of tidal evolution corresponding to $\mathcal{Q} = 11{,}000$, within our constraints on the physical Q or Uranus. The initial orbital elements used in the numerical experiments are $a_M = 4.6361$, $a_A = 6.5110$, $e_M = e_A = 0.005$, $i_M = i_A = 0.005$ radian, $\sigma_M = \pi/2$, $\sigma_A = 3\pi/2$, $\psi_M = 3\pi/2$, and $\psi_A = \pi/2$. In

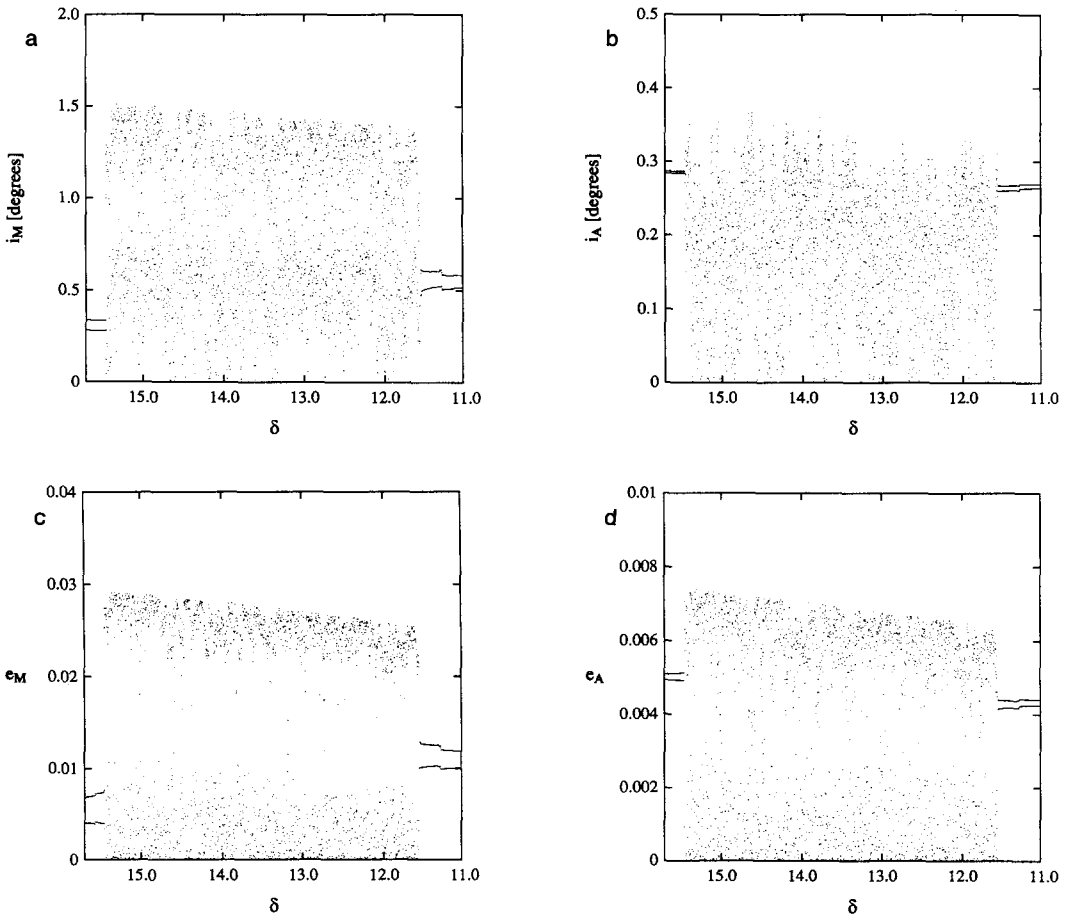

FIG. 18. Variations of the orbital inclinations (a, b) and eccentricities (c, d) of Miranda and Ariel. The rate of evolution is $\dot{a}_A/a_A = 2.4 \times 10^{-13}$ per orbit period ($\mathcal{Q} = 11{,}000$), within our constraints on the physical Q of Uranus. The maximum and minimum values are plotted in intervals of $\Delta\delta = 0.0033$. Both e_M and i_M suddenly jump to moderately large values upon encountering the large chaotic zone, and e_M reaches larger values than in the planar-eccentric approximation. Note that the limits of eccentricity and inclination appear to evolve in a fairly regular manner in the chaotic zone, in contrast with the Miranda–Umbriel 3 : 1 problem (see Figs. 8, 10).

Fig. 18, the maximum and minimum eccentricities and inclinations of Miranda and Ariel are displayed in intervals of $\Delta\delta = 0.0033$. When the trajectory enters the large chaotic zone, the variations in the orbital inclination and eccentricity of Miranda are significant. e_M reaches a maximum value of about 0.03, compared to a value of 0.02 reached in the planar-eccentric model for a comparable initial eccentricity. The inclination reaches a maximum value of about 1.5°. Note that at this simulated rate of tidal evolution, there appear to be relatively smooth "envelopes" of maximum and minimum eccentricity and inclination in the chaotic zone: perhaps there may be an adiabatic invariant for this model at sufficiently slow rates. It is interesting to note that the maximum orbital eccentricity reached by Miranda is only about a factor of 2 lower than the maximum reached at the 3 : 1 commensurability with Umbriel (see Fig. 9).

2.2.3. Secular Perturbations

To take into consideration the effects of other satellites on the Miranda–Ariel 5 : 3 resonance, we used a model that includes secular perturbations due to Umbriel. Figure 19 shows an example of the evolution of the orbital eccentricities of Miranda, Ariel, and Umbriel for a trajectory evolved through the resonance using this model with $\mathcal{Q} = 22$ ($\dot{a}_M/a_M = 1.2 \times 10^{-10}$ per orbit period). The initial orbital parameters for this trajectory were $a_M = 4.6394$, $a_A = 6.5157$, $a_U = 10.056$, $e_M = e_A = e_U = 0.005$, $\phi = 0$, and $\tilde{\omega}_M = \tilde{\omega}_A = \tilde{\omega}_U = -\pi/2$. Shown in the figure are the maximum and minimum eccentricities in intervals of $\Delta\delta = 0.005$. The evolution of Miranda's orbital eccentricity is not markedly different than in the planar-eccentric case involving only Miranda and Ariel: the maximum eccentricity jumps suddenly when the evolution becomes chaotic. There still appear to be well-defined limits to the chaotic variations in e_M as the satellites evolve through the resonance. The average orbital eccentricity after escape from the resonance is about a factor of 2 larger than the initial value. The changes in orbital eccentricity of both Ariel and Umbriel, though chaotic, are not significant.

2.3. The Ariel–Umbriel 2 : 1 Commensurability

2.3.1. The Planar-Eccentric Model

At this commensurability, the semimajor axis of Ariel is increasing much more rapidly than that of Umbriel. The rate at which $\delta = 4n_U - 2n_A - \dot{\tilde{\omega}}_A - \dot{\tilde{\omega}}_U$ increases due to planetary tides is given by (see Appendix II)

$$\dot{\delta} \approx -2\dot{n}_A \approx 3n_A \frac{\dot{a}_M}{a_M}. \tag{7}$$

For the Ariel–Umbriel 2 : 1 resonance, the equilibrium eccentricity of Ariel is approximately 0.02 (see Appendix II) if $Q = 11{,}000$ for Uranus and $Q = 100$ for Ariel.

To determine capture probabilities for this resonance, we numerically integrated six sets of 20 trajectories through the commensurability using the mapping, each with different eccentricities approaching the resonance. Orbital parameters used to calculate the initial states of the trajectories in each run are given in Table III. From the initial state in the table, 19 other initial conditions were computed by integrating the equations of motion forward in time using the mapping without tidal dissipation, with a time interval of 66 mapping iterations ($\Omega = 40.0$ year^{-1}, $\Delta t = 66 \times 2\pi/\Omega = 10.4$ years), yielding a set of trajectories with identical initial values of δ and the Hamiltonian, but with different angular phases. Each of the initial states in the run was then integrated forward in time with tidal dissipation included.

These numerical experiments were carried out using simulated rates of tidal evolution between $\dot{a}_A/a_A = 2.7 \times 10^{-5}$ per orbit period ($\mathcal{Q} = 0.00011$) and $\dot{a}_A/a_A = 2.7 \times 10^{-11}$ per orbit period ($\mathcal{Q} = 110$). At rates slower than about $\dot{a}_A/a_A = 2.7 \times 10^{-7}$ per orbit period ($\mathcal{Q} = 0.011$), all trajectories in runs 1–4 were captured into resonance. Only trajectories from runs 5 and 6 had mea-

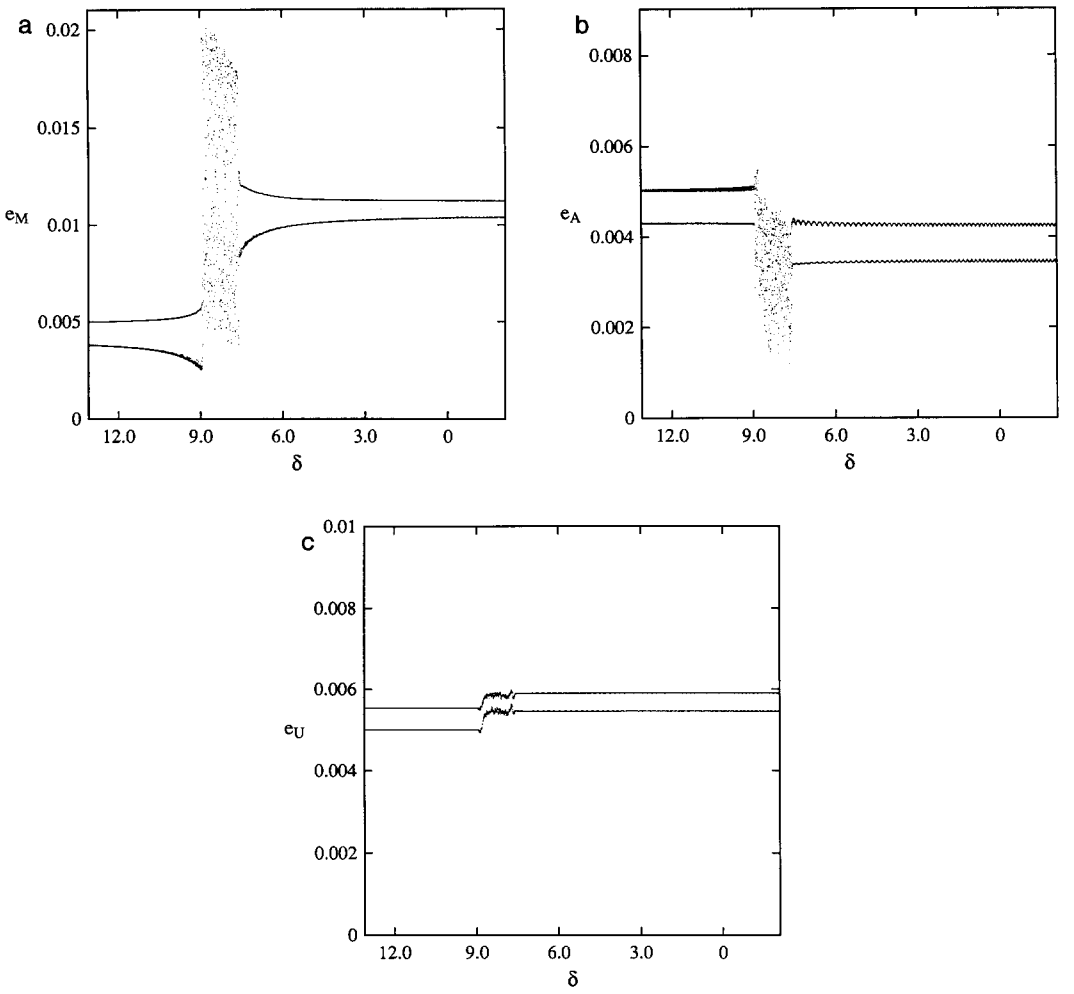

FIG. 19. Variations of the orbital eccentricities of Miranda (a), Ariel (b), and Umbriel (c) during evolution through the Miranda–Ariel 5 : 3 mean-motion commensurability. The maximum and minimum values are plotted in intervals of $\Delta\delta = 0.005$. The orbital elements of all three satellites vary chaotically.

surable probabilities of escape at slow tidal rates ($\mathfrak{Q} = 110$).

This indicates that the probability of escape from the Ariel–Umbriel 2 : 1 resonance is very small if the orbital eccentricities are smaller than about 0.03, much larger than the current values. The capture mechanism for trajectories with low initial eccentricities is very robust: the rate at which artifacts appear is two to three orders of magnitude larger than the rates at which artifacts appeared in the dynamics of the previously considered resonances. This appears to be partly a consequence of the fact that at eccentricities comparable to the current values, the evolution is dominated by quasiperiodic behavior, and trajectories do not cross separatrices associated with the primary mean-motion resonances. Rather, capture occurs via evolution of the energy surface on which a trajectory evolves (see below), analogous to the capture mechanism at the Ariel–Umbriel 5 : 3 resonance (TW-I). The region of escape does not appear until eccentricities are much higher.

Figure 20 is a plot of the maximum and

TABLE III

ARIEL–UMBRIEL 2:1 COMMENSURABILITY: INITIAL PARAMETERS

Run	ΔE	δ	a_A a_U	e_A e_U	σ_A σ_U	x_A x_U	y_A y_U	n
1	-7.7095×10^{-5}	-7.8351	6.3100 10.0400	0.005 0.005	90.0 90.0	0.0 0.0	4.1764×10^{-3} 4.5651×10^{-3}	20
2	-2.7344×10^{-4}	-6.3464	6.3100 10.0400	0.01 0.01	90.0 270.0	0.0 0.0	8.3527×10^{-3} -9.1302×10^{-3}	20
3	-7.3931×10^{-4}	-6.5488	6.3050 10.0400	0.015 0.015	90.0 270.0	0.0 0.0	1.2529×10^{-2} -1.3695×10^{-2}	20
4	-1.4568×10^{-3}	-5.7580	6.3000 10.0400	0.02 0.02	90.0 270.0	0.0 0.0	1.6705×10^{-2} -1.8260×10^{-2}	20
5	-1.0299×10^{-3}	7.1446	6.3055 10.0400	0.03 0.03	90.0 270.0	0.0 0.0	2.5058×10^{-2} -2.7391×10^{-2}	20
6	-9.2686×10^{-4}	21.2018	6.3057 10.0400	0.04 0.04	90.0 270.0	0.0 0.0	3.3411×10^{-2} -3.6521×10^{-2}	20

minimum orbital eccentricities of Ariel and Umbriel in intervals of $\Delta\delta = 0.008$ for a trajectory in run 1, with a simulated tidal evolution rate corresponding to $\mathfrak{Q} = 110$. Both orbits are captured into resonance without displaying significant chaotic behavior. However, there are sudden changes in the amplitudes of oscillation of the eccentricities, for example, at values of δ of about 0.6, 2.7, 4.7, and 7.5. The orbital eccentricity of Ariel reaches its equilibrium value (0.02) without disruption of the resonance.

To understand this complicated behavior, we have computed surfaces of section for the frozen Hamiltonian at various values of δ. The section conditions chosen for study

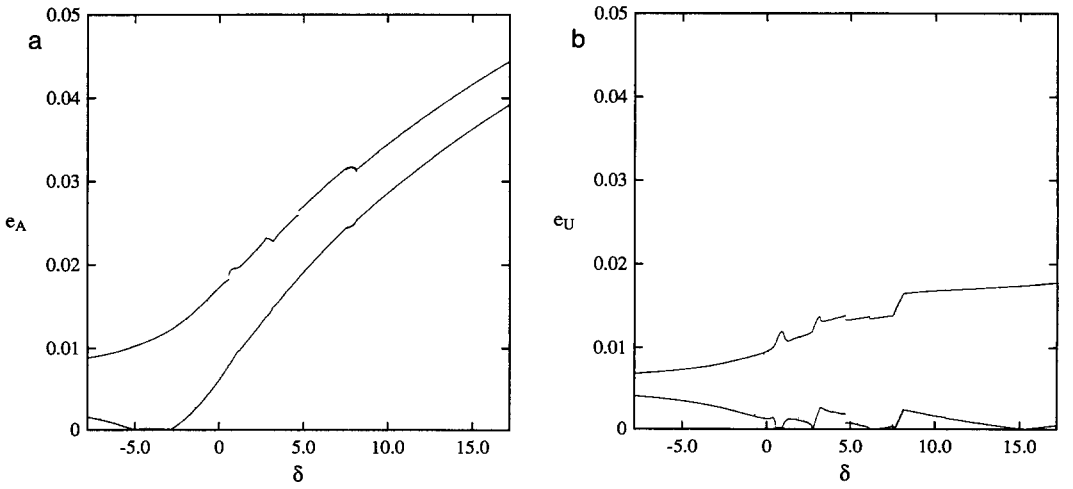

FIG. 20. Orbital eccentricity variations of Ariel (a) and Umbriel (b) of a trajectory from run 1 during evolution through the 2:1 commensurability. Shown are the maximum and minimum eccentricities in intervals of $\Delta\delta = 0.008$. The evolution is primarily quasiperiodic, but with modulations of the oscillation amplitudes of e_A and e_U due to secondary resonances. The trajectory attains the equilibrium eccentricity $e_A = 0.02$ without escaping from the resonance.

are plotting y_A versus x_A when $y_U = 0$, defined to be section I, and plotting y_U versus x_U when $y_A = 0$, defined to be section II. As with the second-order resonant models, initial conditions on the surface of section are determined by solving a quartic equation. Only one quartic root (the one with the lowest value) need be plotted to show the important features of the phase space.

Figure 21 shows section II at $\delta = 2.786$, during one of the aforementioned jumps in the oscillation amplitude of the eccentricity. In this plot, the orbital eccentricity of Umbriel is the radial distance from the origin; the value of the resonant argument $\sigma_U = \frac{1}{2}(2\lambda_U - \lambda_A - \tilde{\omega}_U)$ is measured counterclockwise from the positive abscissa. The heavy solid curve is the energy surface boundary of the surface of section: points generated on the section according to the above criteria are constrained to lie within this boundary. At this point in its evolution, the trajectory displayed in Fig. 21 generates points that form the three quasiperiodic loops in the chain of three resonant islands shown on the figure. Points generated by neighboring trajectories have also been plotted to display the structure of the phase space. Most of the points appear to lie on curves: quasiperiodic behavior dominates the evolution. The trajectory displayed in Fig. 21 has been temporarily captured into a secondary resonance, which is why it occupies the chain of islands. The chaotic separatrix associated with the secondary resonance is also displayed; however, it occupies only a small region of the displayed phase space. During evolution within the secondary resonance, the orbital eccentricity of Umbriel increases slightly. However, evolution within the secondary resonance does not lead to escape from the resonance: the trajectory does not cross a chaotic separatrix associated with the primary resonance. Capture into resonance for low eccentricities occurs via a mechanism analogous to the mechanism found at the Ariel–Umbriel 5:3 resonance (see TW-I): evolution of the energy surface boundary on the surface of section constrains the resonant argument to librate. In Fig. 21, the energy surface boundary still encloses the origin, which means that some trajectories pass through all values of σ_U. However, note that the center of the region of motion is offset from the origin. Eventually, the energy surface boundary no longer encloses the origin, and for all trajectories, σ_U librates about π on the surface of section and in the full phase space.

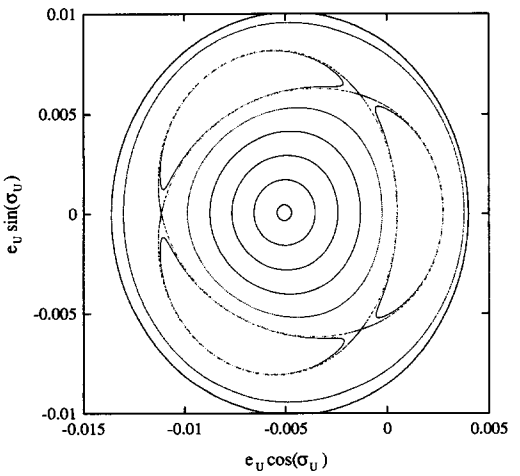

FIG. 21. Section II at $\delta = 3.769$. The trajectory in Fig. 20 generates the three resonant islands. Quasiperiodic behavior dominates the phase space.

For large initial eccentricities, chaotic behavior becomes more important, and the evolution is more complicated. The secondary resonant zones widen and eventually overlap, resulting in a large chaotic sea. At sufficiently large initial eccentricities, the chaotic zones associated with the primary resonances also appear. The initial eccentricities must be quite large, of order 0.03, for the probability of escape from the resonance to become significant. Interestingly, the eccentricity required for escape in our model is similar to the eccentricity below which capture is certain in the single-resonance model (see Peale 1988), even though the behavior is qualitatively quite different when the resonance is encountered at such large values of eccentricity.

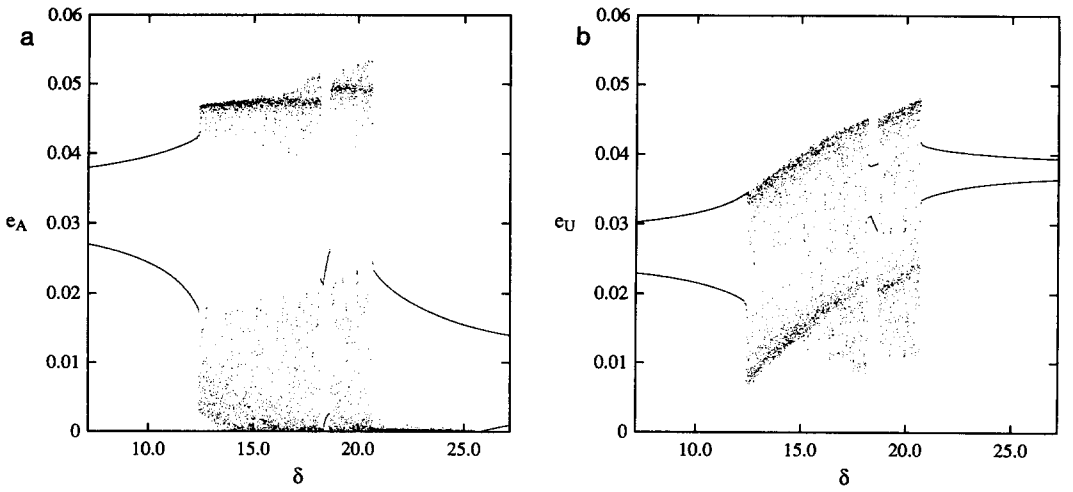

FIG. 22. Orbital eccentricity variations of Ariel (a) and Umbriel (b) during evolution through the 2 : 1 commensurability for a trajectory from run 5. Shown are the maximum and minimum eccentricities in intervals of $\Delta\delta = 0.0066$. The trajectory is chaotic for a significant interval of time during evolution through the resonance, then escapes from the resonance, with $e_U > e_A$.

Figure 22 shows the evolution of the orbital eccentricities for a trajectory from run 5 that escapes from the 2 : 1 commensurability. The maximum and minimum orbital eccentricities of Ariel (Fig. 22a) and Umbriel (Fig. 22b) are plotted in intervals of $\Delta\delta = 0.0066$. Well before the resonance is encountered the evolution is quasiperiodic and dominated by the secular interaction among the satellites. At $\delta \approx 12.3$, the system enters a large chaotic zone, which dominates the evolution until the satellites escape from the resonance at $\delta \approx 20.7$.

Figure 23 shows section II at $\delta = 20.64$, just before the trajectory escapes from the resonance. This picture looks quite different from the surfaces of section for lower initial eccentricities (Fig. 21). At this point in the evolution, the trajectory displayed in Fig. 22 is still in the large chaotic zone, which occupies most of the phase space in the figure. The small crescent-shaped quasiperiodic region to the right of the origin of the figure is the region into which trajectories escape from the resonance. Note that this is well away from the origin: hence, the orbital eccentricity of Umbriel is relatively high upon escape from the resonance (see Fig. 22b). The oval quasiperiodic region near the origin of the figure is a region into which trajectories may escape from the e_U reso-

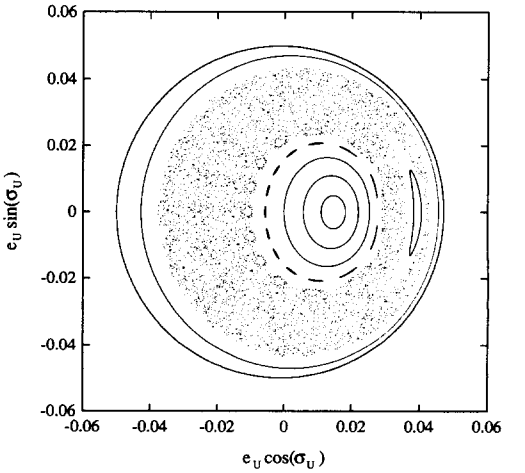

FIG. 23. Section II at $\delta = 20.640$. The trajectory displayed in Fig. 22 is still in the large chaotic zone. Trajectories may escape from the resonance into the small crescent-shaped quasiperiodic region at the right of center. The quasiperiodic region near the origin is associated with capture into the e_A resonance only.

nance, but are captured into the e_A resonance.

2.3.2. *The Eccentric-Inclined Model*

At the Ariel–Umbriel 2:1 mean-motion commensurability, there are two first-order eccentricity resonances, three second-order eccentricity resonances, three second-order inclination resonances, and second-order secular interactions, and the eccentricities are coupled to the inclinations through nonlinear terms. δ is defined to be the nonresonant contributions to $4n_U - 2n_A - \frac{1}{2}(\dot{\bar{\omega}}_A + \dot{\bar{\omega}}_U + \dot{\Omega}_A + \dot{\Omega}_U)$.

Figure 24 displays the evolution of the orbital eccentricities and inclinations of Ariel and Umbriel during evolution through the resonance with $\mathcal{Q} = 11{,}000$ ($\dot{a}_A/a_A =$

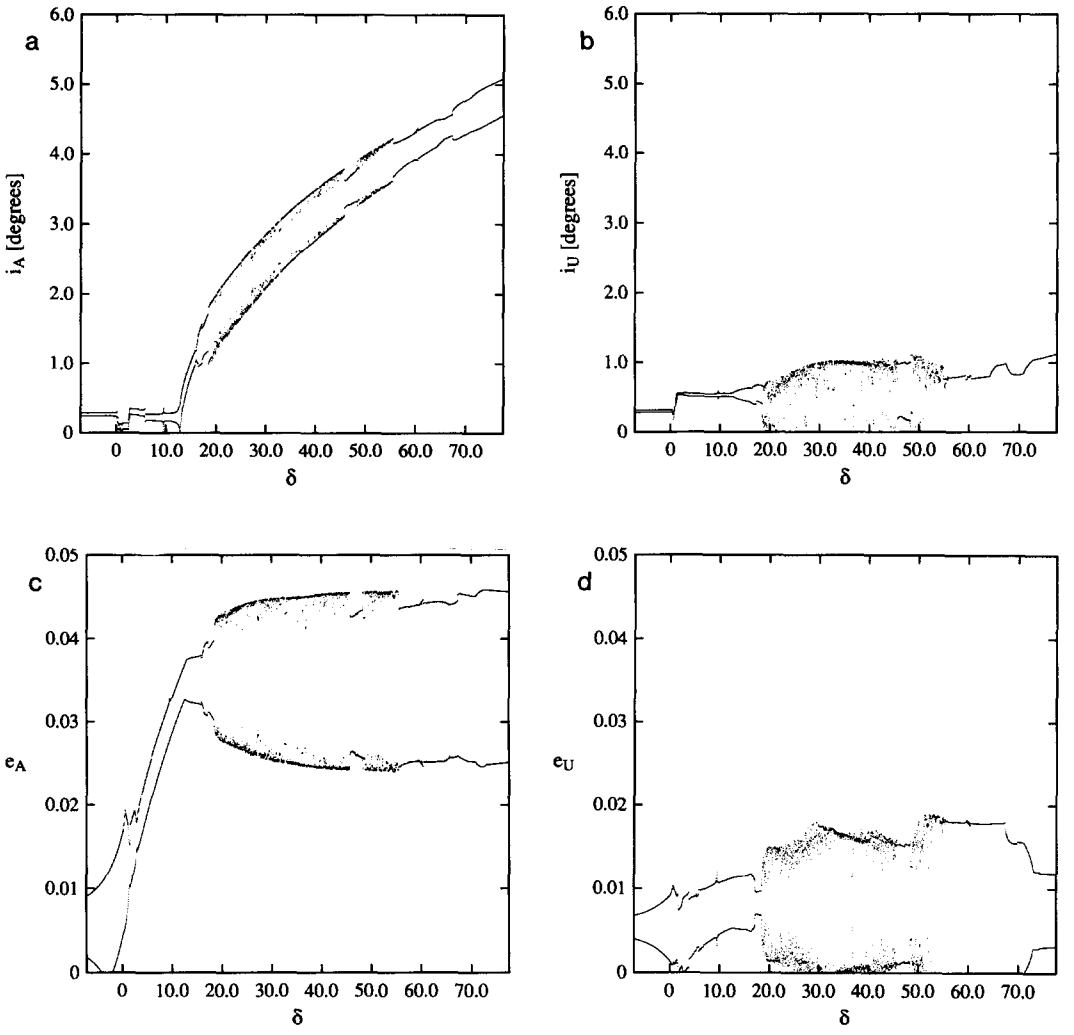

FIG. 24. Variations in orbital inclination [Ariel (a), Umbriel (b)] and eccentricity [Ariel (c), Umbriel (d)] for a trajectory integrated through the 2:1 commensurability using the mapping with $\mathcal{Q} = 11{,}000$. The maximum and minimum values are plotted in intervals of $\Delta\delta = 0.033$. The qualitative behavior is initially similar to the planar-eccentric problem, but at $\delta = 12.6$ the system is captured into the i_A^2 resonance. A period of chaotic behavior at large values of e_A and i_A does not lead to escape from the resonance.

2.7×10^{-13} per orbit period). The initial orbital parameters for this trajectory were $a_A = 6.3100$, $a_U = 10.0400$, $e_A = e_U = 0.005$, $i_A = i_U = 0.005$ radian, $\sigma_A = \sigma_U = \pi/2$, and $\psi_A = \psi_U = \pi/2$. The mapping was used, with $\Omega = 40$ year^{-1}. Maximum and minimum eccentricities are plotted in intervals of $\Delta\delta = 0.033$.

The evolution through the resonance is qualitatively similar to that in the planar-eccentric approximation with similar initial eccentricities (run 1, see Fig. 20), until $\delta = 13.7$. At this point, the trajectory is captured into the i_A^2 resonance. As i_A increases, e_A and e_U maintain constant average values. Eventually, the system becomes chaotic at $i_A \approx 1.3°$. However, this does not lead to escape from the 2 : 1 resonance. Eventually the trajectory becomes quasiperiodic again, remaining captured in the resonance.

Thirteen other trajectories, generated from the above orbital elements, were integrated through the resonance, using a simulated tidal evolution rate corresponding to $\mathfrak{Q} = 110$. All of the trajectories displayed qualitative behavior similar to that displayed in Fig. 20, and all were captured into resonance.

The numerical results indicate that for low initial eccentricities, the interaction between the inclination and eccentricity resonances does not lead to a significantly enhanced probability of escape. Because the inclination resonances are not encountered until after Ariel reaches its equilibrium eccentricity, these interactions would probably never be important. Furthermore, even if the high-inclination chaotic zone were to lead to escape, it would most likely leave Ariel with a substantial orbital inclination, which we do not observe today.

2.3.3. Secular Perturbations

To take into consideration the effects of other satellites on the Ariel–Umbriel 2 : 1 resonance, we used a model that includes secular perturbations due to Titania. Figure 25 shows the evolution of the orbital eccentricities of Ariel, Umbriel, and Titania for a trajectory evolved through the resonance using this model with $\mathfrak{Q} = 220$ ($\dot{a}_A/a_A = 1.4 \times 10^{-11}$ per orbit period). The initial orbital parameters for this trajectory were $a_A = 6.3100$, $a_U = 10.0400$, $a_T = 16.633$, $e_A = e_U = e_T = 0.005$, $\phi = 0.0$, and $\tilde{\omega}_A = \tilde{\omega}_U = \tilde{\omega}_T = -\pi/2$. The maximum and minimum eccentricities are plotted in intervals of $\Delta\delta = 0.01$. The presence of Titania does not affect the evolution much: both resonant arguments are captured into libration. As the trajectory evolves, it encounters various secondary resonances which only change the oscillation amplitudes of the eccentricities. The chaotic zones at these secondary resonances are perhaps somewhat larger than in the two-satellite problem with similar initial eccentricities (run 1), as can be seen from the burst of chaotic behavior in the orbital eccentricities at δ just greater than zero. However, the qualitative behavior of the trajectories does not change much: e_A reaches the equilibrium value without escaping from the resonance. Two other trajectories, with similar initial conditions, and simulated rates of tidal evolution corresponding to $\mathfrak{Q} = 110$, showed similar qualitative behavior.

We have also explored the small chaotic zone, at δ just above zero, using a simulated tidal evolution rate corresponding to $\mathfrak{Q} = 11{,}000$. The initial coordinates of the trajectory were taken from the trajectory displayed in Fig. 25 at $\delta = -0.0608$, and the trajectory was integrated to $\delta = 0.9392$. The trajectory did not escape from the resonance during the chaotic phase of evolution, and eventually became quasiperiodic again.

3. DISCUSSION

At the 3 : 1 commensurability with Umbriel, both the orbital inclination and eccentricity of Miranda undergo large increases. Miranda escapes from the commensurability with a high inclination which is observed today, as we found in TW-II in the circular-inclined approximation.

Miranda displays many features that indicate that it has been strongly heated at some

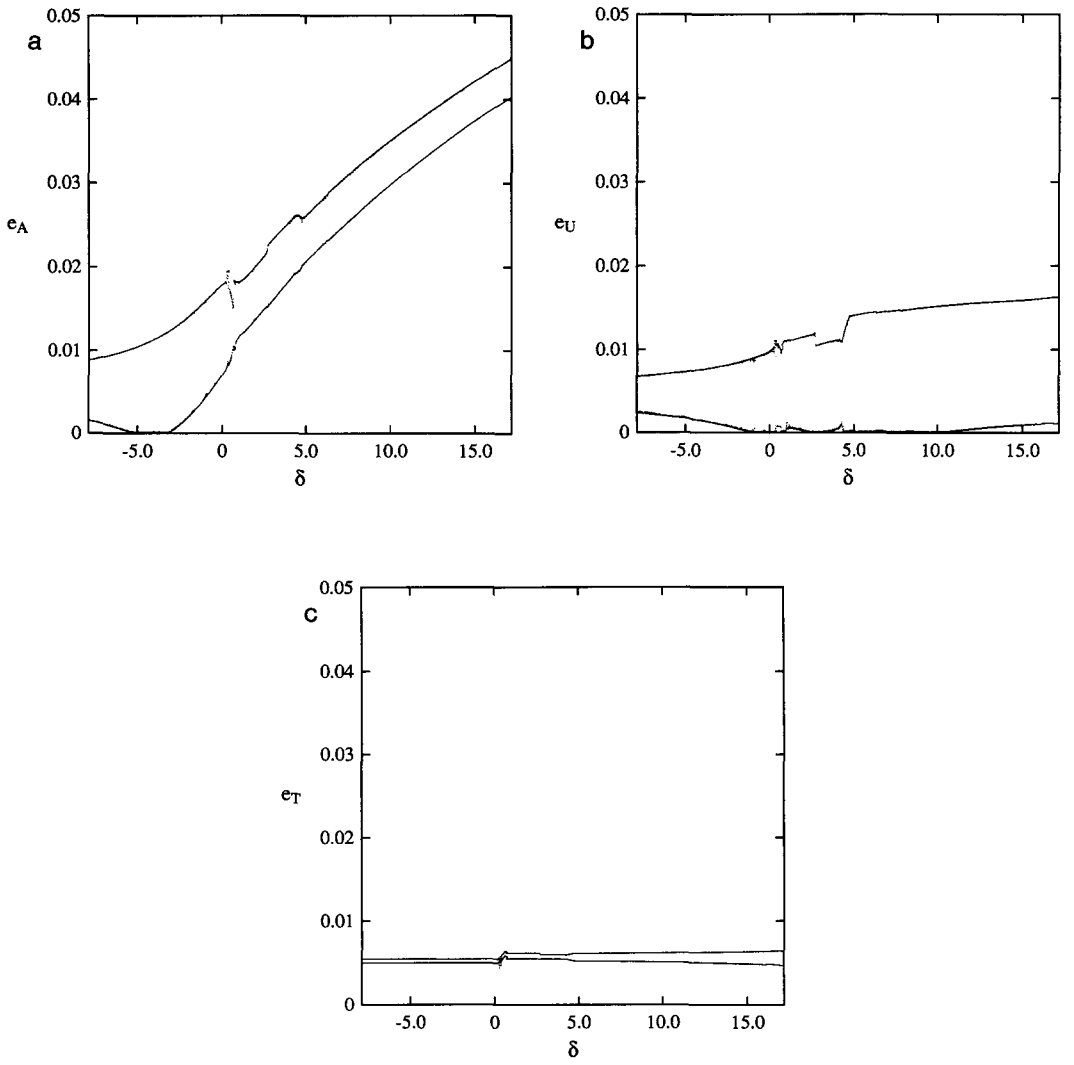

FIG. 25. Orbital eccentricity variations of Ariel (a), Umbriel (b), and Titania (c). The maximum and minimum eccentricities in intervals of $\Delta\delta = 0.01$ are plotted. The trajectory does not escape from the resonance before e_A reaches its equilibrium value.

point in its evolution. The surface of Miranda is very complex (Smith *et al.* 1986). In addition to cratered terrain on the surface, there are regions referred to as "trapezoids," "banded ovoids," and "ridged ovoids" by Smith *et al.* (1986), and named "coronae" by Strobell and Masursky (1987). There are possibly solid-state volcanic flow features on the surface (Jankowski and Squyres 1988).The cratered terrain appears to be the youngest in the Uranian satellite system (Plescia 1988). Could tidal heating of Miranda during passage through the 3 : 1 resonance have driven the processes that altered the surface of this satellite?

We can estimate the rate at which the interior of Miranda was heated during the high-eccentricity phase of evolution through the 3 : 1 commensurability with Umbriel, us-

ing (Peale and Cassen 1978)

$$\frac{dE}{dt} = -\frac{21}{2} k_{2M} \frac{MR_M^5 n_M^3}{a_M^3 Q_M} e_M^2 \approx 7.4 \times 10^{18} e_M^2 \text{ ergs sec}^{-1} \quad (8)$$

using parameters appropriate for this satellite (Tables I and II). Tidal heating due to the nonzero obliquity of Miranda in Cassini state 1 would have been negligible, since the obliquity would have been small (see Tittemore 1988). Based on the results of the numerical integrations using the eccentric-inclined model, the maximum instantaneous tidal heating rate is about 1.9×10^{16} ergs sec^{-1} at $e_M \approx 0.05$. However, this tidal heating rate is not sustained for long periods.

Figure 26 shows a short section of Fig. 10a during the period over which the orbital eccentricity of Miranda reaches its largest values. The time interval represented by this plot is about 4.9×10^7 years ($Q = 11{,}000$). Over this time interval, the eccentricity remains at large values for relatively short periods. For example, at $\delta \approx 16.5$, the average value of e_M is about 0.042 for a period of about 3 million years. At an average heating rate of 1.3×10^{16} ergs sec^{-1} over this time period, the internal thermal energy of the satellite would increase by approximately 1.2×10^{30} ergs, most of which would be retained over such a short time scale. If the heat capacity of the interior of Miranda has a value comparable to that of water ice ($\approx 2 \times 10^7$ ergs g^{-1} sec^{-1}), this would result in a global temperature increase of about 1°K. The tidal heating of a body is not uniformly distributed throughout the interior: the rate of heating at the center of a homogeneous, incompressible body is about three times the globally averaged heating rate (Kaula 1964, Peale and Cassen 1978), so near the center of the satellite the increase in temperature might be a few degrees. Several such bursts of tidal heating are possible during evolution through the chaotic zone; however, it is not expected that the increase in interior temperature would be large if this were the only heating mechanism.

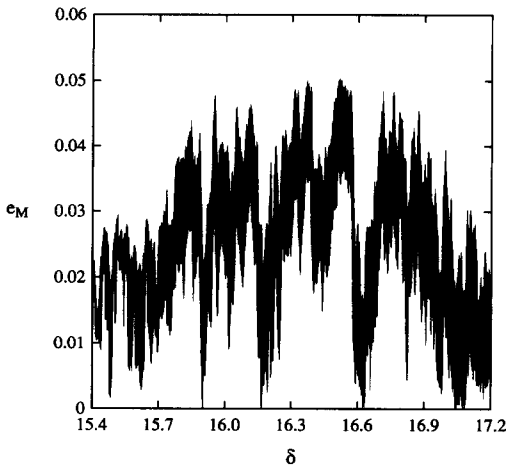

FIG. 26. Orbital eccentricity variations of Miranda during evolution through the 3 : 1 commensurability with Umbriel. This figure is a portion of Fig. 10a with an expanded scale. The time interval represented is about 4.9×10^7 years. Miranda spends relatively short periods of time at large eccentricity.

The time scale of evolution through the commensurability is comparable to the time scale for the eccentricity of Miranda's orbit to damp due to dissipation of tidal energy in the satellite (Appendix II). Satellite tides affect both the values of the eccentricities and the rate of evolution through the resonance. Because the excursions to large values of eccentricity occur on time scales much shorter than the eccentricity damping time scale, the effects of tidal dissipation in the satellites on the chaotic variations of eccentricity are probably not important. It is possible, however, that a quasi-stable state might be reached by the system: chaotic dynamical systems may mimic regular behavior for significant periods of time (see Wisdom 1982, 1983). The equilibrium eccentricity of Miranda in the 3 : 1 resonance is 0.026 (see Appendix II). It is not clear whether an equilibrium eccentricity could be maintained in the chaotic zone; however, it provides an upper limit to the *sustained* rate of heating of the interior of Miranda of about 5×10^{15} ergs sec^{-1} for $Q = 11{,}000$. The central temperature of a uniformly heating spherical body in conductive equilibrium

and with constant thermal conductivity is given by (e.g., Stevenson 1984)

$$T_c = T_s + \frac{H_v}{6k} R^2 \qquad (9)$$

where R is the radius of the satellite, H_v is the volumetric heating rate, k is the thermal conductivity, and T_s is the surface temperature, which is about 70°K for Miranda. The thermal conductivity k of water ice at low temperatures is about 5.3×10^5 erg cm^{-1} sec^{-1} deg^{-1} at 100°K (Hobbs 1974). If an equilibrium tidal heating state were possible, this model predicts that sustained tidal heating of Miranda at the equilibrium eccentricity in the 3 : 1 resonance with Umbriel can raise the central temperature of Miranda by only about 16°K. As mentioned above, however, the central tidal heating rate in a homogeneous body is about three times the global average rate, so the temperature increase near the center may be somewhat larger. In addition, the presence of bubbles and imperfections in the ice, silicate particles, and hydrates and clathrates with relatively low conductivities may lower the thermal conductivity of the interior of Miranda by about a factor of 2 compared to pure water ice (Stevenson 1982), resulting in a steeper temperature gradient. If these effects are important, a stable equilibrium tidal heating configuration could increase the central temperature of Miranda to a value comparable to the eutectic melting temperature of $NH_3 \cdot H_2O$, about 175°K. Whether or not a stable equilibrium state is likely depends on the dynamical effects of tidal dissipation in the satellites, which introduce direct damping terms into the equations of motion. Further work on this problem is currently underway.

Miranda can escape from the 3 : 1 resonance with an orbital eccentricity significantly larger than the value prior to resonance encounter. Our numerical experiments in the planar-eccentric approximation show that the escape eccentricity of Miranda in the absence of satellite dissipation can be larger than 0.06 (see Fig. 2a). The largest escape eccentricity found in the eccentric-inclined model was only 0.02 (Fig. 10b); however, this was based on a more limited set of runs. Tidal damping of the eccentricity following escape from the resonance may have significantly heated Miranda. Dermott *et al.* (1988) estimate that the damping of an eccentricity of 0.07 is required to raise the internal temperature of Miranda to the eutectic melting point of ammonia hydrate. This value is comparable to the largest escape eccentricity we found in our numerical simulations. Their estimate is really a lower limit, though, since it was calculated assuming that all of the tidally generated heat is retained in the interior of Miranda, and it does not take into consideration the possible importance of internal heat transport processes over the eccentricity damping time scale of order 10^8 years. In addition, this value of eccentricity is much larger than the equilibrium eccentricity of 0.026, so it is not clear whether the satellite could reach such a large value before escaping from the resonance. However, it is likely that Miranda left the 3 : 1 resonance with an orbital eccentricity significantly larger than the preencounter value, and that some tidal heating occurred as the eccentricity damped to its current value.

In summary, our numerical experiments indicate that the orbital eccentricity of Miranda may have reached a large enough value to have affected its thermal evolution. A combination of the heating mechanisms discussed above may have raised the internal temperature to a value comparable to the eutectic melting point of ammonia hydrate. Nevertheless, it is not likely that tidal heating of Miranda could have caused significant melting of water ice in the interior of this satellite.

There is a large chaotic zone associated with the Miranda–Ariel 5 : 3 mean-motion commensurability, even in the planar approximation. The orbital eccentricities of both satellites may vary chaotically for a considerable period. After a sudden increase at the point of entering the chaotic

zone, the maximum orbital eccentricity of Miranda gradually decreases until the trajectory escapes from the resonance. The final average orbital eccentricity and inclination of Miranda are most likely, though not necessarily, somewhat higher than the initial values. On average, the average final eccentricity of Ariel is lower than the initial value.

Since the rate of tidal heating depends strongly on the distance to the planet

$$\frac{dE}{dt} \propto \frac{1}{a^{15/2}} \tag{10}$$

a given value of e_M will cause the interior of Miranda to be heated about 40% more at the 5:3 resonance with Ariel than at the 3:1 resonance with Umbriel. The maximum eccentricities achieved at the 5:3 resonance are about half as high as those achieved at the 3:1 resonance with Umbriel, implying a maximum tidal heating rate about a third as large. Considering the uncertainties about the interior of Miranda discussed above, if tidal heating of Miranda was important at the 3:1 resonance with Umbriel, it may have been significant here, too.

Another possibility is that Miranda may have left the 5:3 resonance with an orbital inclination of order one degree. The relatively rapid increase in inclination possible during chaotic evolution through this resonance (e.g., Fig. 19) may have left Miranda with a substantial rotational obliquity; however, this would have quickly damped to the equilibrium Cassini state (see Tittemore 1988). Therefore, a relatively high inclination of Miranda's orbit could have been retained over the time interval between the 5:3 resonance involving Ariel and the 3:1 resonance involving Umbriel, possibly affecting the evolution through the latter commensurability. However, we have shown that even if Miranda approached the 3:1 commensurability involving Umbriel with a relatively high orbital inclination, i_M still may have jumped to its present value (see Fig. 15 of TW-II).

For initial eccentricities approaching the 2:1 commensurability which are comparable to or up to about a factor of 10 higher than the current values, capture into this resonance is very likely. Although even at low eccentricities a series of important secondary resonances between the frequencies of libration of σ_U and σ_A are encountered, they affect only the details of resonance passage, i.e., the oscillation amplitudes of the eccentricities. Interactions between these terms and terms associated with the inclination-type resonant arguments or with secular terms involving the other Uranian satellites may affect the resonant interaction, but do not appear to increase the likelihood of escape from the eccentricity-type resonances.

Could the satellites have encountered the resonance at high eccentricity and escaped? The eccentricities required are of order 0.03, according to the numerical simulations. Are these likely initial values? We can estimate the equilibrium eccentricity of Ariel in the absence of the resonant interaction, using Eqs. (42) and (51) in Appendix II and Q_A = 100, Q = 11,000:

$$e_A = \sqrt{\frac{1}{7D_A}} \approx 0.038. \tag{11}$$

At this eccentricity, the secular increase in semimajor axis due to tides on the planet would just be counterbalanced by the decrease due to dissipation in the satellite; hence, the orbit would not be evolving toward the resonance. Therefore, for the satellites to have evolved into the resonance, e_A must have been less than this. Since this is comparable to the initial eccentricity required to escape from the resonance, it is not likely that Ariel and Umbriel approached the 2:1 resonance with eccentricities large enough to escape from the resonance.

We conclude that it is unlikely that Ariel and Umbriel ever encountered the 2:1 mean-motion commensurability. This implies that the specific dissipation function of Uranus (Q) is greater than about 11,000.

This result, combined with the results from TW-II, constrains Q to within less than a factor of 4, or more tightly than the Q of any other giant planet has been constrained so far [see Burns (1986) for a recent review].

We have found the Uranian satellite system to have a rich variety of dynamical behavior. To summarize, the principal results of our research on the Uranian satellites to date are the following:

- Due to the low oblateness of Uranus ($J_2 = 0.0033$), there are significant chaotic zones at the low-order mean-motion commensurabilities among the Uranian satellites. There are chaotic variations in the eccentricities and/or inclinations for significant intervals of time during evolution through these commensurabilities.
- These chaotic zones have a significant effect on the mechanism of passage through resonance. For example, at both the 5 : 3 and 2 : 1 commensurabilities involving Ariel and Umbriel, trajectories may be captured into resonance while they are still chaotic.
- Simulated evolution through the resonances must be extremely slow to avoid dynamical artifacts: slower than $(1/a)(da/dt) \approx 10^{-11}$ to 10^{-10} per orbit period where chaotic adiabatic invariants are present, and slower than $(1/a)(da/dt) \approx 10^{-14}$ to 10^{-13} per orbit period where higher-dimensional chaotic diffusion is important. For example, to properly represent the dynamics of Miranda and Umbriel during evolution through the 3 : 1 eccentricity resonances, *the simulated tidal evolution rate must be within the physical constraints*, $2 \times 10^{-14} < (1/a)(da/dt) < 6 \times 10^{-14}$ per orbit period.
- At the 5 : 3 Ariel–Umbriel resonance the eccentricities in the chaotic zone are typically a factor of 2 to 3 higher than the preencounter values. Eccentricities large enough to have a significant effect on the thermal evolution of Ariel have not been found so far at this resonance (Tittemore and Wisdom 1988a).
- Evolution through the 3 : 1 Miranda–Umbriel commensurability explains the anomalously high inclination of Miranda. Passage through this resonance involves interesting new dynamical features: escape from the resonance occurs via secondary resonances, which drag trajectories into a chaotic region (Tittemore and Wisdom 1987, 1989).
- There are large increases in the orbital eccentricity of Miranda during chaotic evolution through the 3 : 1 Miranda–Umbriel commensurability. This may have affected the thermal evolution of Miranda, if low temperature melting occurred.
- Passage through the 5 : 3 Miranda–Ariel resonance may have modestly increased the eccentricity and inclination of Miranda.
- Escape from the 2 : 1 Ariel–Umbriel commensurability is not likely at typical satellite eccentricities; therefore, this probably provides a dynamical barrier to the evolution.
- Since the anomalously high orbital inclination of Miranda is a natural outcome of passage through the 3 : 1 commensurability with Umbriel, the requirement that the satellites encountered this resonance places a lower limit on the specific dissipation function (Q) of Uranus of 39,000.
- Since capture into resonance at the 2 : 1 Ariel–Umbriel commensurability is likely at typical satellite orbital eccentricities, the requirement that the satellites did not encounter this resonance constrains Q to be greater than 11,000.
- The requirement that the orbital eccentricity of Miranda damps to its current value since passage through the 3 : 1 commensurability with Umbriel indicates that Q is closer to 11,000.

APPENDIX I: THE AVERAGED RESONANT HAMILTONIAN

In this appendix, we develop the averaged Hamiltonian models used in this paper. Tables IV to VII give expressions and numerical values of the Hamiltonian coefficients. For calculations of the numerical values of the coefficients and other quantities, the adopted unit of time is one year, of mass is the mass of Uranus, $GM_U = 5.794 \times 10^6$

TABLE IV

PLANAR-ECCENTRIC MODEL COEFFICIENTS: EXPRESSIONS

Coefficient	Miranda–Umbriel 3:1	Miranda–Ariel 5:3	Ariel–Umbriel 2:1
A	$-\frac{1}{4}\frac{G^2M^2m_M^2m_M'}{\Gamma_M^3}+\frac{3}{4}\frac{G^2M^2m_U^2m_U'}{\Gamma_U^3}$	$-\frac{3}{4}\frac{G^2M^2m_M^2m_M'}{\Gamma_M^3}+\frac{5}{4}\frac{G^2M^2m_A^2m_A'}{\Gamma_A^3}$	$-\frac{1}{2}\frac{G^2M^2m_A^2m_A'}{\Gamma_A^3}+\frac{G^2M^2m_U^2m_U'}{\Gamma_U^3}$
B	$-\frac{3}{32}\frac{G^2M^2m_M^2m_M'}{\Gamma_M^4}-\frac{27}{32}\frac{G^2M^2m_U^2m_U'}{\Gamma_U^4}$	$-\frac{27}{32}\frac{G^2M^2m_M^2m_M'}{\Gamma_M^4}-\frac{75}{32}\frac{G^2M^2m_A^2m_A'}{\Gamma_A^4}$	$-\frac{3}{8}\frac{G^2M^2m_A^2m_A'}{\Gamma_A^4}-\frac{12}{8}\frac{G^2M^2m_U^2m_U'}{\Gamma_U^4}$
C	$\frac{1}{2}G^4M^4R^2J_2\left[\frac{9m_U^4m_U'^3}{2\Gamma_U^7}-\frac{3m_M^4m_M'^3}{\Gamma_M^7}\right]$ $+\frac{G^2Mm_Mm_U^2m_U'}{4\Gamma_U^2}\left[\frac{3}{\Gamma_U}b_{1/2}^0(\alpha)\right.$ $+\frac{d}{d\alpha}b_{1/2}^0(\alpha)\frac{m_U}{m_M}\frac{m_U'}{m_M'}\left(\frac{\Gamma_M}{\Gamma_U^2}+\frac{3\Gamma_M^2}{\Gamma_U^3}\right)$ $\left.-\frac{(2)^{(0)}}{\Gamma_M}\right]$	$\frac{1}{2}G^4M^4R^2J_2\left[\frac{15m_A^4m_A'^3}{2\Gamma_A^7}-\frac{6m_M^4m_M'^3}{\Gamma_M^7}\right]$ $+\frac{G^2Mm_Mm_A^2m_A'}{4\Gamma_A^2}\left[\frac{5}{\Gamma_A}b_{1/2}^0(\alpha)\right.$ $+\frac{d}{d\alpha}b_{1/2}^0(\alpha)\frac{m_A}{m_M}\frac{m_A'}{m_M'}\left(\frac{3\Gamma_M}{\Gamma_A^2}+\frac{5\Gamma_M^2}{\Gamma_A^3}\right)$ $\left.-\frac{(2)^{(0)}}{\Gamma_M}\right]$	$\frac{1}{2}G^4M^4R^2J_2\left[\frac{6m_U^4m_U'^3}{\Gamma_U^7}-\frac{9m_A^4m_A'^3}{2\Gamma_A^7}\right]$ $+\frac{G^2Mm_Am_U^2m_U'}{4\Gamma_U^2}\left[\frac{2}{\Gamma_U}b_{1/2}^0(\alpha)\right.$ $+\frac{d}{d\alpha}b_{1/2}^0(\alpha)\frac{m_U}{m_A}\frac{m_U'}{m_A'}\left(\frac{\Gamma_A}{\Gamma_U^2}+\frac{2\Gamma_A^2}{\Gamma_U^3}\right)$ $\left.-\frac{(2)^{(0)}}{\Gamma_A}\right]$
D	$\frac{1}{2}G^4M^4R^2J_2\left[\frac{3m_U^4m_U'^3}{\Gamma_U^7}-\frac{3m_M^4m_M'^3}{2\Gamma_M^7}\right]$ $+\frac{G^2Mm_Mm_U^2m_U'}{4\Gamma_U^2}\left[\frac{3}{\Gamma_U}b_{1/2}^0(\alpha)\right.$ $+\frac{d}{d\alpha}b_{1/2}^0(\alpha)\frac{m_U}{m_M}\frac{m_U'}{m_M'}\left(\frac{\Gamma_M}{\Gamma_U^2}+\frac{3\Gamma_M^2}{\Gamma_U^3}\right)$ $\left.-\frac{(3)^{(0)}}{\Gamma_U}\right]$	$\frac{1}{2}G^4M^4R^2J_2\left[\frac{6m_A^4m_A'^3}{\Gamma_A^7}-\frac{9m_M^4m_M'^3}{2\Gamma_M^7}\right]$ $+\frac{G^2Mm_Mm_A^2m_A'}{4\Gamma_A^2}\left[\frac{5}{\Gamma_A}b_{1/2}^0(\alpha)\right.$ $+\frac{d}{d\alpha}b_{1/2}^0(\alpha)\frac{m_A}{m_M}\frac{m_A'}{m_M'}\left(\frac{3\Gamma_M}{\Gamma_A^2}+\frac{5\Gamma_M^2}{\Gamma_A^3}\right)$ $\left.-\frac{(3)^{(0)}}{\Gamma_A}\right]$	$\frac{1}{2}G^4M^4R^2J_2\left[\frac{9m_U^4m_U'^3}{2\Gamma_U^7}-\frac{3m_A^4m_A'^3}{\Gamma_A^7}\right]$ $+\frac{G^2Mm_Am_U^2m_U'}{4\Gamma_U^2}\left[\frac{2}{\Gamma_U}b_{1/2}^0(\alpha)\right.$ $+\frac{d}{d\alpha}b_{1/2}^0(\alpha)\frac{m_U}{m_A}\frac{m_U'}{m_A'}\left(\frac{\Gamma_A}{\Gamma_U^2}+\frac{2\Gamma_A^2}{\Gamma_U^3}\right)$ $\left.-\frac{(3)^{(0)}}{\Gamma_U}\right]$
E	$-\frac{G^2Mm_Mm_U^2m_U'}{4\Gamma_U^2\sqrt{\Gamma_M\Gamma_U}}(21)^{(-1)}$	$-\frac{G^2Mm_Mm_A^2m_A'}{4\Gamma_A^2\sqrt{\Gamma_M\Gamma_A}}(21)^{(-1)}$	$-\frac{G^2Mm_Am_U^2m_U'}{4\Gamma_U^2\sqrt{\Gamma_A\Gamma_U}}(21)^{(-1)}$
F	$-\frac{G^2Mm_Mm_U^2m_U'}{4\Gamma_U^2\Gamma_M}(172)^{(3)}$	$-\frac{G^2Mm_Mm_A^2m_A'}{4\Gamma_A^2\Gamma_M}(172)^{(5)}$	$-\frac{G^2Mm_Am_U^2m_U'}{4\Gamma_U^2\Gamma_A}(172)^{(4)}$
G	$-\frac{G^2Mm_Mm_U^2m_U'}{4\Gamma_U^2\sqrt{\Gamma_M\Gamma_U}}(182)^{(2)}$	$-\frac{G^2Mm_Mm_A^2m_A'}{4\Gamma_A^2\sqrt{\Gamma_M\Gamma_A}}(182)^{(4)}$	$-\frac{G^2Mm_Am_U^2m_U'}{4\Gamma_U^2\sqrt{\Gamma_A\Gamma_U}}(182)^{(3)}$
H	$-\frac{G^2Mm_Mm_U^2m_U'}{4\Gamma_U^3}(192)^{(1)}$	$-\frac{G^2Mm_Mm_A^2m_A'}{4\Gamma_A^3}(192)^{(3)}$	$-\frac{G^2Mm_Am_U^2m_U'}{4\Gamma_U^3}(192)^{(2)}$
I			$-\frac{G^2Mm_Am_U^2m_U'}{2\Gamma_U^2\sqrt{\Gamma_A}}(50)^{(2)}$
J			$-\frac{G^2Mm_Am_U^2m_U'}{2\sqrt{\Gamma_U^5}}(70)^{(1)}$

km^3 sec^{-1} (Stone and Miner 1986), and of length is the radius of Uranus, R_U = 26,200 km (French *et al.* 1985). The Hamiltonians are developed in Jacobi coordinates (see, e.g., Plummer 1960). In the Jacobi coordinate system, the coordinates of the inner satellite are referred to the center of the planet, and the coordinates of the outer satellite are referred to the center of mass of the inner satellite and the planet. The reduced

TABLE V

PLANAR-ECCENTRIC MODEL COEFFICIENTS: NUMERICAL VALUES

Coefficient	Miranda–Umbriel 3 : 1[a]	Miranda–Ariel 5 : 3[b]	Ariel–Umbriel 2 : 1[c]
B	−5164.7	−49209	−1617.0
C	−0.31244	−0.51831	−0.13026
D	−0.14744	−0.35891	−0.073054
E	0.00039381	0.0051029	0.0054908
F	−0.0070667	−0.064822	−0.017678
G	0.0052590	0.037080	0.047364
H	−0.00017401	−0.0052682	−0.031349
I			0.010364
J			−0.0034123

[a] $a_M = 4.8659$, $a_U = 10.1179$.
[b] $a_M = 4.6361$, $a_A = 6.5157$.
[c] $a_A = 6.3255$, $a_U = 10.0400$.

TABLE VI

ECCENTRIC-INCLINED MODEL COEFFICIENTS: EXPRESSIONS

Coefficient	Miranda–Umbriel 3 : 1	Miranda–Ariel 5 : 3	Ariel–Umbriel 2 : 1
K	$\frac{1}{2}G^4M^4R^2J_2\left[\frac{9m_U^4m_U'^3}{2\Gamma_U^7}\right] + \frac{G^2Mm_Mm_U^2m_U'}{4\Gamma_U^2}\left[\frac{3}{\Gamma_U}b_{1/2}^0(\alpha) + \frac{d}{d\alpha}b_{1/2}^0(\alpha)\frac{m_U}{m_M}\frac{m_U'}{m_M'}\left(\frac{\Gamma_M}{\Gamma_U^2}+\frac{3\Gamma_M^2}{\Gamma_U^3}\right) - \frac{(11)^{(0)}}{\Gamma_M}\right]$	$\frac{1}{2}G^4M^4R^2J_2\left[\frac{-15m_A^4m_A'^3}{2\Gamma_A^7}+\frac{3m_M^4m_M'^3}{\Gamma_M^7}\right] + \frac{G^2Mm_Mm_A^2m_A'}{4\Gamma_A^2}\left[\frac{5}{\Gamma_A}b_{1/2}^0(\alpha) + \frac{d}{d\alpha}b_{1/2}^0(\alpha)\frac{m_A}{m_M}\frac{m_A'}{m_M'}\left(\frac{3\Gamma_M}{\Gamma_A^2}+\frac{5\Gamma_M^2}{\Gamma_A^3}\right) - \frac{(11)^{(0)}}{\Gamma_M}\right]$	$\frac{1}{2}G^4M^4R^2J_2\left[\frac{-6m_U^4m_U'^3}{\Gamma_U^7}+\frac{3m_A^4m_A'^3}{2\Gamma_A^7}\right] + \frac{G^2Mm_Am_U^2m_U'}{4\Gamma_U^2}\left[\frac{4}{\Gamma_U}b_{1/2}^0(\alpha) + 2\frac{d}{d\alpha}b_{1/2}^0(\alpha)\frac{m_U}{m_A}\frac{m_U'}{m_A'}\left(\frac{\Gamma_A}{\Gamma_U^2}+\frac{2\Gamma_A^2}{\Gamma_U^3}\right) - \frac{(11)^{(0)}}{\Gamma_A}\right]$
L	$\frac{1}{2}G^4M^4R^2J_2\left[\frac{6m_U^4m_U'^3}{\Gamma_U^7}-\frac{3m_M^4m_M'^3}{2\Gamma_M^7}\right] + \frac{G^2Mm_Mm_U^2m_U'}{4\Gamma_U^2}\left[\frac{3}{\Gamma_U}b_{1/2}^0(\alpha) + \frac{d}{d\alpha}b_{1/2}^0(\alpha)\frac{m_U}{m_M}\frac{m_U'}{m_M'}\left(\frac{\Gamma_M}{\Gamma_U^2}+\frac{3\Gamma_M^2}{\Gamma_U^3}\right) - \frac{(11)^{(0)}}{\Gamma_U}\right]$	$\frac{1}{2}G^4M^4R^2J_2\left[\frac{-9m_A^4m_A'^3}{\Gamma_A^7}+\frac{9m_M^4m_M'^3}{2\Gamma_M^7}\right] + \frac{G^2Mm_Mm_A^2m_A'}{4\Gamma_A^2}\left[\frac{5}{\Gamma_A}b_{1/2}^0(\alpha) + \frac{d}{d\alpha}b_{1/2}^0(\alpha)\frac{m_A}{m_M}\frac{m_A'}{m_M'}\left(\frac{3\Gamma_M}{\Gamma_A^2}+\frac{5\Gamma_M^2}{\Gamma_A^3}\right) - \frac{(11)^{(0)}}{\Gamma_A}\right]$	$\frac{1}{2}G^4M^4R^2J_2\left[\frac{-15m_U^4m_U'^3}{2\Gamma_U^7}+\frac{3m_A^4m_A'^3}{2\Gamma_A^7}\right] + \frac{G^2Mm_Am_U^2m_U'}{4\Gamma_U^2}\left[\frac{4}{\Gamma_U}b_{1/2}^0(\alpha) + 2\frac{d}{d\alpha}b_{1/2}^0(\alpha)\frac{m_U}{m_A}\frac{m_U'}{m_A'}\left(\frac{\Gamma_A}{\Gamma_U^2}+\frac{2\Gamma_A^2}{\Gamma_U^3}\right) - \frac{(11)^{(0)}}{\Gamma_U}\right]$
M	$\frac{G^2Mm_Mm_U^2m_U'}{2\Gamma_U^2\sqrt{\Gamma_M\Gamma_U}}(11)^{(0)}$	$\frac{G^2Mm_Mm_A^2m_A'}{2\Gamma_A^2\sqrt{\Gamma_M\Gamma_A}}(11)^{(0)}$	$\frac{G^2Mm_Am_U^2m_U'}{2\Gamma_U^2\sqrt{\Gamma_A\Gamma_U}}(11)^{(0)}$
N	$-\frac{G^2Mm_Mm_U^2m_U'}{4\Gamma_U^2\Gamma_M}(212)^{(3)}$	$-\frac{G^2Mm_Mm_A^2m_A'}{4\Gamma_A^2\Gamma_M}(212)^{(5)}$	$-\frac{G^2Mm_Am_U^2m_U'}{4\Gamma_U^2\Gamma_A}(212)^{(4)}$
O	$\frac{G^2Mm_Mm_U^2m_U'}{2\Gamma_U^2\sqrt{\Gamma_M\Gamma_U}}(212)^{(3)}$	$\frac{G^2Mm_Mm_A^2m_A'}{2\Gamma_A^2\sqrt{\Gamma_M\Gamma_A}}(212)^{(5)}$	$\frac{G^2Mm_Am_U^2m_U'}{2\Gamma_U^2\sqrt{\Gamma_A\Gamma_U}}(212)^{(4)}$
P	$-\frac{G^2Mm_Mm_U^2m_U'}{4\Gamma_U^3}(212)^{(3)}$	$-\frac{G^2Mm_Mm_A^2m_A'}{4\Gamma_A^3}(212)^{(5)}$	$-\frac{G^2Mm_Am_U^2m_U'}{4\Gamma_U^3}(212)^{(4)}$

TABLE VII

ECCENTRIC-INCLINED MODEL COEFFICIENTS: NUMERICAL VALUES

Coefficient	Miranda–Umbriel 3 : 1[a]	Miranda–Ariel 5 : 3[b]	Ariel–Umbriel 2 : 1[c]
B	−5166.14	−49209	−1617.03
C	−0.31263	−0.51823	−0.13030
D	−0.14783	−0.35883	−0.073083
E	0.00039358	0.005106	0.0054893
F	−0.0070635	−0.064858	−0.017674
G	0.0052572	0.037098	0.047355
H	−0.00017391	−0.0052705	−0.031344
I			0.010362
J			−0.0034115
K	0.044366	−0.070840	0.018914
L	−0.12043	−0.23024	−0.038308
M	−0.00067590	−0.0062127	−0.0073917
N	−0.00097703	−0.0072991	−0.0021365
O	0.00039358	0.0031582	0.0039091
P	−0.000039637	−0.00034162	−0.0017881

[a] $a_M = 4.8652$, $a_U = 10.1179$.
[b] $a_M = 4.6361$, $a_A = 6.5152$.
[c] $a_A = 6.3256$, $a_U = 10.0400$.

masses are $m_1' = m_1(M_U/(M_U + m_1))$ and $m_2' = m_2((M_U + m_1)/(M_U + m_1 + m_2))$ for $(a_1 < a_2)$. A development of the planar second-order resonant mapping is given in TW-I; the other mappings used here are similar in form.

Planar-Eccentric Models

In this section, we summarize the resonant Hamiltonians for the planar-eccentric problems. These can be approximated by two-degree-of-freedom models. We give a brief description of the resonant coordinates and the form of the resonant Hamiltonians. A detailed derivation of the Ariel–Umbriel 5 : 3 resonance planar-eccentric model is given in TW-I. The Hamiltonians of the other resonances are derived in an analogous way, and only the expressions and values of the coefficients are given here.

We consider second-order resonances involving the combination of mean longitudes $i\lambda_2 - j\lambda_1$, $i - j = 2$, where subscripts 1 and 2 refer to the inner and outer satellites, respectively.

The resonance coordinates are defined to be

$$\sigma_1 = \tfrac{1}{2}(i\lambda_2 - j\lambda_1 - 2\tilde{\omega}_1)$$
$$\sigma_2 = \tfrac{1}{2}(i\lambda_2 - j\lambda_1 - 2\tilde{\omega}_2) \qquad (12)$$

and the conjugate momenta are

$$\sum_1 \approx \frac{L_1}{2} e_1^2$$
$$\sum_2 \approx \frac{L_2}{2} e_2^2 \qquad (13)$$

where $L_i \approx m_i\sqrt{GMa_i}$.

The resonant part of the Hamiltonian for a second-order resonance is given by (see, e.g., Leverrier 1855):

$$\mathcal{H}_R = -\frac{Gm_1m_2}{a_2} \times \left[(172)^{(i)} \left(\frac{e_1}{2}\right)^2 \cos(i\lambda_2 - j\lambda_1 - 2\tilde{\omega}_1) + (182)^{(i-1)} \frac{e_1}{2}\frac{e_2}{2} \cos(i\lambda_2 - j\lambda_1 - \tilde{\omega}_1 - \tilde{\omega}_2) + (192)^{(i-2)} \left(\frac{e_2}{2}\right)^2 \cos(i\lambda_2 - j\lambda_1 - 2\tilde{\omega}_2) \right] \qquad (14)$$

where

$$(172)^{(l)} = \frac{1}{2}(-5l + 4l^2)b^l_{1/2}(\alpha) + (-1 + 2l)\,\alpha\frac{d}{d\alpha}b^l_{1/2}(\alpha) + \frac{1}{2}\alpha^2\frac{d^2}{d\alpha^2}b^l_{1/2}(\alpha)$$

$$(182)^{(l)} = (-2 - 4l)lb^l_{1/2}(\alpha) + (-2 - 4l)\,\alpha\frac{d}{d\alpha}b^l_{1/2}(\alpha) - \alpha^2\frac{d^2}{d\alpha^2}b^l_{1/2}(\alpha)$$

$$(192)^{(l)} = \frac{1}{2}(4 + 9l + 4l^2)b^l_{1/2}(\alpha) + (3 + 2l)\,\alpha\frac{d}{d\alpha}b^l_{1/2}(\alpha) + \frac{1}{2}\alpha^2\frac{d^2}{d\alpha^2}b^l_{1/2}(\alpha) \quad (15)$$

where l is an integer, $\alpha = a_1/a_2$ is the ratio of semimajor axes, and $b^l_s(\alpha)$ are Laplace coefficients. For the 3 : 1 resonance, there must also be included the indirect term $-(27/2)\,\alpha$ in the expression for $(192)^{(1)}$.

The form of the Hamiltonian is

$$\begin{aligned}\mathcal{H} = {} & 2A(\Sigma_1 + \Sigma_2) + 4B(\Sigma_1 + \Sigma_2)^2 \\ & + 2C\Sigma_1 + 2D\Sigma_2 \\ & + 2E\sqrt{\Sigma_1\Sigma_2}\cos(\sigma_1 - \sigma_2) \\ & + 2F\Sigma_1\cos(2\sigma_1) \\ & + 2G\sqrt{\Sigma_1\Sigma_2}\cos(\sigma_1 + \sigma_2) \\ & + 2H\Sigma_2\cos(2\sigma_2). \end{aligned} \quad (16)$$

For the 2 : 1 resonance, there are the additional first-order resonance terms in H_R:

$$(50)^{(2)}\left(\frac{e_A}{2}\right)\cos(2\lambda_U - \lambda_A - \tilde{\omega}_A) + (70)^{(1)}\left(\frac{e_U}{2}\right)\cos(2\lambda_U - \lambda_A - \tilde{\omega}_U) \quad (17)$$

where

$$(50)^2 = -4b^2_{1/2}(\alpha) - \alpha\frac{d}{d\alpha}b^2_{1/2}(\alpha)$$

$$(70)^{(1)} = 3b^1_{1/2}(\alpha) + \alpha\frac{d}{d\alpha}b^1_{1/2}(\alpha) - 4\alpha. \quad (18)$$

The last term in the expression for $(70)^{(1)}$ is the indirect term. The first-order resonance terms are included in the resonant Hamiltonian in the following terms:

$$I\sqrt{2\Sigma_1}\cos\sigma_1 + J\sqrt{2\Sigma_2}\cos\sigma_2. \quad (19)$$

In terms of the Cartesian elements

$$y_i = \sqrt{2\Sigma_i}\sin(\sigma_i) \approx e_i\sqrt{L_i}\sin(\sigma_i) \text{ or } i_i\sqrt{L_i}\sin(\sigma_i). \quad (20)$$

and the conjugate momenta

$$x_i = \sqrt{2\Sigma_i}\cos(\sigma_i) \approx e_i\sqrt{L_i}\cos(\sigma_i) \text{ or } i_i\sqrt{L_i}\sin(\sigma_i) \quad (21)$$

the Hamiltonian may be expressed

$$\begin{aligned}\mathcal{H} = {} & \tfrac{1}{4}(\delta - 2(C + D))(x_1^2 + y_1^2 + x_2^2 + y_2^2)^2 \\ & + B(x_1^2 + y_1^2 + x_2^2 + y_2^2)^2 \\ & + C(x_1^2 + y_1^2) + D(x_2^2 + y_2^2) \\ & + E(x_1x_2 + y_1y_2) \\ & + F(x_1^2 - y_1^2) + G(x_1x_2 - y_1y_2) \\ & + H(x_2^2 - y_2^2) \end{aligned} \quad (22)$$

with the additional terms

$$Ix_1 + Jx_2 \quad (23)$$

for the 2 : 1 resonance, and where

$$\delta \equiv 4A + 2(C + D) \approx in_2 - jn_1 - \dot{\tilde{\omega}}_1 - \dot{\tilde{\omega}}_2. \quad (24)$$

This definition of δ is chosen so that the coefficients are evaluated in the middle of the resonance region. Numerical values of the coefficients were calculated at zero eccentricity and $\delta = 0$. Expressions for the coefficients are given in Table IV, and numerical values in Table V. In the evaluation of the coefficients, the unit of mass is the mass of Uranus, the unit of time is one year, and the unit of length is the radius of Uranus. During evolution through the resonance, the quantity $in_2 - jn_1$ changes by a large amount relative to the other coefficients, which are therefore approximated to be constant.

Eccentric-Inclined Models

To include the effects of three-dimensional motion on the interactions at a commensurability, we can develop a resonant Hamiltonian similar to that developed for

the planar-eccentric case, but generalized to include the inclination resonant terms. We define

$$\sigma_1 = \tfrac{1}{2}(i\lambda_2 - j\lambda_1 - 2\tilde{\omega}_1)$$

$$\sigma_2 = \tfrac{1}{2}(i\lambda_2 - j\lambda_1 - 2\tilde{\omega}_2)$$

$$\Sigma_1 \approx \frac{\Gamma_1}{2} e_1^2$$

$$\Sigma_2 \approx \frac{\Gamma_2}{2} e_2^2$$

$$\psi_1 = \tfrac{1}{2}(i\lambda_2 - j\lambda_1 - 2\Omega_1)$$

$$\psi_2 = \tfrac{1}{2}(i\lambda_2 - j\lambda_1 - 2\Omega_2)$$

$$\Psi_1 \approx \frac{\Gamma_1}{2} i_1^2$$

$$\Psi_2 \approx \frac{\Gamma_2}{2} i_2^2$$

$$\Gamma_1 = L_1 + \frac{j}{2}(\Sigma_1 + \Sigma_2 + \Psi_1 + \Psi_2)$$

$$\Gamma_2 = L_2 - \frac{i}{2}(\Sigma_1 + \Sigma_2 + \Psi_1 + \Psi_2). \quad (25)$$

The inclination part of the secular contribution to the Hamiltonian is given by (see, e.g., Leverrier, 1855)

$$\mathcal{H}_S = -\frac{Gm_1m_2}{a_2}\left\{(1)^{(0)} + (11)^{(0)}\left[\left(\frac{i_1}{2}\right)^2 + \left(\frac{i_2}{2}\right)^2 - 2\left(\frac{i_1}{2}\right)\left(\frac{i_2}{2}\right)\cos(\Omega_1 - \Omega_2)\right]\right\} \quad (26)$$

where

$$(1)^{(0)} = \tfrac{1}{2}\alpha b_{1/2}^0(\alpha)$$

$$(11)^{(0)} = -\tfrac{1}{2}\alpha b_{3/2}^1(\alpha) \quad (27)$$

and the inclination part of the resonant contribution is given by

$$\mathcal{H}_R = -\frac{Gm_1m_2}{a_2}(212)^{(i)}\left[\left(\frac{i_1}{2}\right)^2\cos(i\lambda_2 - j\lambda_1 - 2\Omega_1) - 2\frac{i_1}{2}\frac{i_2}{2}\cos(i\lambda_2 - j\lambda_1 - \Omega_1 - \Omega_2) + \left(\frac{i_2}{2}\right)^2\cos(i\lambda_2 - j\lambda_1 - 2\Omega_2)\right] \quad (28)$$

where

$$(212)^{(i)} = \tfrac{1}{2}\alpha b_{3/2}^{(i-1)}(\alpha). \quad (29)$$

α is the ratio of semimajor axes, and $b_s^j(\alpha)$ are Laplace coefficients.

In terms of these coordinates, the Hamiltonian is

$$\begin{aligned}\mathcal{H} = {} & 2A(\Sigma_1 + \Sigma_2 + \Psi_1 + \Psi_2) \\ & + 4B(\Sigma_1 + \Sigma_2 + \Psi_1 + \Psi_2)^2 \\ & + 2C\Sigma_1 + 2D\Sigma_2 \\ & + 2E\sqrt{\Sigma_1\Sigma_2}\cos(\sigma_1 - \sigma_2) \\ & + 2F\Sigma_1\cos(2\sigma_1) \\ & + 2G\sqrt{\Sigma_1\Sigma_2}\cos(\sigma_1 + \sigma_2) \\ & + 2H\Sigma_2\cos(2\sigma_2) \\ & + 2K\Psi_1 + 2L\Psi_2 \\ & + 2M\sqrt{\Psi_1\Psi_2}\cos(\psi_1 - \psi_2) \\ & + 2N\Psi_1\cos(2\psi_1) \\ & + 2O\sqrt{\Psi_1\Psi_2}\cos(\psi_1 + \psi_2) \\ & + 2P\Psi_2\cos(2\psi_2). \end{aligned} \quad (30)$$

For the 2:1 resonance, there are also the terms

$$I\sqrt{2\Sigma_1}\cos\sigma_1 + J\sqrt{2\Sigma_2}\cos\sigma_2. \quad (31)$$

Expressions for the coefficients A through J are the same as in the planar-eccentric model, with the redefined Γ_i given above. δ is defined to be the nonresonant contributions to $in_2 - jn_1 - \frac{1}{2}(\dot{\tilde{\omega}}_1 + \dot{\tilde{\omega}}_2 + \dot{\Omega}_1 + \dot{\Omega}_2) = 4A + (C + D + K + L)$. This definition is chosen so that the coefficients are evaluated in the middle of the resonance region. Expressions for the coefficients are given in Table VIII, and numerical values of the coefficients, evaluated at $\delta = 0$ and zero eccentricity and inclination, are given in Table IX.

[*Note*: For the Miranda–Ariel 5:3 resonance, δ was defined incorrectly to be $5n_A - 3n_M - (\dot{\tilde{\omega}}_M - \dot{\tilde{\omega}}_A - \dot{\Omega}_M - \dot{\Omega}_A) = 4A + 2(C + D + K + L)$. The main effect of this is to slightly change the values of the coefficients in Table VII; however, the differences are not significant.]

TABLE VIII

SECULAR PERTURBED MODEL COEFFICIENTS: EXPRESSIONS

Coefficient	Miranda–Umbriel 3 : 1	Miranda–Ariel 5 : 3	Ariel–Umbriel 2 : 1
C''	$-\frac{3}{4}\frac{G^4M^4m_M^4m_M'^3R^2J_2}{L_M^7}$	$-\frac{3}{4}\frac{G^4M^4m_M^4m_M'^3R^2J_2}{L_M^7}$	$-\frac{3}{4}\frac{G^4M^4m_A^4m_A'^3R^2J_2}{L_A^7}$
	$-\frac{G^2Mm_Mm_A^2m_A'}{4L_A^2}\frac{(2)_{MA}^{(0)}}{L_M}$	$-\frac{G^2Mm_Mm_A^2m_A'}{4L_A^2}\frac{(2)_{MA}^{(0)}}{L_M}$	$-\frac{G^2Mm_Am_U^2m_U'}{4L_U^2}\frac{(2)_{AU}^{(0)}}{L_A}$
	$-\frac{G^2Mm_Mm_U^2m_U'}{4L_U^2}\frac{(2)_{MU}^{(0)}}{L_M}$	$-\frac{G^2Mm_Mm_U^2m_U'}{4L_U^2}\frac{(2)_{MU}^{(0)}}{L_M}$	$-\frac{G^2Mm_Am_T^2m_T'}{4L_T^2}\frac{(2)_{AT}^{(0)}}{L_A}$
D''	$-\frac{3}{4}\frac{G^4M^4m_U^4m_U'^3R^2J_2}{L_U^7}$	$-\frac{3}{4}\frac{G^4M^4m_A^4m_A'^3R^2J_2}{L_A^7}$	$-\frac{3}{4}\frac{G^4M^4m_U^4m_U'^3R^2J_2}{L_U^7}$
	$-\frac{G^2Mm_Mm_U^2m_U'}{4L_U^2}\frac{(3)_{MU}^{(0)}}{L_U}$	$-\frac{G^2Mm_Mm_A^2m_A'}{4L_A^2}\frac{(3)_{MA}^{(0)}}{L_A}$	$-\frac{G^2Mm_Am_U^2m_U'}{4L_U^2}\frac{(3)_{AU}^{(0)}}{L_U}$
	$-\frac{G^2Mm_Am_U^2m_U'}{4L_U^2}\frac{(2)_{AU}^{(0)}}{L_A}$	$-\frac{G^2Mm_Am_U^2m_U'}{4L_U^2}\frac{(2)_{AU}^{(0)}}{L_A}$	$-\frac{G^2Mm_Um_T^2m_T'}{4L_T^2}\frac{(2)_{UT}^{(0)}}{L_U}$
U	$-\frac{3}{4}\frac{G^4M^4m_A^4m_A'^3R^2J_2}{L_A^7}$	$-\frac{3}{4}\frac{G^4M^4m_U^4m_U'^3R^2J_2}{L_U^7}$	$-\frac{3}{4}\frac{G^4M^4m_T^4m_T'^3R^2J_2}{L_A^7}$
	$-\frac{G^2Mm_Mm_A^2m_A'}{4L_A^2}\frac{(3)_{MA}^{(0)}}{L_A}$	$-\frac{G^2Mm_Mm_U^2m_U'}{4L_U^2}\frac{(3)_{MU}^{(0)}}{L_U}$	$-\frac{G^2Mm_Am_T^2m_T'}{4L_T^2}\frac{(3)_{AT}^{(0)}}{L_T}$
	$-\frac{G^2Mm_Am_U^2m_U'}{4L_U^2}\frac{(2)_{AU}^{(0)}}{L_A}$	$-\frac{G^2Mm_Am_U^2m_U'}{4L_U^2}\frac{(3)_{AU}^{(0)}}{L_U}$	$-\frac{G^2Mm_Um_T^2m_T'}{4L_T^2}\frac{(3)_{UT}^{(0)}}{L_T}$
V	$-\frac{G^2Mm_Mm_A^2m_A'}{4L_A^2\sqrt{L_ML_A}}(21)_{MA}^{(-1)}$	$-\frac{G^2Mm_Mm_U^2m_U'}{4L_U^2\sqrt{L_ML_U}}(21)_{MU}^{(-1)}$	$-\frac{G^2Mm_Am_T^2m_T'}{4L_T^2\sqrt{L_AL_T}}(21)_{AT}^{(-1)}$
W	$-\frac{G^2Mm_Am_U^2m_U'}{4L_U^2\sqrt{L_AL_U}}(21)_{AU}^{(-1)}$	$-\frac{G^2Mm_Am_U^2m_U'}{4L_U^2\sqrt{L_AL_U}}(21)_{AU}^{(-1)}$	$-\frac{G^2Mm_Um_T^2m_T'}{4L_T^2\sqrt{L_UL_T}}(21)_{UT}^{(-1)}$

Secular Perturbations

To include the secular perturbations due to other satellites, the development of the Hamiltonian is somewhat different, in order to keep secular variations distinct from resonant variations (see Wisdom 1982). We define as coordinates

$$\phi = j\lambda_1 - i\lambda_2$$
$$p_i \approx e_i\sqrt{L_i}\cos(-\tilde{\omega}_i) \quad \text{or} \quad i_i\sqrt{L_i}\cos(-\Omega_i)$$
$$q_i \approx e_i\sqrt{L_i}\sin(-\tilde{\omega}_i) \quad \text{or} \quad i_i\sqrt{L_i}\sin(-\Omega_i) \qquad (32)$$

and expand the Hamiltonian about the resonant value of L_1 (pendulum approximation). The momentum conjugate to ϕ is $\Phi = (1/j)(L_1 - L_{1R})$, where the resonant value of L_{1R} is defined by setting $\partial\mathcal{H}_0/\partial\Phi = 0$ and where $\mathcal{H}_0$ is the nonresonant part of the Hamiltonian.

The Hamiltonian for the two-body resonance problem can then be expressed as

$$\begin{aligned}\mathcal{H} = {} & \tfrac{1}{2}\alpha\Phi^2 \\ & + C'(p_1^2 + q_1^2) + D'(p_2^2 + q_2^2) \\ & + E(p_1p_2 + q_1q_2) \\ & + F((p_1^2 - q_1^2)\cos\phi + 2p_1q_1\sin\phi) \\ & + G((p_1p_2 - q_1q_2)\cos\phi \\ & + (p_1q_2 + q_1p_2)\sin\phi) \\ & + H((p_2^2 - q_2^2)\cos\phi + 2p_2q_2\sin\phi) \qquad (33)\end{aligned}$$

TABLE IX

SECULAR PERTURBED MODEL COEFFICIENTS: NUMERICAL VALUES

Coefficient	Miranda–Umbriel 3 : 1[a]	Miranda–Ariel 5 : 3[b]	Ariel–Umbriel 2 : 1[c]
α	−165280	-1.5747×10^6	-5.1742×10^4
C''	−0.18896	−0.22521	−0.075839
D''	−0.019399	−0.068809	−0.021761
E	0.00039380	0.0051031	0.0054912
F	−0.0070660	−0.064824	−0.017679
G	0.0052585	0.037081	0.047366
H	−0.00017399	−0.052683	−0.031350
I			0.010364
J			−0.0034125
U	−0.054396	−0.017831	−0.0039395
V	0.0036101	0.00033903	0.00056777
W	0.0098431	0.0063445	0.0033443

[a] $a_M = 4.8658$, $a_A = 7.0846$, $a_U = 10.1179$.
[b] $a_M = 4.6361$, $a_A = 6.5157$, $a_U = 10.0560$.
[c] $a_A = 6.3256$, $a_U = 10.0400$, $a_T = 16.6330$.

where $\alpha \approx 32B$, and where C' and D' contain only precession terms due to planetary oblateness and satellite interactions. For the 2 : 1 resonance, there are the additional terms

$$I(x_1 \cos\phi + y_1 \sin\phi) + J(x_2 \cos\phi + y_2 \sin\phi). \quad (34)$$

To include the perturbations due to a third satellite, we add the terms in the secular part of the disturbing function involving the third satellite and its interactions with the first two. For the Hamiltonian we end up with the expression

$$\begin{aligned}\mathcal{H} = {} & \tfrac{1}{2}\alpha\Phi^2 \\ & + C''(p_1^2 + q_1^2) + D''(p_2^2 + q_2^2) \\ & + E(p_1p_2 + q_1q_2) \\ & + F((p_1^2 - q_1^2)\cos\phi + 2p_1q_1 \sin\phi) \\ & + G((p_1p_2 - q_1q_2)\cos\phi \\ & + (p_1q_2 + q_1p_2)\sin\phi) \\ & + H((p_2^2 - q_2^2)\cos\phi + 2p_2q_2 \sin\phi) \\ & + U(p_3^2 + q_3^2) + V(p_1p_3 + q_1q_3) \\ & + W(p_3p_2 + q_3q_2) \end{aligned} \quad (35)$$

where the perturbing satellite is designated by subscript 3. For the 2 : 1 resonance, there are the additional term

$$I(x_1 \cos\phi + y_1 \sin\phi) + J(x_2 \cos\phi + y_2 \sin\phi). \quad (36)$$

The expressions for the coefficients E–H (and I and J for the 2 : 1 resonance) are the same as those in the two-satellite problem, and $\alpha \approx 32B$, except that in the expressions for the coefficients, L_i should be substituted for Γ_i. Numerical values of the coefficients were evaluated at zero eccentricity. Expressions for the coefficients C'', D'', U, V, and W are given in Table VI, and numerical values of all the coefficients are given in Table VII.

Note. In TW-II (Tittemore and Wisdom 1989), there is an error in the definition of the coefficient of the e_U^2 resonance in the Miranda–Umbriel 3 : 1 eccentric-inclined resonance model. The Leverrier coefficient $(192)^{(1)}$ contains an extra indirect term $-3/2\alpha^2$ which should not have been included. The incorrect definition of this coefficient introduced errors into the numerical integrations of the eccentric-inclined model only, and did not affect the main body of

the paper dealing with the circular-inclined problem. The error does not affect the mechanism that leads to the high orbital inclination of Miranda. The main conclusions drawn from the numerical integrations of the eccentric-inclined model, that the orbital inclination of Miranda remains large during evolution through the chaotic zone associated with the eccentricity resonances and that the orbital eccentricity of Miranda increases significantly during passage through the eccentricity resonances, also remain unchanged.

APPENDIX II: TIDAL EVOLUTION

In planetary satellite systems, tidal evolution is caused by tides raised on the planet by the satellites and tides raised on the satellites by the planet. In the Uranian satellite system, the former tend to the orbital semimajor axes, while the latter act to decrease the semimajor axes and eccentricities.

In the absence of an orbital resonance, the equilibrium eccentricity of a satellite is the value at which there is no net change in the semimajor axis due to tides, because the rate of energy dissipation due to tides raised on the satellite is equal to the rate of energy input to the orbit due to tides raised on the planet.

For satellites involved in an eccentricity resonance, the equilibrium eccentricity has a somewhat different meaning. At the Ariel–Umbriel 5:3, Miranda–Umbriel 3:1, and Ariel–Umbriel 2:1 resonances, planet tides tend to expand the inner satellite orbit (I) relative to the outer orbit (O); therefore, the semimajor axis ratio (a_I/a_O) tends to increase. However, the forced orbital eccentricities resulting from the resonant interaction also increase, so some of the energy gained by the orbits is tidally dissipated in one or both of the satellites. At each of the above resonances in the Uranian system, most of the tidal dissipation occurs in the inner satellite. Under these conditions, the equilibrium eccentricity of the inner satellite is the value at which the semimajor axis ratio of the two satellites (a_I/a_O) remains constant as the orbits expand due to tides (see, e.g., Yoder 1979b, Peale 1988).

We present the calculation of the equilibrium eccentricity for the 2:1 Ariel–Umbriel case in detail; equilibrium eccentricities for the other commensurabilities may be obtained in an analogous manner. Note, however, that the Miranda–Ariel 5:3 commensurability does not have an equilibrium eccentricity because the semimajor axis ratio (a_M/a_A) is decreasing. At the end of this section, we summarize the effective tidal evolution rates due to planetary tides, the equilibrium eccentricities at the resonances, and the eccentricity damping time scales.

Of the various coefficients in the resonance Hamiltonian, only δ depends strongly on the resonant combination of mean motions; during passage through the resonance, the fractional change in the parameter δ is large compared to the fractional changes in the other coefficients. The other coefficients will therefore be taken to be constant. In addition, the value of δ is influenced by the damping of eccentricities due to tidal dissipation in the satellites. For the Ariel–Umbriel 2:1 commensurability, the time rate of change of δ is

$$\dot{\delta} \simeq 4\dot{A}. \tag{37}$$

From the expansion of A to first order in Σ_i,

$$\dot{\delta} \simeq (4\dot{n}_A - 2\dot{n}_M) - 16B(\dot{\Sigma}_M + \dot{\Sigma}_A). \tag{38}$$

The first two terms are due to the tidal expansion of the orbits, and the other terms are due to the exchange of angular momentum between the satellites resulting from dissipation of energy in the satellites (Yoder 1979b). Note that

$$\dot{\Sigma}_i \simeq \Sigma_i \left[-\frac{3}{4}\frac{\dot{n}_i}{4n_i} + 2\frac{\dot{e}_i}{e_i} \right]. \tag{39}$$

Tidal friction results in a secular variation of the mean motions

$$\dot{n}_i = \dot{n}_{ip} + \dot{n}_{is} \tag{40}$$

where the first term is due to tides raised on the planet (e.g., Goldreich 1965)

$$\dot{n}_{ip} = -\frac{9}{2} k_2 n_i^2 \frac{m_i}{M} \left(\frac{R}{a_i}\right)^5 \frac{1}{Q}. \quad (41)$$

The second term is due to tidal dissipation in the satellite, which for a synchronous rotation state must conserve the orbital angular momentum: $\dot{G}_i \simeq d/dt \sqrt{GMa_i(1 - e^2)} = 0$, so $\dot{a} \simeq 2a_i e_i \dot{e}_i$. Therefore,

$$\dot{n}_i = \dot{n}_{ip} - 3n_i e_i \dot{e}_i. \quad (42)$$

Tidal friction also changes the orbital eccentricities (Goldreich, 1963)

$$\dot{e}_i = -\frac{21}{2} k_{2i} n_i \frac{M}{m_i} \left(\frac{R_i}{a_i}\right)^5 \frac{e_i}{Q_i} + \frac{57}{8} k_2 n_i \frac{m_i}{M} \left(\frac{R}{a_i}\right)^5 \frac{e_i}{Q} \quad (43)$$

where k_2 and Q are, respectively, the potential Love number and specific dissipation function for Uranus, and the k_{2i} and Q_i values are the same quantities for the satellites. The first term in the expression for $\dot{e}_i$ is the contribution due to tidal dissipation in the satellite, and the second term is due to tidal dissipation in the planet. The relative contributions of these components is

$$\frac{\dot{e}_s}{\dot{e}_p} = -\frac{28}{19} D_i \quad (44)$$

where

$$D_i = \frac{k_{2i}}{k_2} \left(\frac{M}{m_i}\right)^2 \left(\frac{R_i}{R}\right)^5 \frac{Q}{Q_i} \quad (45)$$

expresses the ratio of the satellite tidal scale factor to that of the planet (e.g., Yoder 1979b). For Ariel, $D_A = 100.7$ ($Q = 11{,}000$ and $Q_A = 100$), and the satellite dissipation term dominates the planet dissipation term by about two orders of magnitude. This is also the case for the other satellites. Since $\dot{n}_p/n$ and $\dot{e}_p/e$ are of the same order, this means that

$$\dot{\Sigma}_i \approx 2\Sigma_i \frac{\dot{e}_i}{e_i} = L_i e_i \dot{e}_i. \quad (46)$$

Using numerical values from Table I to evaluate relative contributions to $\dot{\delta}$,

$$\frac{4\dot{n}_U}{2\dot{n}_A} \simeq \frac{4m_U}{2m_A} \left(\frac{a_A}{a_U}\right)^8 \approx 0.047 \quad (47)$$

so the semimajor axis ratio increases. The ratio of the eccentricity-dependent terms is

$$\frac{\dot{\Sigma}_U}{\dot{\Sigma}_A} \simeq \frac{k_{2U}}{k_{2A}} \frac{m_A}{m_U} \frac{n_U}{n_A} \left(\frac{R_U}{R_A}\right)^5 \left(\frac{a_A}{a_U}\right)^5 \frac{Q_A}{Q_U} \frac{\Sigma_U}{\Sigma_A} \approx 0.06 \left(\frac{e_U}{e_A}\right)^2. \quad (48)$$

The most significant terms in $\dot{\delta}$ are therefore

$$\dot{\delta} = -2\dot{n}_A - 16B\dot{\Sigma}_A. \quad (49)$$

Note that (see Appendix I)

$$16B \approx -6 \frac{n_A}{L_A} \left[1 + 4 \frac{m_A}{m_U} \left(\frac{a_A}{a_U}\right)^2\right] \quad (50)$$

and

$$\frac{\dot{e}_A}{\dot{n}_A} \simeq \frac{7}{3} D_A \frac{e_A}{n_A}. \quad (51)$$

Therefore

$$\dot{\delta} \approx -2\dot{n}_A \left\{1 - 14 D_A e_A^2 \left[1 + 2 \frac{m_A}{m_U} \left(\frac{a_A}{a_U}\right)^2\right]\right\}. \quad (52)$$

The tidal parameter δ will be stationary at the equilibrium eccentricity

$$e_A = \sqrt{\frac{1}{14 D_A \left[1 + 2 \frac{m_A}{m_U} \left(\frac{a_A}{a_U}\right)^2\right]}}. \quad (53)$$

This expression is in agreement with the expressions for the equilibrium eccentricity of the 2 : 1 two-body resonances in the Jovian satellite system found by Yoder (1979b). For the Ariel–Umbriel 2 : 1 resonance, the equilibrium eccentricity of Ariel is

$$e_A = \sqrt{\frac{1}{25.7 D_A}} = 0.02 \quad (54)$$

if $Q = 11{,}000$.

We summarize the effective tidal evolution rates due to planetary tides, the equilibrium eccentricities of the satellites, and the eccentricity damping time scales. These values were computed using $Q = 11{,}000$ for Uranus, $Q = 100$ for the satellites, and the physical parameters given in Tables I and II.

At the Miranda–Umbriel 3 : 1 commensurability

$$\delta = 3n_U - n_M - \dot{\omega}_M - \dot{\omega}_U \quad (55)$$

and

$$\dot{\delta} \approx -\dot{n}_M \approx \frac{3}{2} n_M \frac{\dot{a}_M}{a_M} = 3.71 \times 10^{-8}\,\text{year}^{-2} \quad (56)$$

with $\dot{a}_M/a_M = 5.63 \times 10^{-14}$ per orbit period. The equilibrium eccentricity of Miranda is $e_M = 0.026$, and the eccentricity damping time scales are 10^8 years for Miranda and 10^9 years for Umbriel.

At the Miranda–Ariel 5 : 3 commensurability,

$$\delta = 5n_A - 3n_M - \dot{\omega}_M - \dot{\omega}_A \quad (57)$$

and

$$\dot{\delta} \approx 0.492(5\dot{n}_A) \approx -0.492 \frac{15}{2} n_A \frac{\dot{a}_A}{a_A} = -1.60 \times 10^{-7}\,\text{year}^{-2} \quad (58)$$

with $\dot{a}_A/a_A = 2.35 \times 10^{-13}$ per orbit period. The eccentricity damping time-scale of both satellites is about 10^8 years.

At the Ariel–Umbriel 2 : 1 commensurability

$$\delta = 4n_U - 2n_U - \dot{\omega}_A - \dot{\omega}_U \quad (59)$$

and

$$\dot{\delta} \approx -2\dot{n}_A \approx 3n_A \frac{\dot{a}_A}{a_A} = 1.65 \times 10^{-7}\,\text{year}^{-2} \quad (60)$$

with $\dot{a}_A/a_A = 2.73 \times 10^{-13}$ per orbit period. The equilibrium eccentricity of Ariel is approximately 0.02. The eccentricity damping time scale of Ariel is about 6×10^7 years, and that of Umbriel is about 10^9 years.

ACKNOWLEDGMENTS

This research was supported in part by the NASA Planetary Geology and Geophysics Program under Grants NAGW-706 and NAGW-1720, in part by the Presidential Young Investigator Award AST-8857365, and in part by the Lunar and Planetary Laboratory of the University of Arizona. The authors thank Stan Peale and Carl Murray for careful reviews of the manuscript.

REFERENCES

ARNOLD, V. I. 1963. Small denominators and problems of stability of motion in classical and celestial mechanics. *Russ. Math. Surv.* **18,** 85–91.

BORDERIES, N., AND P. GOLDREICH 1984. A simple derivation of capture probabilities for the $J+1:J$ and $J+2:J$ orbit–orbit resonance problems. *Celest. Mech.* **32,** 127–136.

BROWN, R., E. OTT, AND C. GREBOGI 1987. The goodness of ergodic adiabatic invariants. *J. Stat. Phys.* **49,** 511–550.

BULIRSCH, R., AND J. STOER 1966a. Numerical treatment of ordinary differential equations by extrapolation methods. *Numer. Math.* **8,** 1–13.

BULIRSCH, R., AND J. STOER 1966b. Asymptotic upper and lower bounds for results of extrapolation methods. *Numer. Math.* **8,** 93–104.

BURNS, J. A. 1986. The evolution of satellite orbits. In *Satellites* (J. Burns and M. Matthews, Eds.), pp. 117–158. Univ. of Arizona Press, Tucson.

CHIRIKOV, B. V. 1979. A universal instability of many dimensional oscillator systems. *Phys. Rep.* **52,** 263–379.

COUNSELMAN, C. C., III AND I. I. SHAPIRO 1970. Spin–orbit resonance of Mercury. *Symp. Math.* **3,** 121–169.

CROFT, S. K., J. I. LUNINE, AND J. KARGEL 1988. Equation of state ammonia–water liquid: Derivation and planetological applications. *Icarus* **73,** 279–293.

DARWIN, G. H. 1880. On the secular changes in the elements of the orbit of a satellite revolving about a tidally distorted planet. *Phil. Trans. R. Soc. (London)* **171,** 713–891.

DERMOTT, S. F. 1979. Tidal dissipation in the solid cores of the major planets. *Icarus* **37,** 310–325.

DERMOTT, S. F. 1984. Origin and evolution of the Uranian and Neptunian satellites: Some dynamical considerations. In *Uranus and Neptune* (J. Bergstralh, Ed.), NASA Conference Publication 2330, pp. 377–404.

DERMOTT, S. F., R. MALHOTRA, AND C. D. MURRAY 1988. Dynamics of the Uranian and Saturnian satellites: A chaotic route to melting Miranda? *Icarus* **76,** 295–334.

DERMOTT, S. F., AND P. D. NICHOLSON 1986. Masses of the satellites of Uranus. *Nature* **319,** 115–120.

FRENCH, R. G., J. L. ELLIOT, AND S. L. LEVINE 1985.

Structure of the Uranian rings. II. Perturbations of the ring orbits and widths. *Icarus* **67,** 134–163.

GAVRILOV, S. V., AND V. N. ZHARKOV 1977. Love numbers of the giant planets. *Icarus* **32,** 443–449.

GOLDREICH, P. 1963. On the eccentricity of satellite orbits in the solar system. *Mon. Not. R. Astron. Soc.* **126,** 257–268.

GOLDREICH, P. 1965. An explanation of the frequent occurrence of commensurable mean motions in the solar system. *Mon. Not. R. Astron. Soc.* **130,** 159–181.

GOLDREICH, P., AND P. D. NICHOLSON 1977. Turbulent viscosity and Jupiter's tidal Q. *Icarus* **30,** 301–304.

GOLDREICH, P., AND S. J. PEALE 1966. Spin–orbit coupling in the solar system. *Astron. J.* **71,** 425–438.

GOLDREICH, P., AND S. SOTER 1966. Q in the solar system. *Icarus* **5,** 375–389.

GREENBERG, R. 1975. Commensurabilities of satellites' apsidal precession periods. *Mon. Not. R. Astron. Soc.* **170,** 295–303.

HÉNON, M. 1983. Numerical exploration of Hamiltonian systems. In *Chaotic Behaviour of Dynamical Systems*. North-Holland, Amsterdam.

HÉNON, M., AND C. HEILES 1964. The applicability of the third integral of motion: Some numerical experiments. *Astron. J.* **69,** 73–79.

HENRARD, J. 1982. Capture into resonance: An extension of the use of adiabatic invariants. *Celest. Mech.* **27,** 3–22.

HENRARD, J., AND A. LEMAITRE 1983. A second fundamental model for resonance. *Celest. Mech.* **30,** 197–218.

HOBBS, P. 1974. *Ice Physics*. Oxford Univ. Press (Clarendon), London.

JANKOWSKI, D. G., AND S. W. SQUYRES 1988. Solid-state ice volcanism on the satellites of Uranus. *Science* **241,** 1322–1325.

KAULA, W. M. 1964. Tidal dissipation by solid friction and the resulting orbital evolution. *Rev. Geophys.* **2,** 661–682.

KAULA, W. M. 1968. *An Introduction to Planetary Physics: The Terrestrial Planets*. Wiley, New York.

KRUSKAL, M. 1962. Asymptotic theory of Hamiltonian and other systems with solutions nearly periodic. *J. Math. Phys.* **3,** 806–828.

KULSRUD, R. M. 1957. Adiabatic invariant of the harmonic oscillator. *Phys. Rev.* **106,** 205–207.

LASKAR, J. 1986. A general theory for the Uranian satellites. *Astron. Astrophys.* **166,** 349–358.

LEMAITRE, A. 1984. High-order resonances in the restricted three-body problem. *Celest. Mech.* **32,** 109–126.

LENARD, A. 1959. Adiabatic invariance to all orders. *Ann. Phys.* **6,** 261–276.

LEVERRIER, U.-J. 1855. Développement de la fonction qui sert de base au calcul des perturbations des mouvements des planètes. *Ann. Obs. Paris, Mém.* **1.**

MARCIALIS, R., AND R. GREENBERG 1987. Warming of Miranda during chaotic rotation. *Nature* **328,** 227–229.

PEALE, S. J. 1986. Orbital resonances, unusual configurations, and exotic rotation states among planetary satellites. In *Satellites* (J. Burns and M. Matthews, Eds.), pp. 159–223. Univ. of Arizona Press, Tucson.

PEALE, S. J. 1988. Speculative histories of the Uranian satellite system. *Icarus* **74,** 153–171.

PEALE, S. J., AND P. CASSEN 1978. Contribution of tidal dissipation to lunar thermal history. *Icarus* **36,** 245–269.

PEALE, S. J., P. CASSEN, AND R. T. REYNOLDS 1979. Melting of Io by tidal dissipation. *Science* **203,** 892–894.

PLESCIA, J. B. 1988. Cratering history of Miranda: Implications for geologic processes. *Icarus* **73,** 442–461.

PLUMMER, H. C. 1960. *An Introductory Treatise on Dynamical Astronomy*. Dover, New York.

SMITH, B. A. L. A. SODERBLOM, R. BEEBE, D. BLISS, J. M. BOYCE, A. BRAHIC, G. A. BRIGGS, R. H. BROWN, S. A. COLLINS, A. F. COOK II, S. K. CROFT, J. N. CUZZI, G. E. DANIELSON, M. E. DAVIES, T. E. DOWLING, D. GODFREY, C. J. HANSEN, C. HARRIS, G. E. HUNT, A. P. INGERSOLL, T. V. JOHNSON, R. J. KRAUSS, H. MASURSKY, D. MORRISON, T. OWEN, J. B. POLLACK, C. C. PORCO, K. RAGES, C. SAGAN, E. M. SHOEMAKER, L. A. SROMOVSKY, C. STOKER, R. G. STROM, V. E. SUOMI, S. P. SYNNOTT, R. J. TERRILE, P. THOMAS, W. R. THOMPSON, AND J. VEVERKA 1986. Voyager 2 in the Uranian system: Imaging science results. *Science* **233,** 43–64.

SQUYRES, S. W., R. T. REYNOLDS, AND J. J. LISSAUER 1985. The enigma of the Uranian satellites' orbital eccentricities. *Icarus* **61,** 218–233.

STEVENSON, D. J. 1982. Volcanism and igneous processes in small icy satellites. *Nature* **298,** 142–144.

STEVENSON, D. J. 1983. Anomalous bulk viscosity of two-phase fluids and implications for planetary interiors. *J. Geophys. Res.* **88,** 2445–2455.

STEVENSON, D. J. 1984. Composition, structure, and evolution of Uranian and Neptunian satellites. In *Uranus and Neptune* (J. Bergstralh, Ed.), NASA Conference Publication 2330, pp. 405–423.

STONE, E. C., AND E. D. MINER 1986. The Voyager 2 encounter with the Uranian system. *Science* **233,** 39–43.

STROBELL, M. E., AND H. MASURSKY 1987. New named features on the Moon and Uranian satellites. *Proc. Lunar Planet. Sci. Conf. 18th,* 964–965.

TITTEMORE, W. C. 1988. *Tidal Evolution of the Uranian Satellites*. Ph.D. thesis, Massachusetts Institute of Technology.

TITTEMORE, W. C., AND J. WISDOM 1987. Tidal evolution of the Uranian satellites. *Bull. Amer. Astron. Soc.* **19,** 821.

TITTEMORE, W. C., AND J. WISDOM 1988a. Tidal evolution of the Uranian satellites. I. Passage of Ariel and

Umbriel through the 5 : 3 mean-motion commensurability. *Icarus* **74,** 174–230.

TITTEMORE, W. C., AND J. WISDOM 1988b. Tidal evolution of the Uranian satellites. *Bull. Amer. Astron. Soc.* **20,** 873.

TITTEMORE, W. C., AND J. WISDOM 1989. Tidal evolution of the Uranian satellites. II. An explanation of the anomalously high orbital inclination of Miranda. *Icarus* **78,** 63–89.

VEILLET, C. 1983. *De l'observation et du mouvement des satellites d'Uranus.* Thèse de Doctorate d'Etat, Université de Paris.

WHITAKER, E. A., AND R. J. GREENBERG 1973. Eccentricity and inclination of Miranda's orbit. *Mon. Not. R. Astron. Soc.* **165,** 15P–18P.

WISDOM, J. 1982. The origin of the Kirkwood gaps: A mapping for asteroidal motion near the 3/1 commensurability. *Astron. J.* **87,** 577–593.

WISDOM, J. 1983. Chaotic behavior and the origin of the 3/1 Kirkwood gap. *Icarus* **56,** 51–74.

WISDOM, J. 1987a. Rotational dynamics of irregularly shaped natural satellites. *Astron. J.* **94,** 1350–1360.

WISDOM, J. 1987b. Chaotic dynamics in the solar system. *Icarus* **72,** 241–275.

WISDOM, J., S. J. PEALE, AND F. MIGNARD 1984. The chaotic rotation of Hyperion. *Icarus* **58,** 137–152.

YODER, C. F. 1979a. Diagrammatic theory of transition of pendulum-like systems. *Celest. Mech.* **19,** 3–29.

YODER, C. F. 1979b. How tidal heating in Io drives the Galilean orbital resonance locks. *Nature* **279,** 767–770.